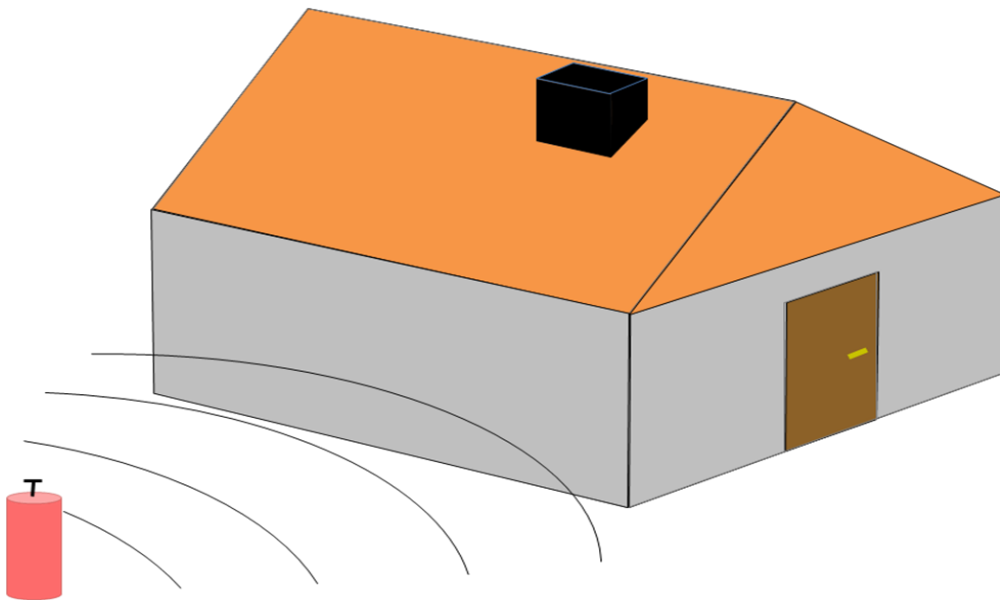


CHALMERS



Design of reinforced concrete slab with regard to explosions

Master of Science Thesis in the Master's Programme Structural engineering and building performance design

**RICKARD AUGUSTSSON
MARKUS HÄRENSTAM**

Department of Civil and Environmental Engineering
Division of Structural Engineering
Concrete structures
CHALMERS UNIVERSITY OF TECHNOLOGY
Göteborg, Sweden 2010
Master's Thesis 2010:38

MASTER'S THESIS 2010:38

Design of reinforced concrete slab with regard to explosions

*Master of Science Thesis in the Master's Programme Structural engineering and
building performance design*

RICKARD AUGUSTSSON

MARKUS HÄRENSTAM

Department of Civil and Environmental Engineering
*Division of Structural Engineering
Concrete structures*

CHALMERS UNIVERSITY OF TECHNOLOGY

Göteborg, Sweden 2010

Design of reinforced concrete slab with regard to explosions

Master of Science Thesis in the Master's Programme Structural engineering and building performance design

RICKARD AUGUSTSSON

MARKUS HÄRENSTAM

© RICKARD AUGUSTSSON & MARKUS HÄRENSTAM, 2010

Examensarbete / Institutionen för bygg- och miljöteknik,
Chalmers tekniska högskola 2010:38

Department of Civil and Environmental Engineering

Division of Structural Engineering

Concrete structures

Chalmers University of Technology

SE-412 96 Göteborg

Sweden

Telephone: + 46 (0)31-772 1000

Chalmers Reproservice / Department of Civil and Environmental Engineering
Göteborg, Sweden 2010

Design of reinforced concrete slab with regard to explosions

Master of Science Thesis in the Master's Programme Structural engineering and building performance design

RICKARD AUGUSTSSON

MARKUS HÄRENSTAM

Department of Civil and Environmental Engineering

Division of Structural Engineering

Concrete structures

Chalmers University of Technology

ABSTRACT

The design approach for structures submitted to explosions differ from the common statically approach and are not well documented. This master thesis compiles simplified methods used to design reinforced concrete beams and slabs against impulse loads and will verify the reliability of these methods.

Two simplified methods are presented here, hand calculations based on energy equations and a numerical solution method based on the equation of motion. Both methods are based on that the structure can be reduced to a one degree of freedom system (SDOF-system). The study is performed for elastic, plastic and elastoplastic material response and is compared to results from the FE software ADINA (2009), which is here assumed to correspond to a real structural response.

A comparison of the generated results concludes that the reliability for the SDOF analyses, assuming elastic response, is good for both beams and slabs. A divergence is found for the hand calculations which increase the longer the load is applied, but this divergence is known and can be predetermined. For the plastic material a divergence is found for both the beams and slabs. The analysis will approach the FE-analysis when an increased load duration is used, but is not a reliable method for impulse loaded structures. However, the results are on the safe side and can be used for preliminary design. When assuming an elastoplastic response for the beams there is certainly a good agreement between SDOF and FE-analysis, but because of the large divergence in the plastic analysis more studies are needed before it can be assumed to be reliable. The elastoplastic analysis for the slabs needs to be modified to receive relatively acceptable results, this modification is described in the thesis.

Key words: Reinforced concrete, slab, beam, explosion, impulse load, dynamic, SDOF system, equivalent static load, non-linear FEM

Dimensionering av armerad betongplatta med avseende på explosioner
Examensarbete inom Structural Engineering and Building Performance Design
RICKARD AUGUSTSSON & MARKUS HÄRENSTAM
Institutionen för bygg- och miljöteknik
Avdelningen för Konstruktionsteknik
Chalmers tekniska högskola

SAMMANFATTNING

Tillvägagångssättet vid dimensionering mot explosioner skiljer sig från den traditionella statiska dimensioneringen och är dåligt dokumenterad. Detta examensarbete sammanställer förenklade metoder som används vid dimensionering av armerade betongbalkar och plattor samt verifierar tillförlitligheten för dessa metoder.

Två förenklade metoder presenteras här, handberäkningar baserade på energiekvationer och en numerisk lösningsmetod baserad på rörelseekvationen. Båda metoderna antar att den utsatta konstruktionen kan reduceras till ett enfrihetsgradsystem (SDOF). Studien är utförd för elastiskt, plastiskt och elastoplastisk materialrespons samt jämförs med resultat från FE-programmet ADINA (2009), som här antas ge en respons motsvarande den för en riktig konstruktion.

Jämförelse mellan utförda resultat fastställer att tillförlitligheten för SDOF analyserna vid elastisk respons är god för både balkar och plattor. En avvikelse synes för handberäkningarna som avtar desto längre lasten appliceras, men denna avvikelse är känd från tidigare och kan förutbestämmas. Däremot fås en avvikelse för både balkar och plattor när en plastisk respons antas. Analysen närmar sig FE-analysen desto längre lastvaraktighet som antas, men kan inte anses ha en bra tillförlitlighet för impulsbelastade konstruktioner. Resultaten är dock på den säkra sidan och kan användas som en preliminär dimensionering. När en elastoplastisk respons antas för balkarna uppnås visserligen en bra överensstämmelse, men på grund av avvikelsen vid plastisk analys behövs fler studier göras för att ett uttalande om dimensioneringsmetodens tillförlitlighet kan göras. Den elastoplastiska analysen för plattor behöver modifieras för att ge relativt acceptabla resultat, denna modifiering är beskriven i rapporten.

Nyckelord: Armerad betong, platta, balk, explosion, impuls last, dynamik, SDOF system, ekvivalent statisk last, olinjär FEM

Contents

ABSTRACT	I
SAMMANFATTNING	II
CONTENTS	III
PREFACE	VII
NOTATIONS	VIII
1 INTRODUCTION	1
1.1 Background	1
1.2 Aim	1
1.3 Method	1
1.4 Limitations	2
1.5 Outline of the report	2
2 BACKGROUND THEORY	3
2.1 What is an explosion?	3
2.2 Simplified shockwave and load	4
2.3 Materials	5
2.3.1 Material behaviour	5
2.3.2 Simplified material behaviour	6
2.3.3 Theory of plasticity and plastic hinges	8
2.3.4 Plastic rotation capacity	11
2.4 Basic dynamics	12
2.4.1 Introduction	12
2.4.2 Velocity and acceleration	12
2.4.3 Force and pressure	13
2.4.4 Momentum, impulse and impulse intensity	13
2.4.5 Work	14
2.4.6 Equation of motion	18
2.5 Plate theory	20
2.5.1 Introduction	20
2.5.2 Elastic behaviour	20
2.5.3 Plastic behaviour	21
2.6 SDOF system	24
3 BEAMS	27
3.1 Introduction	27
3.2 Response of beams subjected to impulse load	27
3.3 Equation of motion	30
3.3.1 Introduction	30
3.3.2 Transformation factor for the mass κ_m	30

3.3.3	Transformation factor for the load κ_F	31
3.3.4	Examples of tabulated transformation factors	32
3.3.5	Solving the equation of motion	33
3.4	Hand calculation	33
3.5	FE-analysis	34
3.5.1	Restrictions	34
3.5.2	Cracked elasticity modulus	34
3.5.3	Choice of material responses in different sections	35
3.5.4	Element integration points	35
3.6	Example	37
3.6.1	Scenario	37
3.6.2	Assumptions and simplifications	37
3.6.3	Transformed mass	38
3.6.4	Stiffness and internal resistance	38
3.6.5	Required deformations	41
3.6.6	Equivalent static load	42
3.6.7	Maximum deformation capacity	43
3.6.8	Results	45
3.7	Comments to divergence between analysis	50
3.7.1	Elastic response	50
3.7.2	Ideal plastic response	51
3.7.3	Elastoplastic response	54
3.7.4	Numerical solution methods	56
4	SLABS	58
4.1	Introduction	58
4.2	Response of slabs subjected to impulse load	58
4.3	Transformation from slab to SDOF-system	61
4.3.1	Introduction	61
4.3.2	Transformation factor for the mass κ_m	61
4.3.3	Transformation factor for the load κ_F	62
4.3.4	Tabulated transformation factors	63
4.4	Equation of motion	64
4.5	Hand calculations	64
4.6	FE-analysis	64
4.6.1	Restrictions	64
4.6.2	How to model in ADINA	64
4.6.3	Verification of the model	69
4.7	Example – Simply supported slab	71
4.7.1	Scenario	71
4.7.2	Assumptions and simplifications	71
4.7.3	Transformed mass	72
4.7.4	Maximum static load	72
4.7.5	Stiffness and internal resistance	74
4.7.6	Required deformations	76

4.7.7	Equivalent static load	77
4.7.8	Maximum deformation capacity	78
4.7.9	Results	80
4.8	Example – Fully fixed slab	86
4.8.1	Scenario, assumptions and simplifications	86
4.8.2	Transformed mass	86
4.8.3	Maximum static load	86
4.8.4	Stiffness and internal resistance	88
4.8.5	Required deformations	89
4.8.6	Maximum deformation capacity	90
4.8.7	Results	91
4.9	Comments to divergence between analysis	92
4.9.1	Introduction	92
4.9.2	Elastic	93
4.9.3	Ideal plastic	93
4.9.4	Elastoplastic	95
5	FINAL REMARKS	98
5.1	Conclusions	98
5.2	Further studies	98
6	REFERENCES	99
APPENDIX A	CENTRAL DIFFERENCE METHOD	101
APPENDIX B	MODIFIED TRANSFORMATION FACTOR FOR THE IDEAL PLASTIC MATERIAL FOR A BEAM	102
APPENDIX C	MODIFIED TRANSFORMATION FACTOR FOR THE ELASTOPLASTIC MATERIAL FOR A BEAM	104
APPENDIX D	ELASTIC TRANSFORMATION FACTORS FOR A SIMPLY SUPPORTED SLAB WITH UNIFORMLY DISTRIBUTED LOAD	106
D.1	Indata	106
D.2	Transformation factor for the mass κ_m	106
D.3	Transformation factor for the load κ_F	107
APPENDIX E	PLASTIC TRANSFORMATION FACTORS FOR A SIMPLY SUPPORTED AND FULLY FIXED SLAB WITH UNIFORMLY DISTRIBUTED LOAD	108
E.1	Indata	108
E.2	Transformation factor for the mass κ_m	108
E.3	Transformation factor for the load κ_F	110

APPENDIX F MODIFIED ALPHA FACTOR FOR THE FICTITIOUS YIELD
STRESS WHEN USING SEVEN INTEGRATION POINTS 112

APPENDIX G TRANSFORMATION FACTORS FOR ELASTOPLASTIC SLAB
114

Preface

In this Master's thesis simplified design approaches for impulse loaded reinforced concrete beams and slabs are compiled and investigated. The study has been carried out in cooperation with Reinertsen Sverige AB and the Division of Structural Engineering at Chalmers University of Technology. The work has been done at Reinertsen's office in Göteborg between January 2010 and June 2010.

Many thanks go out to Morgan Johansson, PhD, who has been our supervisor and has helped us through harsh time. Thanks also to Håkan Lantz at Reinertsen who has helped us with ADINA and to Reinertsen itself, which has provided us access to helpful documents. Finally, thanks to Kent Gylltoft who has been our examination during this project.

Göteborg June 2010

Rickard Augustsson, Markus Härenstam

Notations

Roman upper case letters

A	Area
A_s	Area of reinforcement
C	Damping
D	Flexural rigidity of a plate
E	Modulus of elasticity
E_c	Young's modulus for concrete
E_s	Young's modulus for steel
E_k	Kinetic energy
F	External force
F_e	Equivalent external force
I	Moment of inertia
I	Impulse (general)
I_c	Characteristic impulse
K	Stiffness
K_v	Torsional stiffness
M	Moment
M_{rd}	Moment capacity
M_{el}	Elastic moment
M_{pl}	Ultimate moment
P	Pressure load
P_1	Peak pressure load
R	Internal resisting force
R_e	Equivalent internal force
R_m	Maximum internal force
W_e	External work
W_i	Internal work
$W_{i,el}$	Elastic internal work
$W_{i,pl}$	Plastic internal work
$W_{i,ep}$	Elastoplastic internal work
W_{el}	Elastic bending resistance
Q	Total load

Roman lower case letters

a	Acceleration
a	Length of middle yield line for slabs
\bar{a}	Mean acceleration
c	Distance of concrete layer
d	Effective height of cross section
f_y	Yield stress (general)

f_{sy}	Yield stress for reinforcement
f_{su}	Ultimate capacity for reinforcement
f_{cc}	Concrete compression strength
f'_y	Fictitious yield stress
f_y^{mod}	Modified fictitious yield stress
h	Height of cross-section
i	Impulse intensity
k	Stiffness
l	Length of beam / width of slab
m	Mass
m'	Mass per unit length
m_e	Equivalent mass
s	Spacing between reinforcement steel
q	Distributed load
q_e	Equivalent static load
q_{el}	Equivalent static load with elastic response
q_{pl}	Equivalent static load with plastic response
p	Momentum
t	Time
t_1	Total time duration of transient load
u	Deformation
\dot{u}	Velocity, first derivative of u with respect to time t
\ddot{u}	Acceleration, second derivative of u with respect to time t
u_{el}	Elastic deformation
u_{pl}	Plastic deformation
u_{ep}	Elastoplastic deformation
u_s	Deformation of system point
v	Velocity
\bar{v}	Mean velocity
v_s	Velocity in the system point
w	Width of cross-section / length of slab
x	Coordinate
y	Coordinate

Greek lower case letters

α	Quota between the Young's modulus for the reinforcement and concrete
α	Stress block factor
α	Modification factor for Young's modulus
α	Modification factor for the maximal moment
β	Stress block factor
δ	Deformation
ε	Strain

ε_s	Reinforcement strain
ε_{el}	Elastic strain
ε_{su}	Ultimate reinforcement strain
ε_{pl}	Plastic strain
ε_{sy}	Strain when yielding starts for the reinforcement
κ_K	Transformation factor for the internal force
κ_m	Transformation factor for the mass
κ_{mF}	Transformation factor for the mass and external load
κ_F	Transformation factor for the external load
λ	Slenderness
θ	Rotation
θ_{pl}	Plastic rotation
ρ	Density
σ	Stress
ω	Angular frequency
μ	Number of the statically indeterminacy
ν	Poisson's ratio

1 Introduction

1.1 Background

An explosion is a huge release of energy and it creates a shockwave that acts as an impulse load on structures. In many applications it is of great importance to take this accidental action in consideration when designing structures, for example in civil defense, military installations, tunnels and processing industry. The methods used to design against impulse loads are today not well documented and few controls of the reliability for these methods can be found.

This master thesis is a continuation of earlier master thesis carried out by Nyström (2006) and Ek and Mattsson (2010).

1.2 Aim

The aim of this master theses project is to put together information about design approaches for impact loading on concrete structures. Since the knowledge regarding designing with impulse loading is limited and engineers in practice are not used to apply dynamic calculations there is a need to find simple calculation models that are accurate to reality. From previous master theses carried out 2006 and 2009 by Nyström respective Ek and Mattsson impulse loaded beams were investigated. However, this master thesis will take the next step and investigate the response of slabs.

Questions that will be considered in the project:

- What is the response of a concrete slab subjected to impulse loading by means of simple hand calculation approaches? What is the agreement between such simple methods and more advanced analyses as FE-analyses? How should such a FE-analysis be done in order to be both easy to carry out and yield correct results?
- What is the difference in response of a structural member when it has a plastic response instead of a linear elastic response?

1.3 Method

Literature studies are carried out to get a deeper understanding on how a concrete structure responds when exposed to an explosion. This is done by first searching for present hand calculations on the subject and by studying the previous master theses on beams.

A simplified hand calculation model describing the response of a concrete slab subjected to an impulse load is established. To verify this model a FE model in the FE software ADINA (2009) is done. There are no possibilities to perform any real tests and the FE model is therefore considered to simulate the real behaviour of the concrete slab. A comparison between the FE model and the simplified hand calculations for linear elastic and plastic response is done separately. The elastic model is expected to coincide well between the different analyses, while the plastic analysis is expected to be more complicated and therefore be a main factor in this

thesis. A study of beams is carried out before advancing to slabs, this is done in order to get a better understanding of the behaviour for impulse loaded structures.

1.4 Limitations

Because of the complex material behaviour that arises for reinforced concrete structures, the beam and slab is here modelled as a homogenous material. This means that the strength of the reinforcement in one direction is smeared out over the entire cross section. Also, only idealized material behaviour, i.e. linear elastic, ideal plastic and elastoplastic, are used in the models. This is to simplify the calculations and to reduce the parameters that can affect the results.

The explosion studied arises from a detonation of explosives in the air. Different phenomenon, as reflection of the shockwave and vibrations in the ground, will not be taken into account. The impact from the fragments of the bomb will also be neglected.

1.5 Outline of the report

The report is divided into Background theory (Chapter 2), Beams (Chapter 3), Slabs (Chapter 4) and Final remarks (Chapter 5).

In Chapter 2, basic theory for explosion, material response, dynamic, plate and SDOF system are explained to understand the rest of the report.

Chapter 3 explain the behaviour and the different approaches used to control the resistance for a beam subjected to an impulse load. An example is established and is followed by comments to the results obtained.

Chapter 4 has the same structure as Chapter 3 but here, slabs are investigated. It starts with an explanation of the behaviour and the different approaches used for an impulse loaded slab. Then, two examples are established, one with a simply supported slab and the other with a fully fixed slab, and it followed by comments to the results obtained.

Chapter 5 summarises the conclusions from the studies and give suggestions to further studies.

2 Background theory

2.1 What is an explosion?

An explosion is an exothermal reaction, i.e. a sudden release of energy that creates a shockwave. When a charge detonates its energy is suddenly released, the entire explosion process is over in a couple of microseconds. The release will create a shockwave front, i.e. a fast rise in pressure, temperature and density which will move with a supersonic speed through the air. This initial energy will decrease with increased distance to the centre of detonation as illustrated in Figure 2.1.

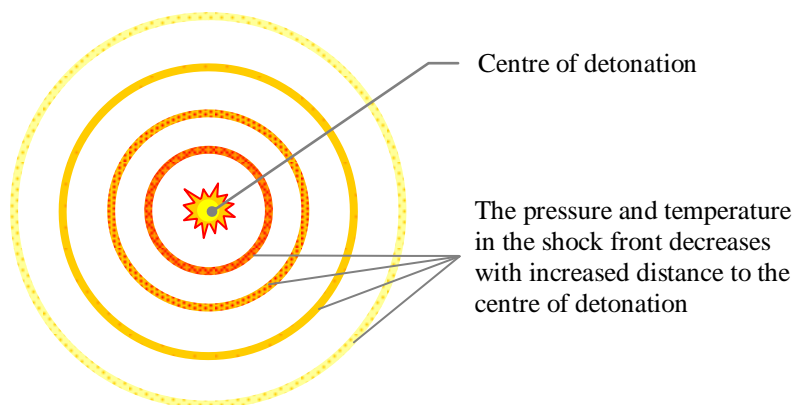


Figure 2.1 Shockwave with decreasing pressure and temperature outward from the explosion centre.

The pressure in a point when an idealized shockwave, i.e. a shockwave that is not disturbed by any reflections, passes through will first have an initially positive pressure phase and then a negative pressure phase, see Figure 2.2, Johansson and Laine (2007).

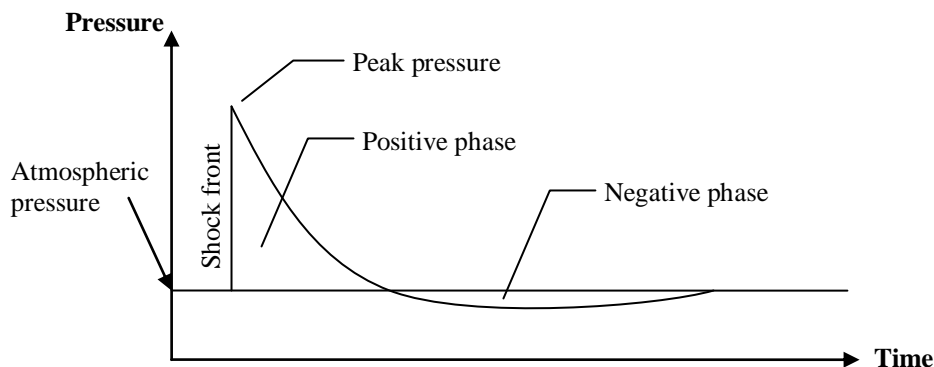


Figure 2.2 Idealized shockwave pressure in time.

As can be seen the shockwave front caused by the detonation is instantaneously increased from normal atmospheric pressure to a higher pressure which can be seen as a “wall” of compressed air molecules moving through space. When the shockwave front is moving forward it compresses the air molecules that come in its way and as a result of this a negative pressure arises behind the shockwave front where it is “a lack of” air molecules. However, the shockwave front “borrows” air molecules from the

bypassing area. With time and distance from the blast the energy and shockwave decreases. The air molecules that were moved away in the shockwave front will return to the zone where the pressure is negative. Finally, there is equilibrium between air molecules.

In case of a reflected shockwave the pressure over time will not have the same appearance as the idealized shockwave shown in Figure 2.2. Instead, the distribution of the pressure over time will vary depending on how the shockwave is reflected, Johansson (2002). Figure 2.3 shows an unreflected and reflected hit on a building. The reflected hit is a so called normal reflection, i.e. the shockwave hits the building perpendicular to the surface, and can be up many times larger than the unreflected shockwave.

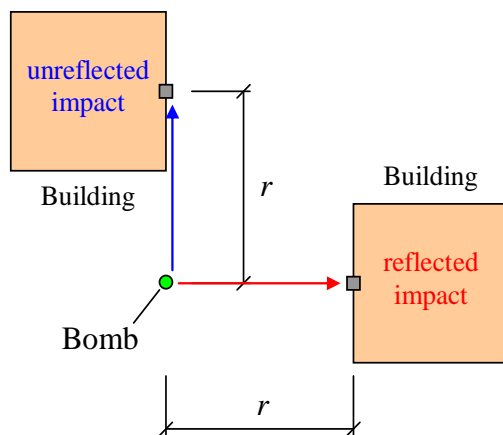


Figure 2.3 Reflected and unreflected shockwave. From Johansson and Laine (2009).

There is two main different degrees of explosives, called high and low. When using low explosives the movement of the shockwave happens in subsonic, i.e. with a velocity under speed of sound. This ignition of low explosive explosion is called deflagration. In contrast to low explosives the high explosive shockwave moves in supersonic, i.e. with a velocity over speed of sound. The ignition of a high explosive explosion is called detonation, Johansson (2002).

2.2 Simplified shockwave and load

In Figure 2.2 the pressure variation at a point is illustrated. A simplification of the shockwave is done to easier be able to calculate the intensity and the load it will give rise to. This is done by assuming a linear decrease of pressure in time and also, because of the relatively small peak pressure in the negative phase, by neglecting the negative phase, see Figure 2.4a. From now on this idealization of the impulse load is to be used. However, a modification has been made with a small inclination from zero pressure to the peak pressure for the FE-analysis due to convergence problems in model, see Figure 2.4b.

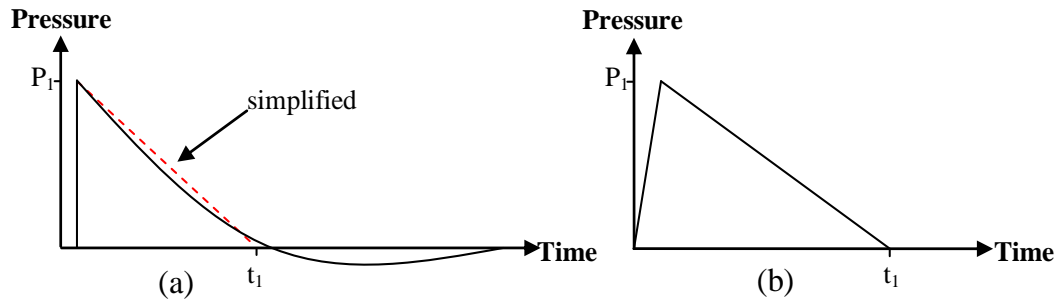


Figure 2.4 Simplified shockwave.

Due to limitations in performing a real test or doing a nonlinear numerical calculation empirical expressions are used to calculate the impulse load from an explosion. These empirical expressions from e.g. Baker (1973) can be used in order to compile parameters like peak pressure and impulse intensity. For a deeper investigation and understanding about how to define an impulse load the reader is referred to Johansson and Laine (2007) and Johansson (2002).

In this master thesis, a reference bomb provided by the authority will be used. It consists of 125 kg high explosive TNT with a distance of 5 meter from the studied structure.

2.3 Materials

2.3.1 Material behaviour

The material studied in this master thesis is reinforced concrete. The material behaviour of reinforcement and reinforced concrete is shown in Figure 2.5.

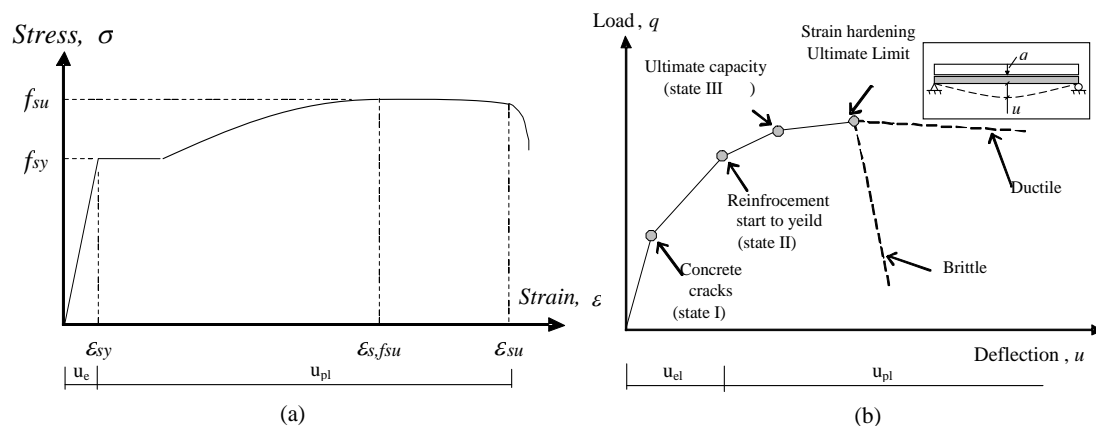


Figure 2.5 Material behaviour for (a) reinforcement and (b) reinforced concrete.

The reinforcement behaviour is linear elastic until it yields, which happens when the stress reaches the yield limit f_{sy} . The stress can then increase further to the ultimate capacity f_{su} because of a phenomenon called strain hardening. When the ultimate strain ϵ_{su} is reached the reinforcement cannot deform anymore and will be torn off. The value of the total strain will depend on the plastic rotation capacity, which is

essential for the capacity of a concrete structure and will be described further in Section 2.3.4.

Because of the high stiffness of uncracked concrete the reinforced concrete will have a high stiffness in the beginning, called state I, and only small deformations will occur. However, the concrete has a low tensile capacity and when it cracks, state II, it will leave the reinforcement to resist the tensile stresses. When designing a reinforced concrete structure it is assured that the reinforcement in the tensile zone can develop its ultimate capacity, state III, before the structure collapse. Assuming this, the reinforced concrete will have a similar material behaviour after it has cracked as the reinforcement. Note here that the load in Figure 2.5 increases for state III while the stress remains constant at f_{sy} . This is because the structure will start to redistribute the moment to other parts where the yield moment not is reached.

Depending on how the reinforced concrete structure is designed, i.e. amount and location of reinforcement, the structure can have a ductile or brittle response. The response that will arise depends on the plastic rotation capacity and will be presented in Section 2.3.4. A general rule is that a ductile response is preferred since the structure can then deform more and that crushing of concrete should occur and not a torn off of the reinforcement.

As can be seen the response may be rather complex and further studies will not be done here. Instead, simplified models of reinforcement and reinforced concrete are established to simplify the different methods used in this master thesis.

2.3.2 Simplified material behaviour

2.3.2.1 Reinforcement

A common simplification of the behaviour of reinforcement is to neglect the strain hardening. It can then be described as in Figure 2.6, with the maximum capacity set to the yield limit, f_{sy} .

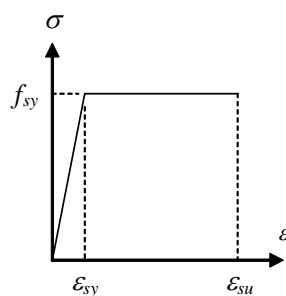


Figure 2.6 Simplified reinforcement behaviour.

2.3.2.2 Linear elastic

The uncracked and cracked part of the concrete, state I and II, is following Hooke's law

$$\sigma = E \varepsilon \quad (2.1)$$

where σ is stress, E is Young's modulus and ε is concrete strain. To simplify calculations here either a case with uncracked concrete or with cracked concrete will be assumed. The internal resisting force R can for the cracked case be calculated as

$$R = ku \tag{2.2}$$

where u is the deflection and k is the stiffness, see Figure 2.7.

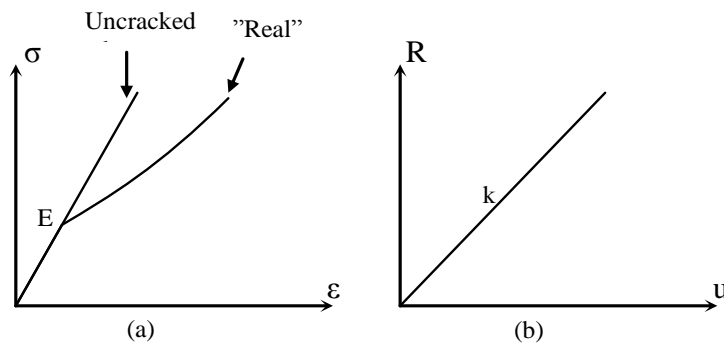


Figure 2.7 Linear elastic uncracked case (a) material response (b) structural response.

The stiffness k depends on Young's modulus and the moment of inertia. Its function will differ depending on the system, i.e. boundary conditions, choice of material and form of structure. For the cracked part the moment of inertia will be lower than for the uncracked part, resulting in a lower stiffness. The cracked case is assumed to have a constant stiffness and the internal resisting force can then be calculated in the same way as for the cracked case, equation (2.2), but with a lower stiffness and hence a higher deformation, see Figure 2.8.

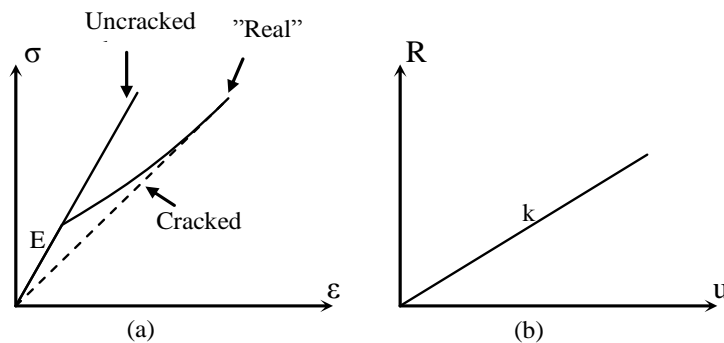


Figure 2.8 Linear elastic cracked case (a) material response (b) structural response.

2.3.2.3 Ideal plastic

Since strain hardening is neglected for the reinforcement the idealized plastic, state III, material behaviour for reinforced concrete will be assumed to have a constant value equal to the yield stress, see Figure 2.9. A result from this assumption is that no deformations will occur until the stress has reached the yield stress. If a system is subjected to a load F the relation can be written as

$$\begin{aligned} R &= F & \text{for} & & F < R_m & \text{and} & u = 0 \\ R &= R_m & \text{for} & & F \geq R_m & \text{and} & u \geq 0 \end{aligned} \tag{2.3}$$

where R_m is the maximum value of the internal force, i.e the resisting internal force when the steel is yielding.

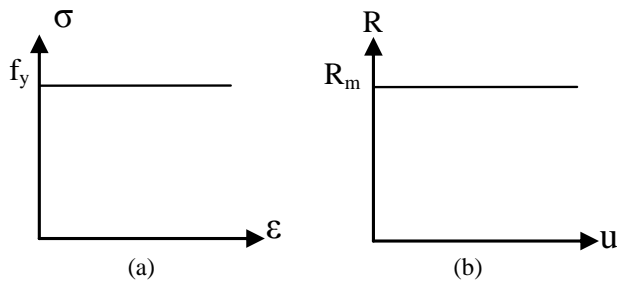


Figure 2.9 Idealized plastic case (a) material response (b) structural response.

2.3.2.4 Elastoplastic

The simplified elastoplastic material is more similar to the “real behaviour”, see Figure 2.5, than the elastic and the ideal plastic material. It will have an elastic part equal to the cracked concrete and when the stress equals the yield stress it will enter the plastic part, see Figure 2.10. Note here that when unloading the system the elastic deformation will go back while the plastic deformation will remain. So if a system is subjected to a load P the relation can be written as

$$\begin{aligned} R &= ku_{el} \quad \text{for} \quad F < R_m \\ R &= R_m \quad \text{for} \quad F \geq R_m \end{aligned} \quad (2.4)$$

where u_{el} is the elastic part of the deformations. The cracked case has been chosen because it gives an upper limit for the elastic deformations and the model will therefore be a “worst case scenario”.

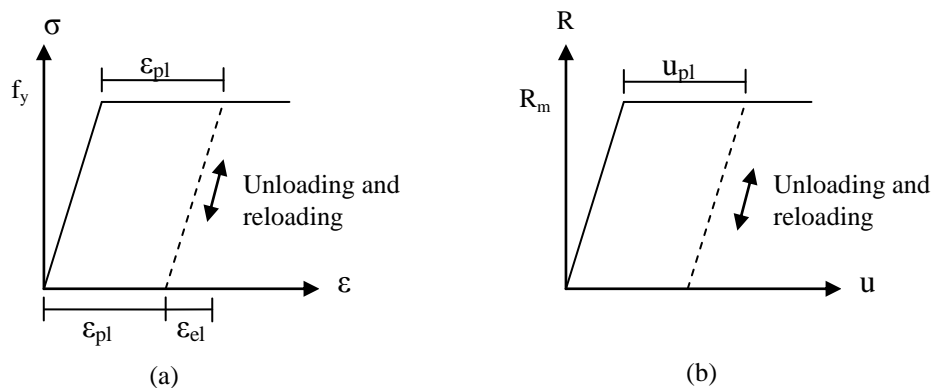


Figure 2.10 Elastoplastic case (a) material response (b) structural response.

2.3.3 Theory of plasticity and plastic hinges

As long as the stress in the most stressed fibres in the cross section is less than the yield stress the cross section will have an elastic response and Hooke’s law, equation (2.1), will apply. For a rectangular double symmetric cross section the stress and strain distribution will be symmetric as shown in Figure 2.11. The elastic moment for a rectangular cross section is

$$M_{el} = \frac{\sigma I}{h/2} \quad (2.5)$$

where I is the moment of inertia which for a rectangular cross section can be calculated as

$$I = \frac{wh^3}{12} \quad (2.6)$$

where w is the width and h is the height of the cross section. A limiting case is when the maximum stress equals the yield stress, Figure 2.12a, the moment is then equal to

$$M_{el} = \frac{f_y I}{h/2} \quad (2.7)$$

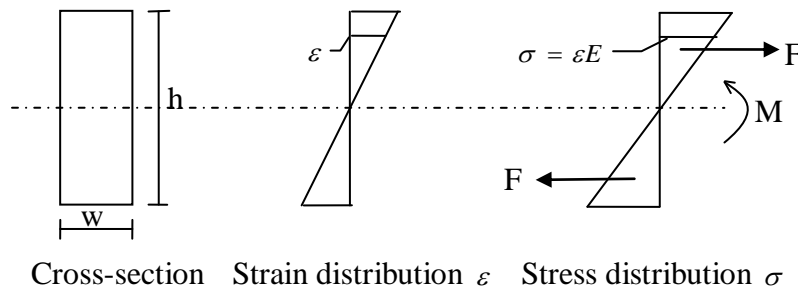


Figure 2.11 Stress- and strain distribution for a double symmetric cross section.

If the load is increased further the cross section will enter an elastoplastic state. Hooke's law will only apply for the elastic part while the plastic part will have a linear strain response but the stresses will be modified so it doesn't exceed the yield limit, see Figure 2.12b. The maximum moment capacity is reached when the whole cross section has plasticised, as shown in Figure 2.12c. It can be calculated for a rectangular cross section to be

$$M_{pl} = f_y \frac{wh^2}{4} \quad (2.8)$$

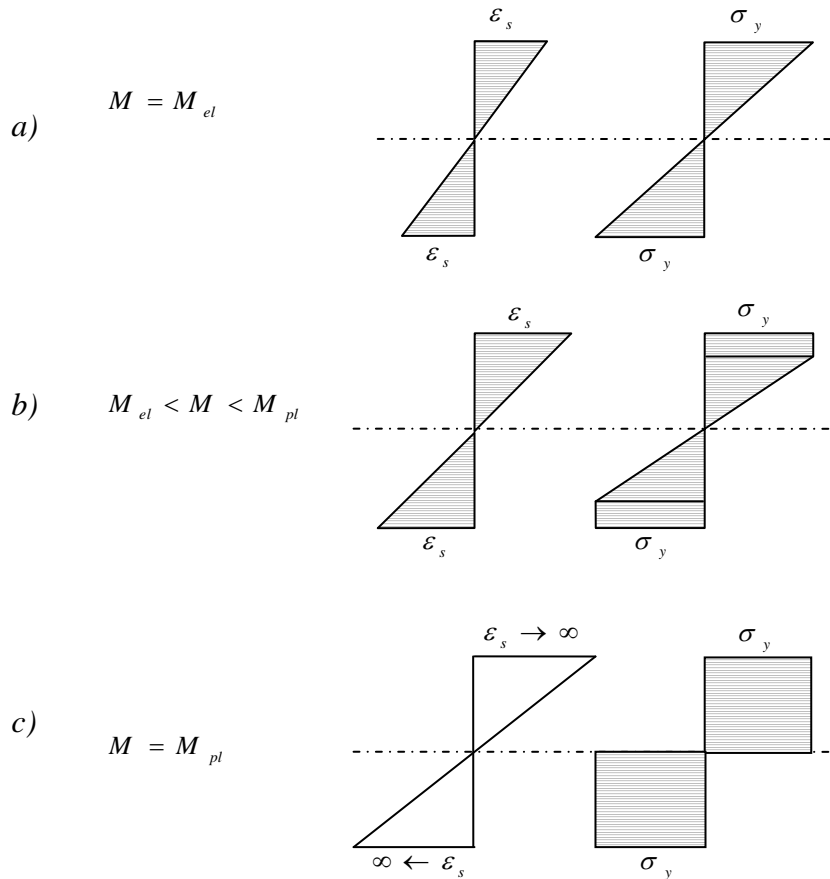


Figure 2.12 Stress- and strain distribution for (a) yielding starts (b) part of the cross section is yielding (c) the whole cross section is yielding (ultimate moment capacity).

When the ultimate moment capacity M_{pl} is reached in a section the deformations will increase rapidly in the affected area. Because the yield area is small it can be assumed that all the deformations take place in one small deformable element called a plastic hinge. If the structure is statically determined, for example for a simply supported beam, a plastic hinge will lead to a mechanism, see Figure 2.13a. In other cases when the structure is statically indeterminate, for example for a fully fixed beam or a slab, more plastic hinges are needed to form a mechanism, see Figure 2.13b. The number of plastic hinges needed is equal to

$$\text{number plastic hinges} = \mu + 1 \quad (2.9)$$

where μ is the number of the statically indeterminacy for the structure. This means that although the ultimate moment capacity is reached in one part of the structure more load can be applied since the moments are distributed to other parts.

For a statically loaded structure a mechanism will lead to a collapse of the structure. This is however not true for a dynamic loaded structure. Here, the only limit is the maximum internal force R_m of the structure.

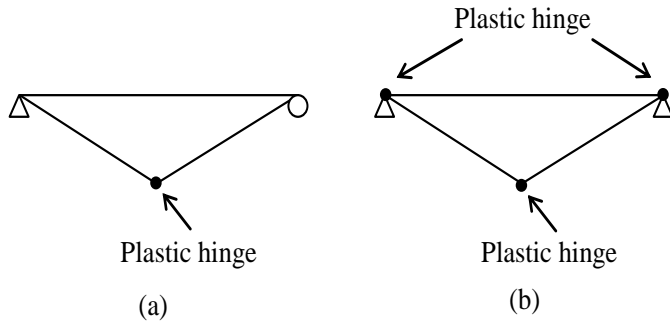


Figure 2.13 A mechanism for (a) statically determinate structure (b) statically indeterminate structure

2.3.4 Plastic rotation capacity

As mentioned above the maximum moment capacity is reached when the whole cross section yields. This is however an idealized state where the strains are infinite large and the real maximum moment capacity may be reached before. The limit depends on how much the deformable element can deform before a plastic hinge is created. The deformations that start after yield limit is reached are called plastic deformations and will give rise to plastic rotations in the region. The plastic rotation capacity is a measure of the maximum plastic rotation, i.e. the plastic rotation when a plastic hinge is formed. This means that although the yield stress is reached the deformations can increase further, see Figure 2.14.

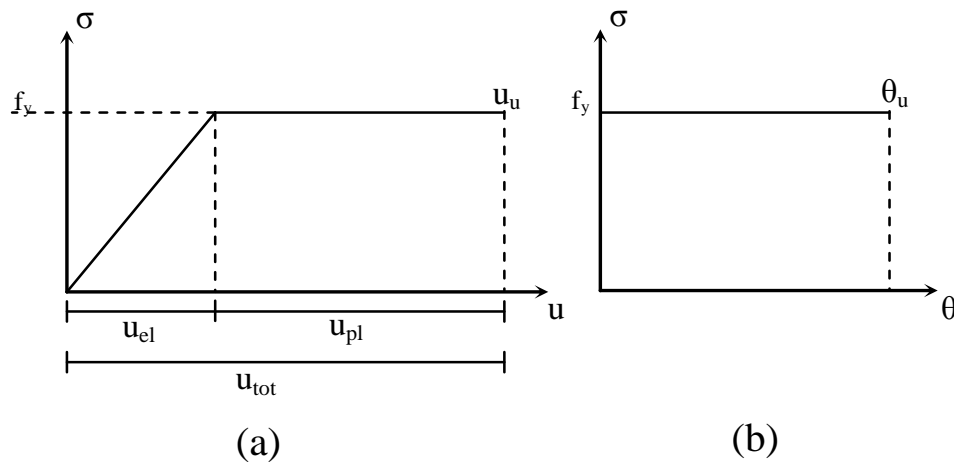


Figure 2.14 Plastic capacity for (a) deformation (b) rotation.

In Eurocode 2 CEN (2004) the maximum allowed plastic rotation is presented in a diagram, shown in Figure 2.15.

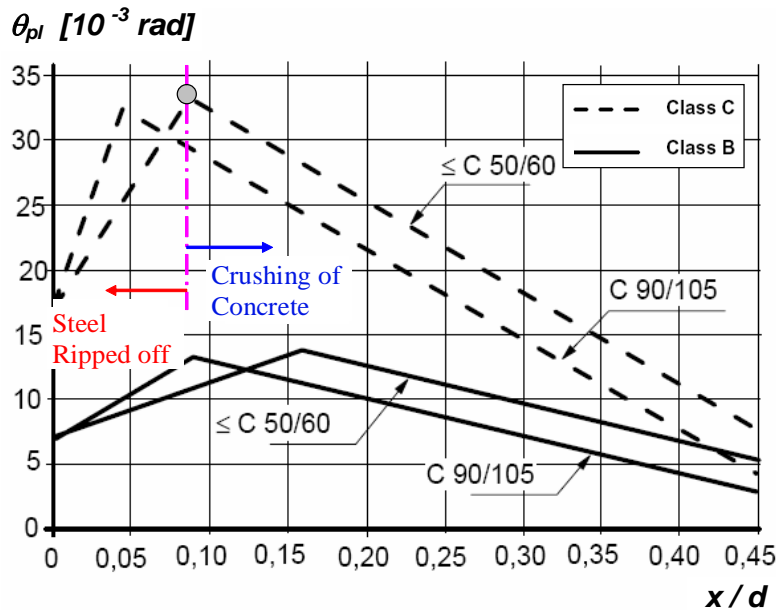


Figure 2.15 Diagram from Eurocode 2 CEN (2004) describing maximum allowed plastic rotation.

Here, the plastic rotation capacity is based on the quality of the concrete, the reinforcement class and the ratio between the height of the compressed zone and the effective height.

2.4 Basic dynamics

2.4.1 Introduction

An explosion will give rise to a high pressure under a short amount of time. This pressure will be much larger than the static pressure the structure is normally designed for and still the structure will not always collapse. The reason for this is that the static pressure is applied on the structure for infinite time while the explosion only has a short duration and hence, can have a larger maximum pressure. This means that another way of resolving the problem has to be used. One way to do this is by considering the energy applied by the explosion and the energy the structure can absorb before it collapses. In this chapter basic dynamics needed to understand this way of designing will be presented.

2.4.2 Velocity and acceleration

The velocity is defined as the movement over time. If a particle moves from u_0 to u_1 over the time t_0 to t_1 the mean velocity is

$$\bar{v} = \frac{u_1 - u_0}{t_1 - t_0} \quad (2.10)$$

By letting the time difference $t_1 - t_0$ go towards zero the difference in distance will also go towards zero and the velocity of the particle will approach a value defined as the velocity at time t . The equation is

$$v(t) = v = \lim_{t_0 \rightarrow t_1} \frac{u_1 - u_0}{t_1 - t_0} = \frac{du}{dt} = \dot{u} \quad (2.11)$$

The acceleration is defined as the difference in velocity over time, i.e. if the velocity increases from v_0 to v_1 over the time t_0 to t_1 the mean acceleration is

$$\bar{a} = \frac{v_1 - v_0}{t_1 - t_0} \quad (2.12)$$

Analogous with the velocity the acceleration will reach a value at time t when the time difference goes toward zero. The equation is

$$a(t) = a = \lim_{t_0 \rightarrow t_1} \frac{v_1 - v_0}{t_1 - t_0} = \frac{dv}{dt} = \ddot{u} \quad (2.13)$$

2.4.3 Force and pressure

The force is according to Newton's second law

$$F = ma \quad (2.14)$$

where m is the mass and a the acceleration of the body, respectively.

The pressure P is defined as the force acting on an area, i.e.

$$P = \frac{F}{A} \quad (2.15)$$

where F is the force acting on the area A .

2.4.4 Momentum, impulse and impulse intensity

The momentum p for a body with the mass m and velocity v is defined as

$$p = mv \quad (2.16)$$

If the body is moving with the velocity v_0 and is subjected to a force F under the time t_0 - t_1 , see Figure 2.16, the new momentum can be calculated as

$$mv_1 = mv_0 + \int_{t_0}^{t_1} F(t) dt \quad (2.17)$$

where v_1 is the new velocity of the body and the integral to the right is defined as the impulse I transferred to the body, i.e.

$$I = \int_{t_0}^{t_1} F(t) dt \quad (2.18)$$

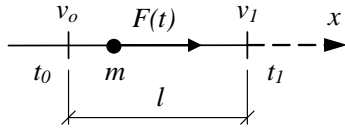


Figure 2.16 Difference in momentum when a body is subjected to an external force.

By inserting equation (2.13) and (2.14) into (2.18) the impulse can be redefined as

$$I = \int_{t_0}^{t_1} F(t) dt = \int_{t_0}^{t_1} ma(t) dt = m \int_{t_0}^{t_1} a(t) dt = mv \quad (2.19)$$

If the body instead is subjected to a pressure P under the time t_0-t_1 the new momentum is calculated as

$$mv_1 = mv_0 + A \int_{t_0}^{t_1} P(t) dt \quad (2.20)$$

where the integral is defined as the impulse intensity i transferred to the body, i.e.

$$i = \int_{t_0}^{t_1} P(t) dt \quad (2.21)$$

By looking at Figure 2.4 again the impulse intensity can be illustrated as the area under the force-time relation. From Figure 2.17 and by combining equations (2.15), (2.18) and (2.21) it can be seen that

$$I = Ai \quad (2.22)$$

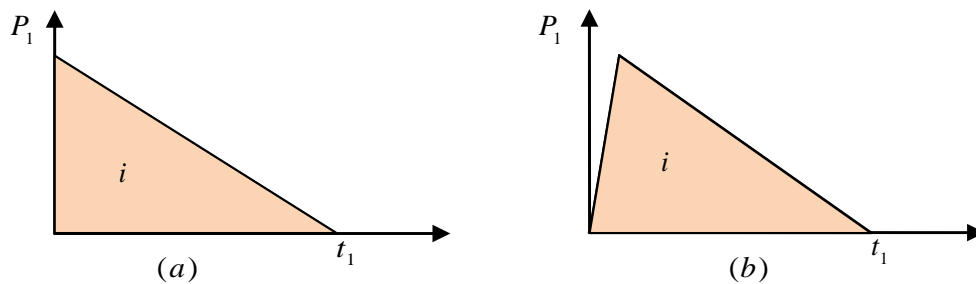


Figure 2.17 Impulse intensity for an idealized shockwave.

2.4.5 Work

2.4.5.1 External

The kinetic energy E_k for a body with the mass m and velocity v is defined as

$$E_k = \frac{mv^2}{2} \quad (2.23)$$

By inserting the equation (2.19) into (2.23) the external work W_e , i.e. the kinetic energy E_k , for a body with the mass m and subjected to an impulse load I can be expressed as

$$W_e = E_k = \frac{I^2}{2m} \quad (2.24)$$

However, this equation is only correct when the impulse is infinitely short. In other cases a resistance against transferring the kinetic energy into the structure must be considered. This resistance depends on the stiffness of the structure and will increase with time. By introducing a so called characterized impulse I_c that has an infinite high pressure and infinite short duration, see Figure 2.18, the equation (2.24) can be stated in a more correct way as

$$W_e = E_k = \frac{I_c^2}{2m} \quad (2.25)$$

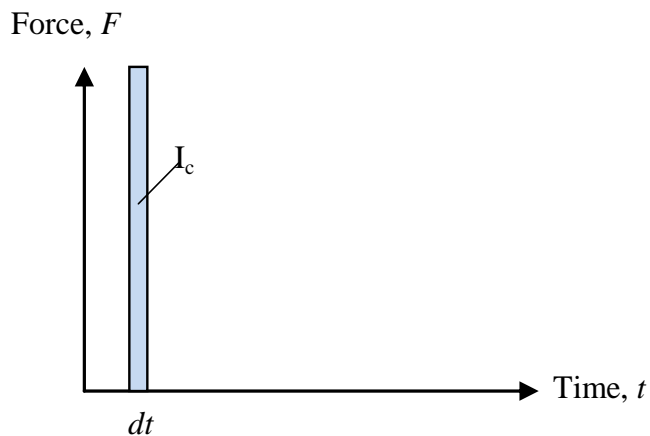


Figure 2.18 Characterized impulse.

This means that when comparing the external work for an impulse load with longer duration the longer impulse will result in a lower external work on the structure. Study for example the impulse for the idealized shockwave shown in Figure 2.4. The external work for this idealized shockwave will be lower than for a characterized impulse load with the same total impulse, see Figure 2.19.

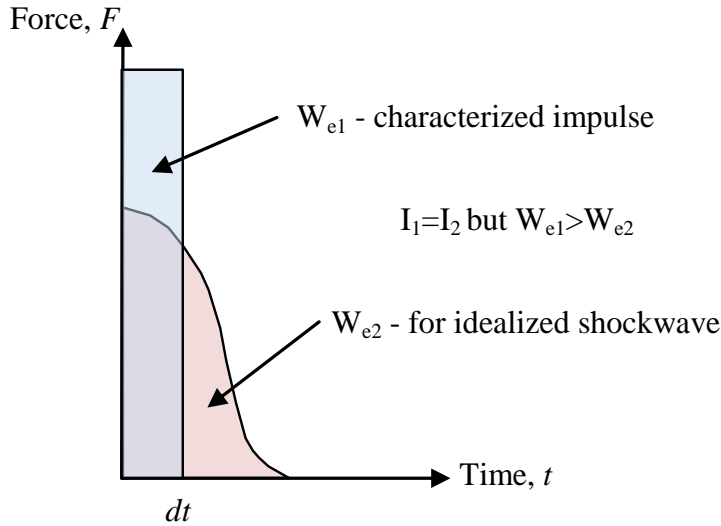


Figure 2.19 Different external work on the structure for the same total impulse but with different durations.

2.4.5.2 Internal

The internal work of a body is defined as

$$W_i = \int_{u_0}^{u_1} R(u) \quad (2.26)$$

where u is the deformation and $R(u)$ is the internal resisting force of the structure. Note here that this resisting force is not the same as the resistance against transferring the kinetic energy into the structure mentioned in Section 2.4.5.1. The internal work can be illustrated by the area under the structural response curve described in Section 2.3.2, see Figure 2.20. As can be seen the internal work will develop differently in time depending on what material is used, but the final internal work will always be the same.

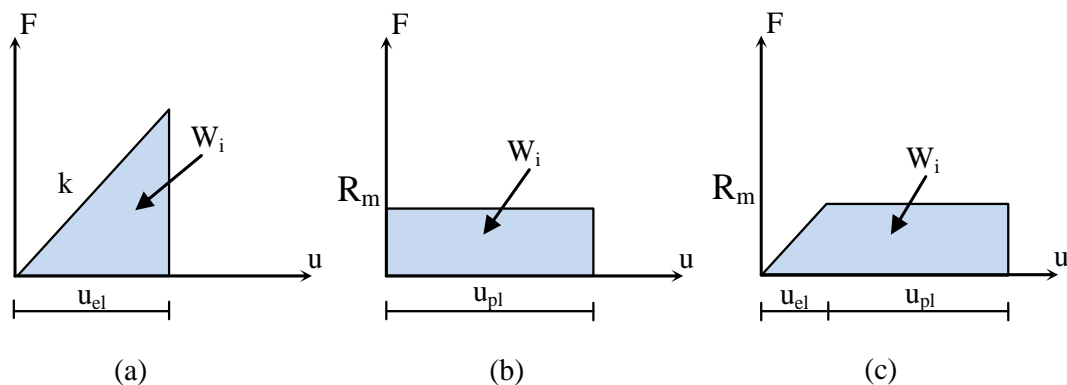


Figure 2.20 The internal work for the materials (a) elastic (b) plastic (c) elastoplastic.

By combining equation (2.2) and (2.26) the elastic internal work can be stated as

$$W_{i.el} = \int_0^{u_{el}} R(u_{el}) = \int_0^{u_{el}} ku_{el} = \frac{ku_{el}^2}{2} \quad (2.27)$$

By combining equation (2.3) and (2.24) the ideal plastic work can be stated as

$$W_{i.pl} = \int_0^{u_{pl}} R(u_{pl}) = \int_0^{u_{pl}} P + \int_0^{u_{pl}} R = 0 + Ru_{pl} = Ru_{pl} \quad (2.28)$$

By combining equation (2.4) and (2.24) the elastoplastic work can be stated as

$$W_{i.ep} = \int_0^{u_{tot}} R(u_{pl}) = \int_0^{u_{el}} ku_{el} + \int_{u_{el}}^{u_{tot}} R = \frac{ku_{el}^2}{2} + Ru_{pl} \quad (2.29)$$

2.4.5.3 Equilibrium

For a body to be in energy equilibrium the external work must be equal to the internal work, i.e.

$$W_e = W_i \quad (2.30)$$

By combining equation (2.25), (2.27) and (2.30) the elastic deformations that will arise in the structure can be calculated to

$$u_{el} = \frac{I_c}{\sqrt{km}} = \frac{I_c}{m\omega} \quad (2.31)$$

where ω is the angular frequency. In the same way the plastic deformations can be calculated by combining equation (2.25), (2.28) and (2.30) to

$$u_{pl} = \frac{I_c^2}{2mR_m} \quad (2.32)$$

and the elastoplastic deformations can be calculated as

$$u_{ep} = u_{ep.el} + u_{ep.pl} \quad (2.33)$$

where $u_{ep.el}$ and $u_{ep.pl}$ is the elastic respectively plastic parts of the deformations. Note here that for the elastoplastic case the elastic part will add additional resistance and therefore less plastic deformation is needed. However, since the elastic part has a linear response and is limited by the ultimate internal resistance, the deformation will be twice as large compared with the plastic contribution, see Figure 2.21.

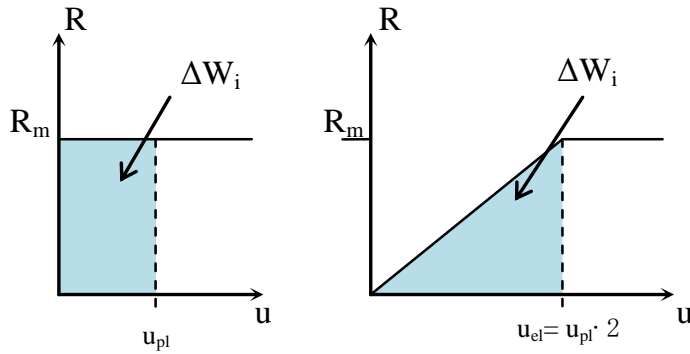


Figure 2.21 Difference in required deformation for same internal energy.

This will result in a larger total deformation for the beam than if an ideal plastic material was used. The maximum elastic deformation can be calculated as

$$u_{ep.el} = \frac{R}{k} \quad (2.34)$$

and the plastic reductions will then be according to Figure 2.21.

$$\Delta u_{pl} = \frac{u_{ep.el}}{2} \quad (2.35)$$

This will give the plastic deformation

$$u_{ep.pl} = u_{pl} - \Delta u_{pl} \quad (2.36)$$

2.4.6 Equation of motion

Study Figure 2.22a, the rigid mass m is attached to a spring with the internal force R and the force $F(t)$ and damping C acting on the system. If the system is vibrating with help of an external force the motion is referred to as forced vibration. Since an impulse load will hit the structure when it is exposed to explosions this will be the case in the beginning. But the impulse load has a short duration and the force is after only a short time equal to zero and the continued motion can then be described as a damped free vibration. The damping on the system will have a positive effect since it reduces the displacement for the system and hence, the work done by the system. Due to the short time duration, the effect of damping is, on the safe side, often neglected when considering explosions. The system will then only consist of a rigid mass attached to a spring with a force $F(t)$ acting on it, see Figure 2.22b. In this master thesis the focus will lie on the time when the impulse load is acting and shortly after so whenever the equation of motion is mentioned it is this undamped forced vibration system, shown in Figure 2.22b, that is considered. It should be kept in mind, though, that when the load duration is short and when the impulse load has expired, the force $F(t)$ will be equal to zero and the system will act as an undamped free vibration system.

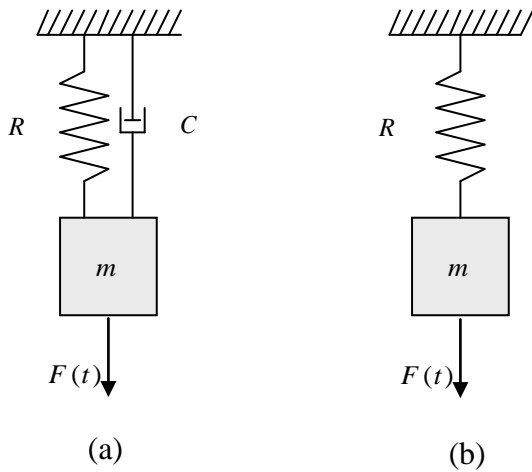


Figure 2.22 Mechanical forced vibration system a) damped b) undamped.

The impulse load will result in a deformation u for the mass as shown in Figure 2.23a. The body will then start to oscillate around its equilibrium point. Since the system is undamped the same deformation will occur in the opposite direction and in the same direction again for infinity or until the oscillation is interrupted. This means that the same work will be done in both directions and also that the gravitation must be neglected since it will accelerate in one direction and retard in the other direction. By isolating the rigid body m the Figure 2.23b can be established. For the body to be in equilibrium the sum of all forces must equal zero. With this condition the equation of motion for an undamped forced vibration can be stated as

$$m\ddot{u} + R = F(t) \quad (2.37)$$

Combining equation (2.37) with (2.2) a linear elastic equation of motion can be expressed as

$$m\ddot{u} + Ku = F(t) \quad (2.38)$$

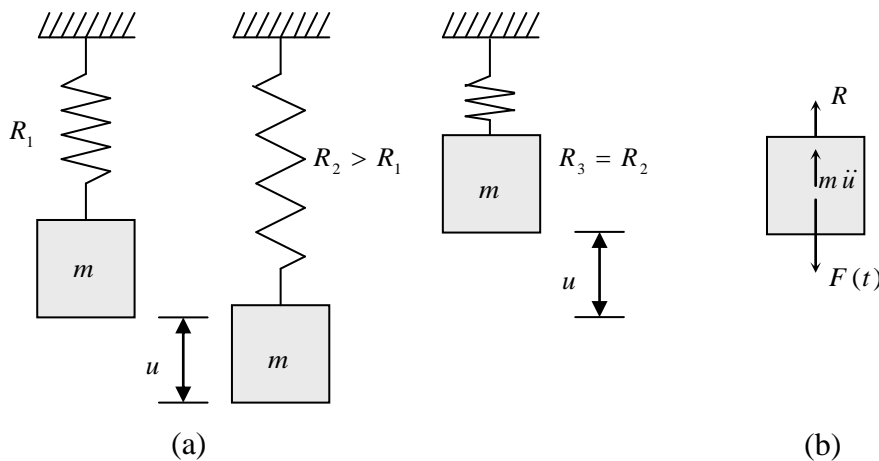


Figure 2.23 a) Rigid body undergoing undamped forced vibration b) forces acting on the rigid body.

2.5 Plate theory

2.5.1 Introduction

A plate is a flat body with a relatively thin thickness compared to its length and width. The bending properties of the plate depend strongly on its thickness compared to the size of the flat area. According to Timoshenko (1959) the plates are divided into three different sub categories: thin plates with small deformations, thin plates with large deformations and thick plates. The slabs studied in this master thesis will have a relatively small thickness compared to its other dimensions and the deformations will be relatively small. Therefore, the slab can be assumed to have the same behaviour as a thin plate with small deformations. In this chapter and further on, only theory of thin plates with small deformations will be presented. However, the structural behaviour of plates is rather complex and will in some extent be simplified.

2.5.2 Elastic behaviour

If the plate is studied from the side it will have the same deformation shape as a beam. By combining the two beams in different directions the final shape for the elastic plate is established. To easier be able to calculate the deformations it is assumed that the plate has a sinusoidal shape, Timoshenko (1959). The deformations along the plate can then be expressed as

$$u(x, y) = \sin(\pi x / w) \cdot \sin(\pi y / l) \cdot u_{\max} \quad (2.39)$$

where w is the width, x is the width coordinate, l is the length, y is the length coordinate and u_{\max} is the maximum deformation, i.e. the deformation in the middle of the plate, see Figure 2.24.

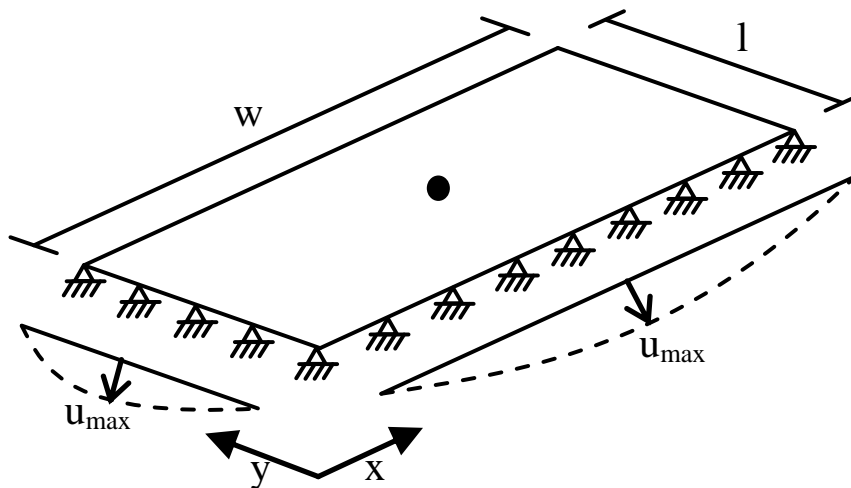


Figure 2.24 Elastic deformation for a plate.

The maximum deformation for a simply supported plate with uniformly distributed load is, according to Timoshenko (1959), equal to

$$u_{\max} = \frac{16q}{\pi^6 D} \sum_{m=1}^{\infty} \sum_{n=1}^{\infty} \frac{(-1)^{\frac{m+n}{2}-1}}{mn \left(\frac{m^2}{w^2} + \frac{n^2}{l^2} \right)^2} \quad (2.40)$$

where q is a uniformly distributed load, m and n are an odd series as $m=1,3,5\dots$ $n=1,3,5\dots$ and D is the flexural rigidity of a plate defined as

$$D = \frac{EI}{1-\nu^2} \quad (2.41)$$

where ν is the Poisson's ratio and I is the moment of inertia per meter .

2.5.3 Plastic behaviour

2.5.3.1 Method

The plastic behaviour of the plate is here described according to the yield line method in Hultin (1983). This method is a so called upper bound approach, meaning that it's an upper limit for the capacity of the plate and hence, an upper limit for the deformations.

2.5.3.2 Yield line figure

The plastic behaviour will start when the yield limit is reached for the most stressed fiber in the plate and a hinge is formed. For a rectangular plate with uniformly distributed load this will happen in the middle. The hinge will then spread along a yield line and eventually branch off to the corners. When the hinge lines reaches the corners a mechanism is formed and the full capacity of the plate is reached, see Figure 2.25.

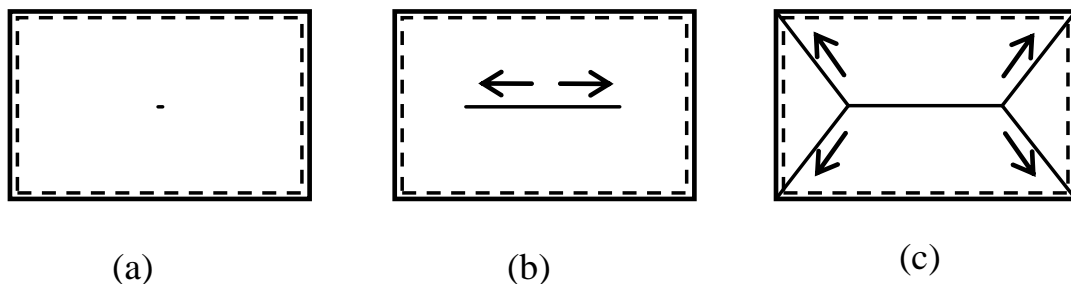


Figure 2.25 a) A hinge is formed in the middle b) The hinge is spreading along the yield line c) The yield line branches off to the corners and a mechanism is formed.

The assumed yield line figure must be kinematic possible, meaning that the different plate portions divided by the yield lines must fit together when the plate deflects. This criterion is fulfilled as long as the yield line between two slab portions or the yield lines extension passes through the intersection of the rotation axes for the two slab parts. The principle is illustrated for Figure 2.25c. The yield line in the corner between

slab portions 1 and 2 will pass through the intersections of the rotation axes A-A and B-B, see Figure 2.26a. The same can be said for all yield lines in the corners. However, the yield line in the middle is an exception. Since it is parallel to its rotation axes, A-A and D-D, either the rotation axes or the yield line will intersect. One way to bypass this is by extending the axes and line to eternity. This will create an optical illusion that the axes and line will intersect, see Figure 2.26b.

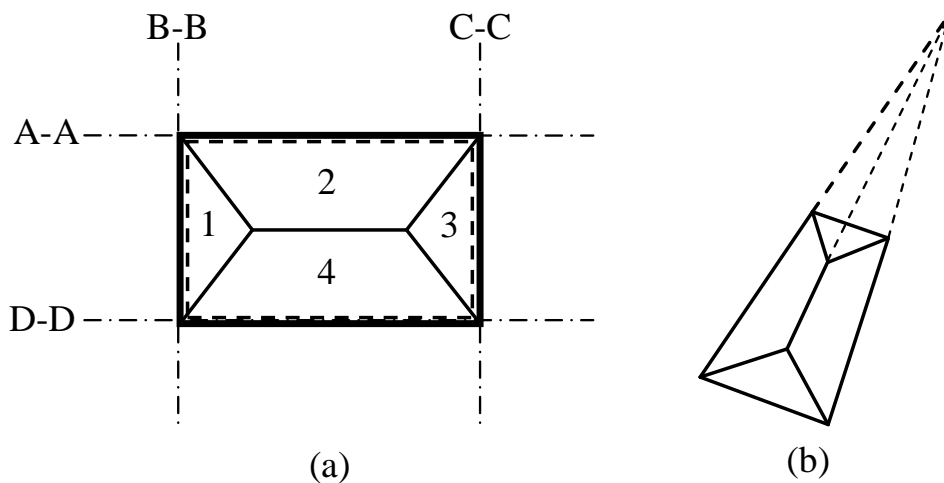


Figure 2.26 Criterion for the yield line method (a) The corner yield lines passes through the intersection of the affected rotation axes (b) By letting the axes and line extend to eternity an optical illusion will arise that the axes intersect the line.

A phenomenon that can arise in the plate corners is the so called corner demerging. What happens then is that the corners of the plate rises above their support, resulting in a split of the corner yield line into two lines, see Figure 2.27. However, according to Hultin (1983) this phenomenon has a very small impact on four sided plates with uniformly distributed loads and is therefore here neglected.

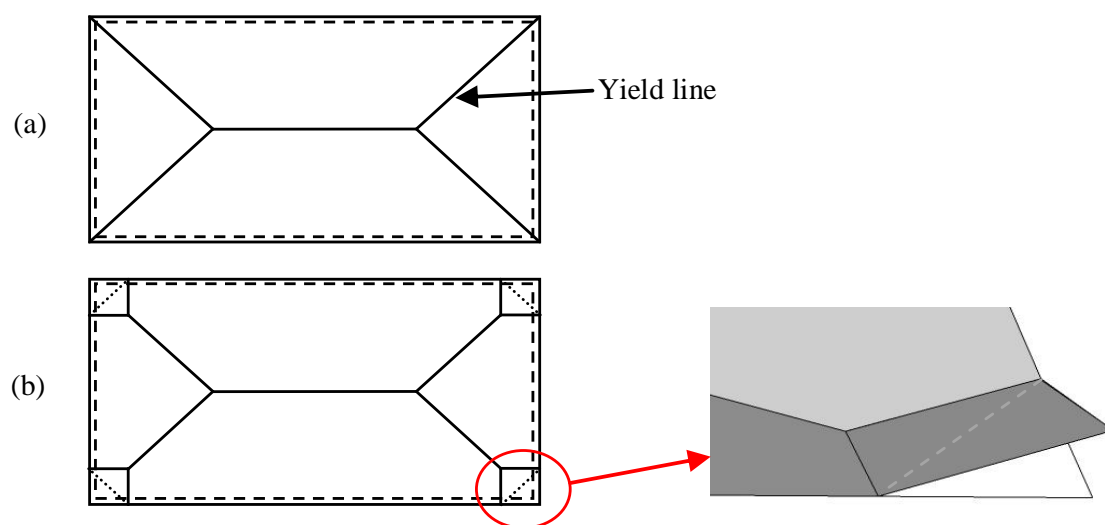


Figure 2.27 (a) Yield line figure according to yield line theory (b) yield line figure with corner demerging.

2.5.3.3 Maximum load capacity

When a yield line figure has been established the maximum capacity for the plate can be calculated with either equilibrium equations or with the virtual work principle.

The internal virtual work for the slab is

$$W_i = \sum M_i l_i \theta_i \quad (2.42)$$

where M_i is the moment, l_i the length of the affected yield line and θ_i is the angel between the undeformed and deformed shape, see Figure 2.28. Since the deformations are small the angel can be calculated to

$$\theta_1 = \frac{\delta}{x} \quad (2.43)$$

$$\theta_2 = \frac{\delta}{y} \quad (2.44)$$

where δ is the deformation for the plate.

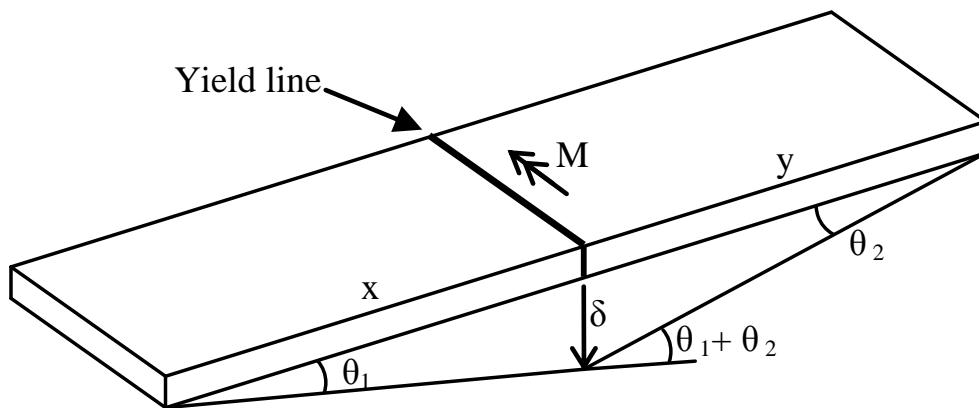


Figure 2.28 Yield line figure for a simply supported one-way plate.

The external virtual work done by the load is

$$W_e = \sum q_i A_i \delta_{TP,i} \quad (2.45)$$

where $\delta_{TP,i}$ is the deformation in the centre of gravity for each part.

By setting the internal work equal to the external work ($W_i = W_e$) the maximum uniformly distributed load on the plate can be calculated to

$$q = \frac{\sum m_i l_i \theta_i}{\sum A_i \delta_{TP,i}} \quad (2.46)$$

2.6 SDOF system

When considering a beam or a slab it can be of interest to reduce the entire structure to a single degree of freedom system (SDOF), i.e. describing the behaviour of a system in one point. This will simplify the structure and make it easier to calculate its response. In Figure 2.29 an illustration of the transformation concept for both a beam and a slab is presented.

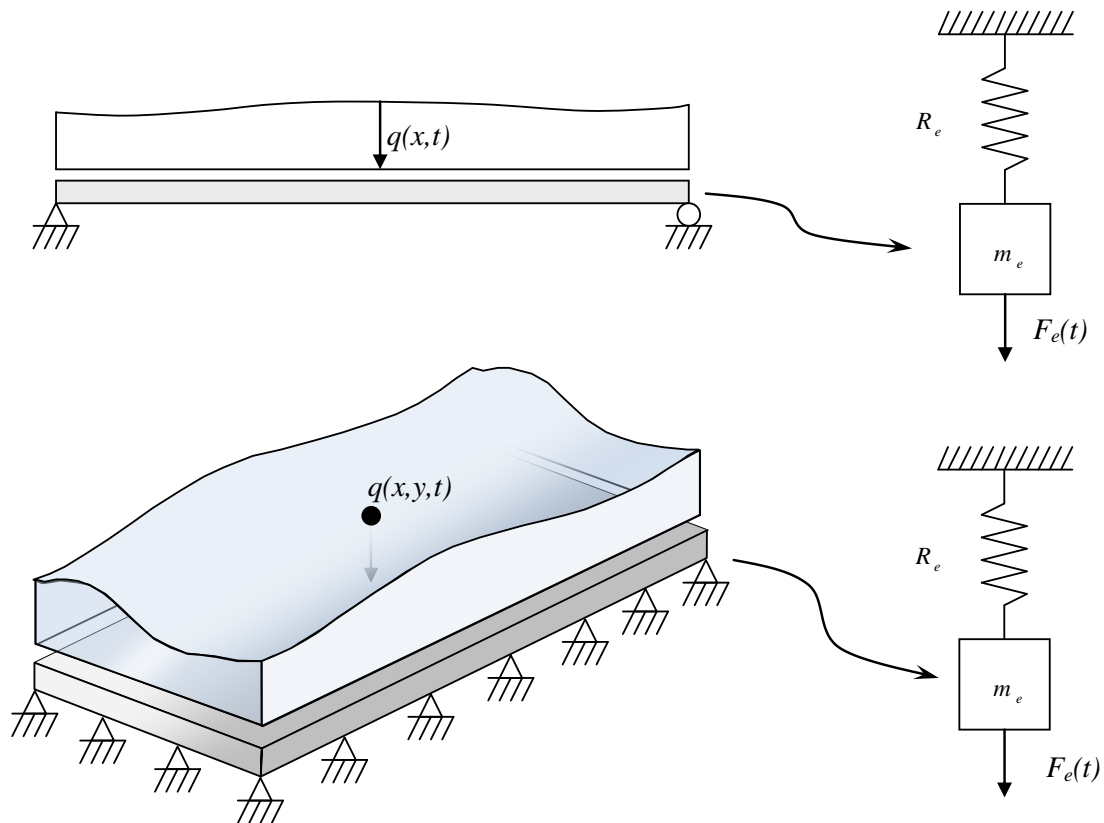


Figure 2.29 Concept of transforming a beam and a slab to a SDOF system.

The SDOF-system has one dimension and is therefore prevented from movements in other undescribed directions. For a multi degree of freedom system (MDOF), as the beam and slab, there are three-dimensions resulting in 3 directions where the body is able to move.

It is possible to reduce a MDOF-system to a SDOF-system which describes the response of the structure in one point called the system point, see Figure 2.30. It is also possible to choose position of the system point anywhere, but it is often of interest to place this point where maximum deformation occurs.

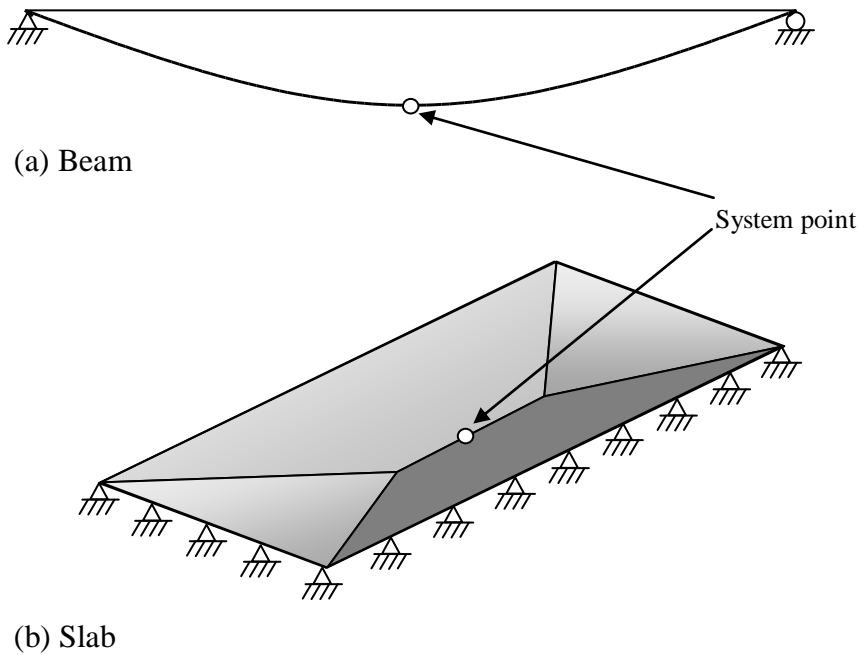


Figure 2.30 System point in the middle of (a) a simply supported beam (b) a simply supported slab.

In order to reduce the beam or the slab to a SDOF-system a deflection shape of the structure has to be assumed. Here, the assumed deflection shape for linear elastic case is chosen from elementary cases as the first eigen mode and for the plastic case a mechanism form is used for the deflection shape, see Figure 2.31.

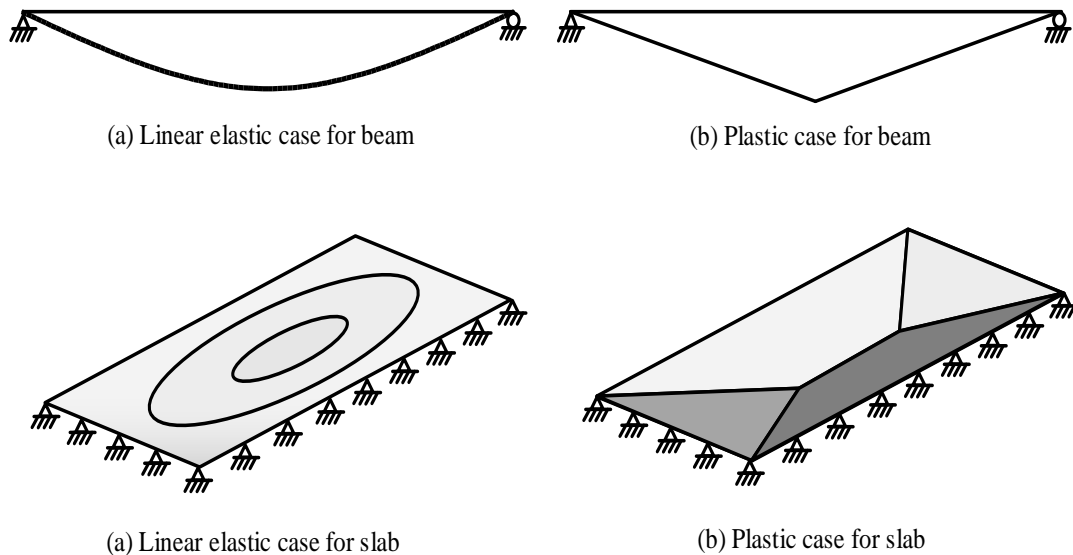


Figure 2.31 Assumed mode shapes for elastic and plastic material.

Now when the deformation shapes are established the equation of motion can be calculated as

$$m\ddot{u} + R = F(t) \quad (2.47)$$

where m is the total mass for the untransformed body, \ddot{u} is the acceleration, R is the internal force and $F(t)$ is the external force acting on the untransformed body. The untransformed MDOF body has a different physical behaviour than a SDOF-system which is assumed to have a rigid body. To solve this problem so called transformation factors are added to each quantity so the equivalent quantities in the SDOF-system equal the quantities in the untransformed body. The definition of the transformation factors for each quantity is

$$\kappa_m = \frac{m_e}{m} \quad (2.48)$$

$$\kappa_K = \frac{R_e}{R} \quad (2.49)$$

$$\kappa_F = \frac{F_e(t)}{F(t)} \quad (2.50)$$

where the index e is for the equivalent body (SDOF) and without an index is for the untransformed body. Inserting equations (2.48) to (2.50) into (2.47) the equation of motion for a transformed body, i.e. a SDOF-system as the beam or slab, can be written as

$$\kappa_m m \ddot{u} + \kappa_K R = \kappa_F F(t) \quad (2.51)$$

By dividing all terms with κ_F the equation can be rewritten as

$$\frac{\kappa_m}{\kappa_F} m \ddot{u} + \frac{\kappa_K}{\kappa_F} R = F(t) \quad (2.52)$$

According to Biggs (1964) the relation between κ_K and κ_F is

$$\kappa_K = \kappa_F \quad (2.53)$$

and together with a new transformation factor defined as

$$\kappa_{mF} = \frac{\kappa_m}{\kappa_F} \quad (2.54)$$

the equation of motion can finally be expressed as

$$\kappa_{mF} m \ddot{u} + R = F(t) \quad (2.55)$$

3 Beams

3.1 Introduction

A beam can be seen as a one way slab, i.e. a slab with supports and reinforcement in one direction. Therefore, as an introduction to slabs, beams and their behaviour under impulse load is briefly studied. From previous master thesis by Nyström (2006) simplified models and FE-analysis to describe the response of the beam have been established and a short summary is presented in this chapter. Special attention is given to the plastic and elastoplastic cases, which has given a large divergence between the FE-analyses, equation of motion and hand calculations for the previous master thesis Ek and Mattsson (2010).

3.2 Response of beams subjected to impulse load

The response of a beam subjected to a uniformly distributed impulse load is illustrated in Figure 3.1. The impulse load has a triangular shape as shown in Figure 2.4b. Figure 3.1a shows the response when the impulse load is zero and the beam is unloaded. Figure 3.1b shows the response of the beam subjected to the impulse load when the load has reached its peak and the beam has just started to deform. It may be noted here that the maximum deformation is not in the centre. This is because the wave velocity is about 3500 m/s in longitudinal direction for concrete and the middle of the beam is not yet aware of the existence of any supports. One way to describe this phenomenon is to look at it as transport of information. When the impulse hit the beam, information of the load will spread through the beam with the velocity of 3500 m/s. The information will travel through the beam and when reaching the two supports it will turn back with this information to the rest of the beam again, see Figure 3.2.

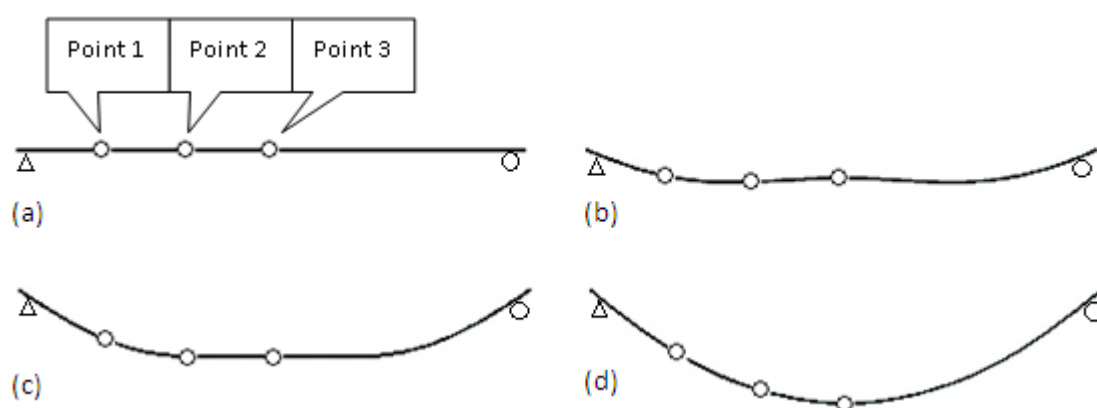


Figure 3.1 Response of beam at different time.

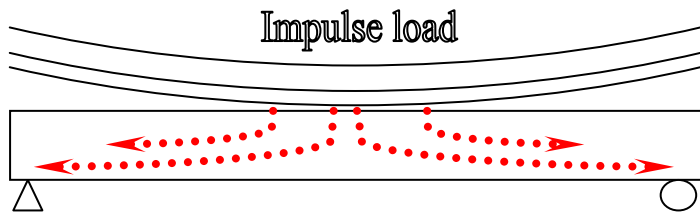


Figure 3.2 Transportation of load through a beam.

This means that if the beam is 2.7 m long and the impulse is a characteristic impulse with an infinite small duration, see Figure 2.18, it will take about 0.39 ms $((2.7/2)/3500)$ for the supports to be aware of the entire load. After this the information will spread through the beam again making it deform accordingly to the boundary condition between the beam and the support. So, in Figure 3.1c the information has gone further through the beam but the information about the full load has still not reached the middle of the beam. Finally, in the last picture, the entire impulse has reached the middle of the beam resulting in the maximum deformation which has the same appearance as a statically loaded beam. This happens after 0.78 ms when the information has travelled another 1.35 m $(2.7/2)$. It can further be pointed out here that the maximum deformation happens after the impulse has ended.

The deformation in different points along the beam can be seen in Figure 3.3 where point 1 - 3 are located as shown in Figure 3.1. Figure 3.3 is illustrative in order to get a better understanding on how the impulse loaded beam behaves. It is a clear difference in behaviour from a statically loaded beam to an impulse loaded beam. The deformation for each point is similar to each other in the initial part, see Figure 3.4, of the impulse and will then increase almost sinusoidal.

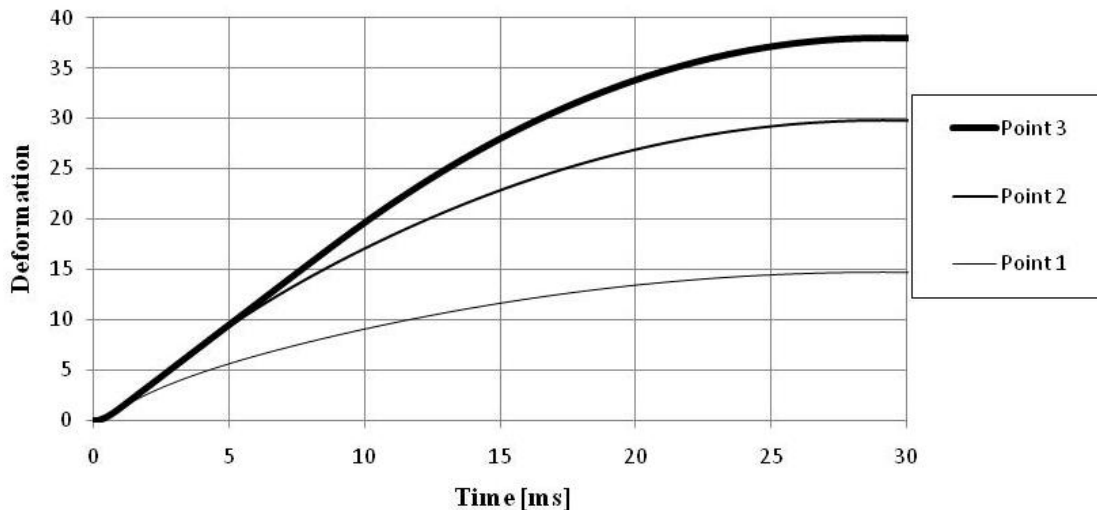


Figure 3.3 Deformation in different points along the impulse loaded beam.

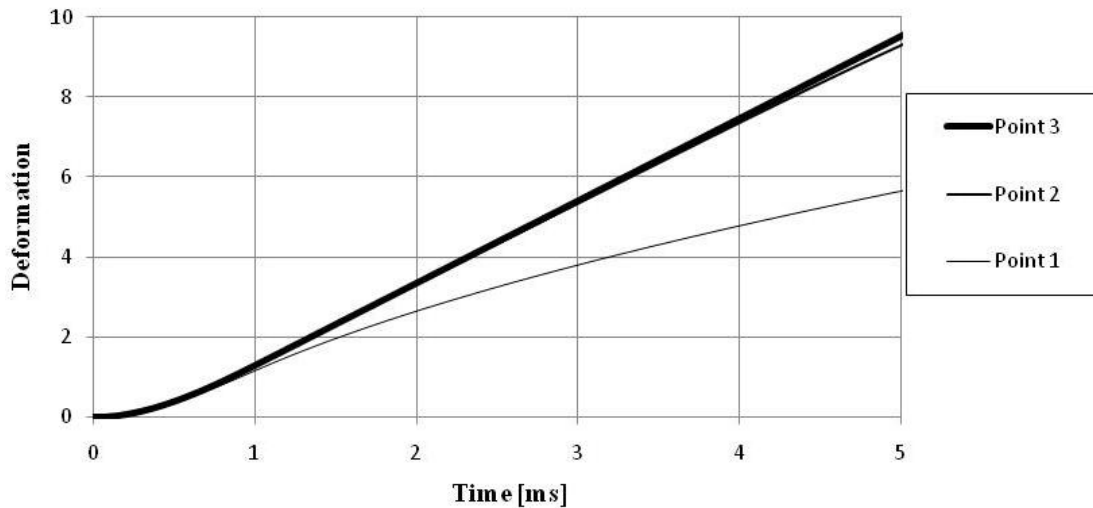


Figure 3.4 Deformation in different points along the beam in an early stage.

This is however not the case for a statically loaded beam. When applying a load gradually and slowly, i.e. statically, the deformation can often be simplified with the form of a half sinus wave from the beginning and until the full load is applied. However, for the static loaded beam the curvatures in Figure 3.3 will never coincide with each other, as for the impulse loaded beam. The difference is clearly shown in Figure 3.5.

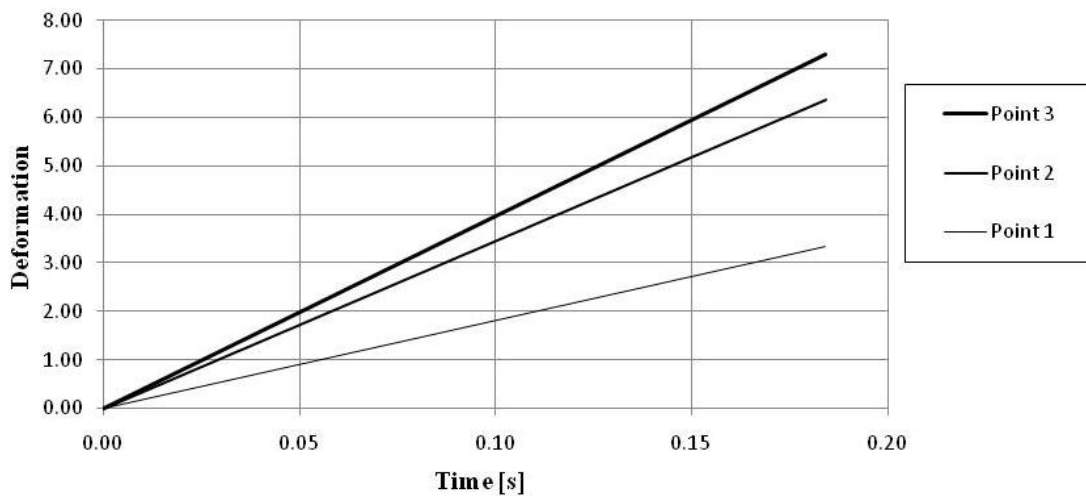


Figure 3.5 Deformation in different points along the static loaded beam.

As mentioned in Section 2.4.6 a dynamic load will make the mass, here the beam, oscillate around its equilibrium point. If no damping is assumed the deformation of the beam will be the same in both vertical directions. Consequently, when designing a beam subjected to a dynamic load, in contrast to static case, the dynamic case need to be designed for maximum displacement in both vertical directions.

In an early stage there is a significant deformation near the supports compared to the deformation in the mid section of the structure, see Figure 3.6. These deformations will give rise to large shear stresses which results in a large risk of cracking. However, although this problem requires more investigation it is outside the limits of this master thesis and will therefore not be further investigated.

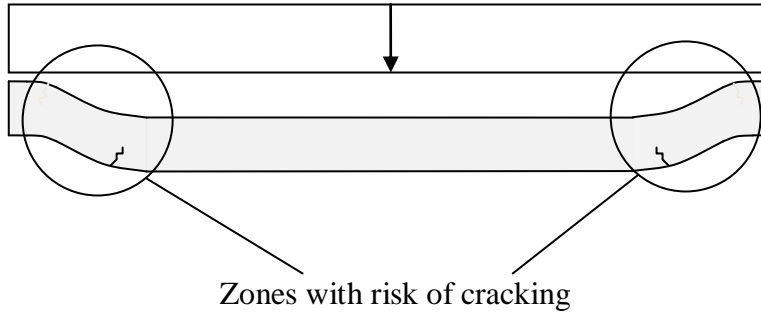


Figure 3.6 Zone where there is a high risk of cracking in the early stage. From Nyström (2006).

3.3 Equation of motion

3.3.1 Introduction

As mentioned in Section 2.4 it is the energy that can be absorbed by the structure that is of main interest. This can be calculated by studying a point on the beam where the maximum deformations occur, i.e. in the middle of the beam. Henceforth this point, denoted the system point, can be used to transform the beam to an undamped SDOF-system. According to Section 2.6 the equation of motion is

$$\kappa_{mF} m \ddot{u} + R = F(t) \quad (3.1)$$

where m , R and $F(t)$ are properties of the untransformed beam and κ_{mF} is the transformation factor that is based on a division between the transformation factors κ_m and κ_F as

$$\kappa_{mF} = \frac{\kappa_m}{\kappa_F} \quad (3.2)$$

3.3.2 Transformation factor for the mass κ_m

The transformation factor for the mass is derived based on the requirement that the kinetic energy for the untransformed beam is the same as the kinetic energy for the point in the SDOF-system. The kinetic energy for an untransformed beam and SDOF-system can then be expressed as

$$E_k^{beam} = \int_{x=0}^{x=l} \frac{m'(x) \cdot v(x)^2}{2} dx \quad (3.3)$$

$$E_k^{SDOF} = \frac{m_e v_s^2}{2} \quad (3.4)$$

Where $m'(x)$ is the mass per unit length, v_s is the velocity in the system point and m_e is the equivalent mass.

The velocity in both cases can be written as

$$v(x) = \frac{du(x)}{dt} \quad (3.5)$$

$$v_s = \frac{du_s}{dt} \quad (3.6)$$

Combining equations (3.3) to (3.6) with the requirement of equal kinetic energy for both systems results in the equation

$$m_e u_s^2 = \int_{x=0}^{x=l} m'(x) \cdot u(x)^2 dx \quad (3.7)$$

Thus, the equivalent mass m_e can be expressed as

$$m_e = \kappa_m m \quad (3.8)$$

and together with equation (3.7) and (3.8) the general equation for the mass transformation factor can be stated as

$$\kappa_m = \frac{\int_{x=0}^{x=l} m'(x) \cdot u(x)^2 dx}{m u_s^2} \quad (3.9)$$

When considering a case when the mass along the beam is constant the equation (3.9) can be rewritten with

$$m = m' l \quad (3.10)$$

to be

$$\kappa_m = \frac{1}{l} \frac{\int_{x=0}^{x=l} u(x)^2 dx}{u_s^2} \quad (3.11)$$

3.3.3 Transformation factor for the load κ_F

The same principle is used for the load as for the mass but here, the untransformed beam shall absorb the same amount of external work as the SDOF-system. The external work done by a static external load for an untransformed beam and a SDOF-system is

$$W_e^{beam} = \int_{x=0}^{x=l} q(x) \cdot u(x) dx \quad (3.12)$$

$$W_e^{beam} = F_e u_s \quad (3.13)$$

As defined in Section 2.6 the equivalent load for the SDOF-system is

$$F_e = \kappa_F F \quad (3.14)$$

By using equations (3.12) to (3.14) and the requirement of equal external work for both systems the expression for the transformation factor can be written as

$$\kappa_F = \frac{\int_{x=0}^{x=l} q(x) \cdot u(x) dx}{F u_s} \quad (3.15)$$

When considering a case where the load along the beam is constant the equation (3.15) can be rewritten together with

$$F = \int_{x=0}^{x=l} q(x) dx = ql \quad (3.16)$$

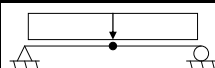
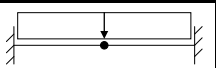
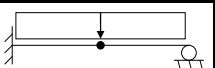
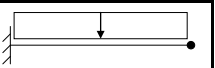
to be

$$\kappa_F = \frac{1}{l} \frac{\int_{x=0}^{x=l} u(x) dx}{u_s} \quad (3.17)$$

3.3.4 Examples of tabulated transformation factors

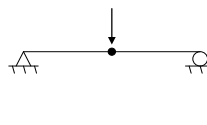
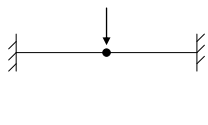
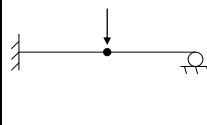

The transformation factors for beams are not derived in this master thesis since the emphasis of this project is to study the plate. Instead, examples of tabulated transformation factors collected from Johansson and Laine (2009) are presented in Table 3.1 and Table 3.2.

Table 3.1 Tabulated transformation factors for distributed load. From Johansson and Laine (2009).

	Uniformly distributed load			
				
	Deformation curve elastic case			
κ_m	0.504	0.406	0.483	0.257
κ_F	0.640	0.533	0.600	0.400
κ_{mF}	0.787	0.762	0.805	0.642
	Deformation curve plastic case			

κ_m	0.333	0.333	0.333	0.333
κ_F	0.500	0.500	0.500	0.500
κ_{mF}	0.667	0.667	0.667	0.667

Table 3.2 Tabulated transformation factors for point load. From Johansson and Laine (2009).

	Point load			
				
	Deformation curve elastic case			
κ_m	0.486	0.371	0.445	0.236
κ_F	1.000	1.000	1.000	1.000
κ_{mF}	0.486	0.371	0.446	0.236
	Deformation curve plastic case			
κ_m	0.333	0.333	0.333	0.333
κ_F	1.000	1.000	1.000	1.000
κ_{mF}	0.333	0.333	0.333	0.333

3.3.5 Solving the equation of motion

The equation of motion can be solved analytically. However, this may be a very time consuming solution depending on what case is studied. Another way to solve it is by using numerical solution methods. Such methods are approximate but will, correctly handled, give a result close to the analytical methods. In this master thesis the “central difference method” is used together with the software Matlab. This method is an explicit method, meaning that the new calculated value is based on the previous time step value. The algorithm for this method is adopted from Johansson and Laine (2009) and is presented in APPENDIX A.

3.4 Hand calculation

As in the equation of motion model the hand calculations can be based on the SDOF-system and the information of energy balance. It is important to know that the hand calculation model is only to be used in the preliminary design to get a rough estimation of the response for the structural element. Even though simple, it may still be very useful in order to get an estimate of the final response of the structure.

The capacity of the beam is decided by how much the beam can deform before it collapses. From Section 2.4.5 the deformations can be calculated as

$$u_{el} = \frac{I_c}{\sqrt{km_e}} = \frac{I_c}{\sqrt{k\kappa_{mF} m}} \quad (3.18)$$

for an elastic material,

$$u_{pl} = \frac{I_c^2}{2m_e R_m} = \frac{I_c^2}{2\kappa_{mF} m R_m} \quad (3.19)$$

for a plastic material, and

$$u_{ep} = u_{ep.el} + u_{ep.pl} \quad (3.20)$$

for an elastoplastic material where

$$u_{ep.el} = \frac{R}{k} \quad (3.21)$$

and

$$u_{ep.pl} = u_{pl} - \frac{u_{ep.el}}{2} \quad (3.22)$$

3.5 FE-analysis

3.5.1 Restrictions

The finite element (FE) analysis is carried out in the software ADINA. 2-D beam elements will be used in order to simplify the analysis. The reinforcement and concrete is modelled as an equivalent material. Because of this, some special cautions have been made. The following Sections describe the modifications made in order to model the reinforced concrete.

3.5.2 Cracked elasticity modulus

In the uncracked state the reinforcement have almost no effect at all and the beam can be modelled as a solid concrete beam. However, when the beam is in the cracked state the reinforcement have a large impact and need to be considered. To capture the stiffness for the cracked reinforced concrete a new Young's modulus has been calculated as

$$E_{II} = \frac{I_{II}}{I_I} E_I \quad (3.23)$$

where E_I , I_I and E_{II} , I_{II} is the Young's modulus and moment of inertia for uncracked and cracked state, respectively. Note here that this is only done in order to capture the stiffness of the equivalent material and that Young's modulus in reality is constant.

3.5.3 Choice of material responses in different sections

The only difference between the plastic and elastoplastic case is the choice of Young's modulus. The ideal plastic material shown in Figure 2.9 cannot be modelled in ADINA. Instead, the Young's modulus has been multiplied with 100 times the uncracked stiffness which will result in a response that is close enough to the ideal plastic case. For the elastoplastic case the stiffness is chosen to be the same as in the cracked state and can be calculated according to (3.23). This assumption will result in a larger deformation than if the bilinear model of both uncracked and cracked modulus would have been used.

The earlier Master theses, Nyström (2006) and Ek and Mattsson (2010), have modelled the beam with a plastic or elastoplastic element in the middle and elastic elements in the rest of the beam. The problem with such modelling is that when the middle element plasticises the elastic elements will start to oscillate on each side of the plasticised element as shown in Figure 3.7. This is believed to be one of the reasons why the earlier Master theses, Nyström (2006) and Ek and Mattsson (2010), have found a divergence between FE-analysis and the calculations based on the equation of motion. To avoid this problem here, all the elements will be modelled as plastic or elastoplastic depending on which case is of interested.

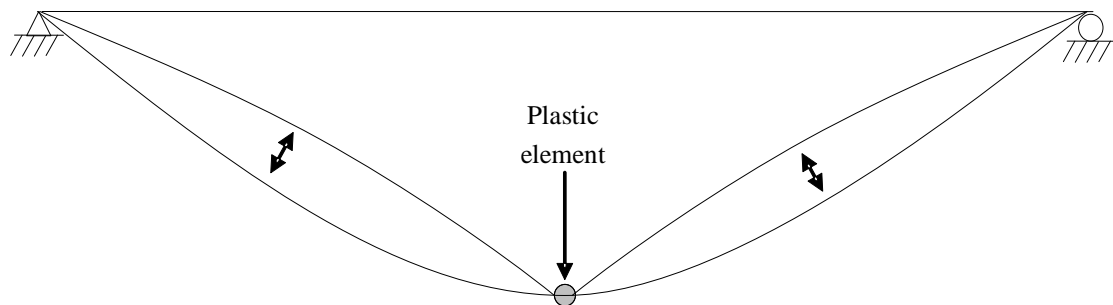


Figure 3.7 The elastic element oscillates on each side of the plastic element.

3.5.4 Element integration points

In this master thesis, compared to previous master thesis, there has been an interest of changing the ultimate moment capacity from a shape of nearly ideal plastic to a shape where yielding in the outer fibers is the limit, see Figure 3.8. Previous studies by Ek and Mattsson (2010) with 7 integration points over the height showed that the output moment capacity was not equal to the expected moment capacity. The change of the shape of ultimate moment capacity to 3 integration points is done in order to get the expected moment capacity.

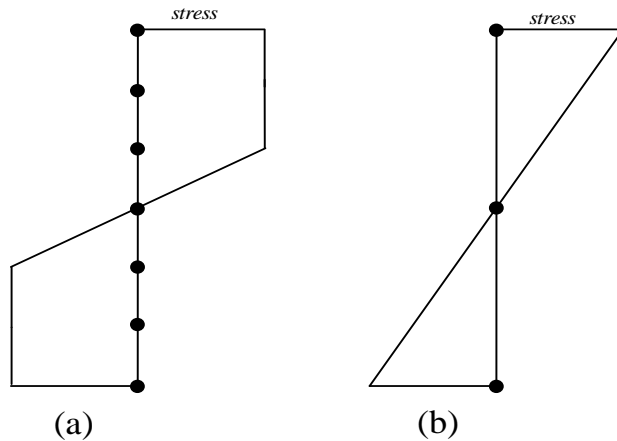


Figure 3.8 The Stress distribution over the height of the beam for (a) 7 integration points (b) 3 integration points.

Since the FE-model is simplified to a homogenous and isotropic material there is a need to calculate a so called fictitious yield stress. This fictitious yield stress will be inserted in ADINA to get the same material response as the reinforced concrete beam. From basic equations a required moment capacity, M_{rd} , can be calculated and with this information the fictitious yield stress f'_y can be expressed as

$$f'_y = \frac{W_{el}}{M_{rd}} \quad (3.24)$$

where W_{el} is the elastic bending resistance, for a stress distribution shown in Figure 3.8b, may be expressed as

$$W_{el} = \frac{wh^2}{6} \quad (3.25)$$

The integration method, Newton-Cotes, is here chosen for the stiffness matrix in the FE equations. This choice is done because the positions of the outer integration points are located in the edge fibers in the height direction of the element, and the limit for the yield stress is located at the outmost fibers. The positions of the integration points in Newton-Cotes can be seen in Figure 3.9. This method is default in ADINA when using beam elements.

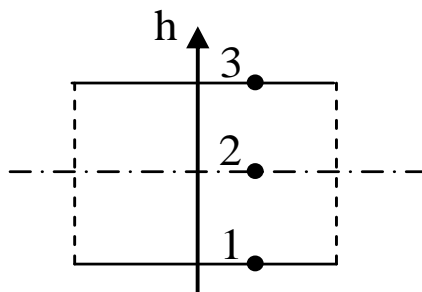


Figure 3.9 The position of the integration point in height direction for the Newton-Cotes method.

It is of importance to choose 2D-beam elements when using 3 integration points due to limitations in the software program ADINA. Otherwise, when choosing 3D-beam elements, ADINA automatically sets to 7 integration points.

3.6 Example

3.6.1 Scenario

A charge of 125 kg TNT detonates on a distance of 5 m from a building resulting in an impulse load of 2800 Ns/m^2 , with a maximum peak pressure of 5000 kPa, hitting one of the building sides. The building is a multi-story building with a height of 2.7 m for each floor. The wall facing the explosion is a reinforced concrete wall with a cross-section as shown in Figure 3.10. The concrete is of quality C20/25 and the reinforcement is in class B500. Will the wall be able to resist the explosion?

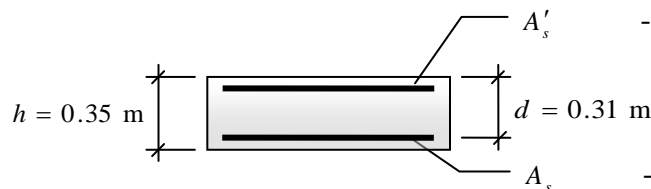


Figure 3.10 Cross-Section of the studied wall.

The control will be made for four cases – uncracked (state I), cracked (state II), ideal plastic (state III) and the elastoplastic case which is the case most accurate to reality.

3.6.2 Assumptions and simplifications

- The load is assumed to be triangular and uniformly distributed over the entire wall.
- There are no windows or other irregularities in the wall.
- The connection wall to slab is free to rotate and the wall is not continuous over the floor slabs.
- The supports are rigid.
- The wall is simplified to a beam with only supported at two opposite sides.

With these assumptions the wall can be simplified to a 2.7 m long simply supported beam with a wide per unit length, i.e. a width of 1 m, see Figure 3.11.

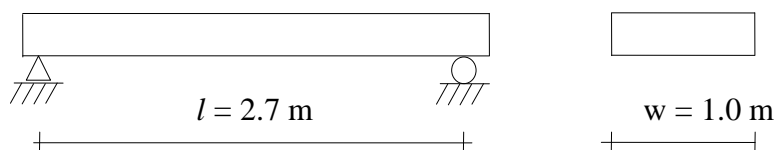


Figure 3.11 Dimensions of the wall.

This system can then be simplified further to the SDOF-system described in Section 2.6. Note here that the equation of motion for the SDOF-system is

$$\kappa_{mF} m \ddot{u} + R = F(t) \quad (3.26)$$

which means that only the mass needs to be transformed to an equivalent quantity while the stiffness and load will remain the same.

3.6.3 Transformed mass

The total mass of the beam is

$$m = \rho \cdot w \cdot h \cdot l = 2400 \cdot 1.0 \cdot 0.35 \cdot 2.7 = 2268 \text{ kg} \quad (3.27)$$

This will then be modified with the factor κ_{mF} , which depends on the boundary conditions, type of load and if the beam has an elastic or plastic response. According to Table 3.1 κ_{mF} is

$$\kappa_{mF, I} = \kappa_{mF, II} = 0.788 \quad (3.28)$$

for the elastic cases and

$$\kappa_{mF, III} = 0.667 \quad (3.29)$$

for the plastic and elastoplastic cases, and the equivalent mass will finally be

$$m_I = m_{II} = \kappa_{mF, I} \cdot m = 0.788 \cdot 2268 = 1787 \text{ kg} \quad (3.30)$$

$$m_{III} = \kappa_{mF, III} \cdot m = 0.667 \cdot 2268 = 1512 \text{ kg} \quad (3.31)$$

3.6.4 Stiffness and internal resistance

The deformation of a simply supported beam subjected to a uniformly distributed load is according to Johannesson and Vretblad (2005) equal to

$$u = \frac{5}{384} \cdot \frac{ql^4}{EI} \quad (3.32)$$

which will give the stiffness

$$k = \frac{Q}{u} = \frac{ql}{u} = \frac{384}{5} \cdot \frac{EI}{l^3} \quad (3.33)$$

The moment of inertia for the uncracked beam is approximately

$$I_I = \frac{wh^3}{12} = \frac{1000 \cdot 350^3}{12} = 3.57 \cdot 10^9 \text{ mm}^4 \quad (3.34)$$

where w and h is the width and height of the beam. The moment of inertia for the cracked beam is determined approximately, i.e. assuming pure bending and neglecting the effect of the top reinforcement. The equation is

$$I_{II} = \frac{wx^3}{3} + \alpha A_s (d - x)^2 \quad (3.35)$$

where x is the height of the compressed zone, α is the ratio between the Young's modulus for the reinforcement and concrete as

$$\alpha = \frac{E_s}{E_c} = \frac{200}{30} = 6.7 \quad (3.36)$$

A_s is the amount of reinforcement

$$A_s = \frac{A_{\phi 16}}{s} = \frac{201}{0.200} = 1005 \text{ mm}^2 \quad (3.37)$$

and d is the effective height

$$d = h - c = 350 - 40 = 310 \text{ mm} \quad (3.38)$$

The height of the compressed zone can now be expressed with help of equilibrium

$$x = \frac{wx \frac{x}{2} + \alpha A_s d}{wx + \alpha A_s} \quad (3.39)$$

and can be rearranged to

$$x^2 + \frac{2\alpha A_s}{w}(x - d) = 0 \quad (3.40)$$

The equation (3.40) is solved to

$$x = -\frac{\alpha A_s}{w} + \sqrt{\left(\frac{\alpha A_s}{w}\right)^2 + \frac{2\alpha A_s d}{w}} = -\frac{6.7 \cdot 1005}{1000} + \sqrt{\left(\frac{6.7 \cdot 1005}{1000}\right)^2 + \frac{2 \cdot 6.7 \cdot 1005 \cdot 310}{1000}} = 58 \text{ mm} \quad (3.41)$$

and inserting this in (3.35) gives

$$I_{II} = \frac{1000 \cdot 58^3}{3} + 6.7 \cdot 1005 \cdot (310 - 58)^2 = 4.8 \cdot 10^8 \text{ mm}^4 \quad (3.42)$$

The ratio between the uncracked respectively cracked moment of inertia is

$$\gamma = \frac{I_l}{I_{II}} = 7.438 \quad (3.43)$$

Finally, the stiffness for an uncracked and a cracked beam can be calculated as

$$k_l = \frac{384}{5} \cdot \frac{30 \cdot 10^3 \cdot 3.57 \cdot 10^9}{2700^3} = 4.2 \cdot 10^8 \text{ N/m} \quad (3.44)$$

$$k_{II} = \frac{384}{5} \cdot \frac{30 \cdot 10^3 \cdot 4.8 \cdot 10^8}{2700^3} = 5.6 \cdot 10^7 \text{ N/m} \quad (3.45)$$

When the plastic case is studied the deformation of the beam is no longer following the elastic deformation shape and the stiffness is of no importance. Instead, it is the internal resistance which is of importance and it can be calculated by setting the moment capacity equal to the maximum field moment. The moment capacity for a rectangular beam is

$$M_{rd} = f_y A_s (d - \beta x) \quad (3.46)$$

where f_y is the yield stress for the reinforcement and β is a stress block factor from Eurocode 2 CEN (2004). The height of the compressed zone x is calculated as

$$x = \frac{f_y A_s}{\alpha f_{cc} w} = \frac{500 \cdot 1005}{0.81 \cdot 20 \cdot 1000} = 31 \text{ mm} \quad (3.47)$$

where f_{cc} is the concrete compression strength and α is another stress block factor from Eurocode 2 CEN (2004). Equation (3.46) together with (3.47) gives the final moment capacity as

$$M_{rd} = 500 \cdot 1005 \cdot (310 - 0.416 \cdot 31) = 150 \text{ kNm} \quad (3.48)$$

The maximum field moment for a simply supported beam is

$$M_{fd} = \frac{ql^2}{8} \quad (3.49)$$

where q is a static load and together with equation (3.48) the internal resistance can be calculated to

$$R = ql = \frac{8M_{rd}}{l} = \frac{8 \cdot 150}{2.7} = 444 \text{ kN} \quad (3.50)$$

For the elastoplastic case the stiffness of the elastic part is approximated to correspond to that of the cracked state. This will give a larger deflection than in reality and is therefore on the safe side, see Figure 3.12. When the ultimate internal resistance R is reached the material will enter the plastic state and start to yield.

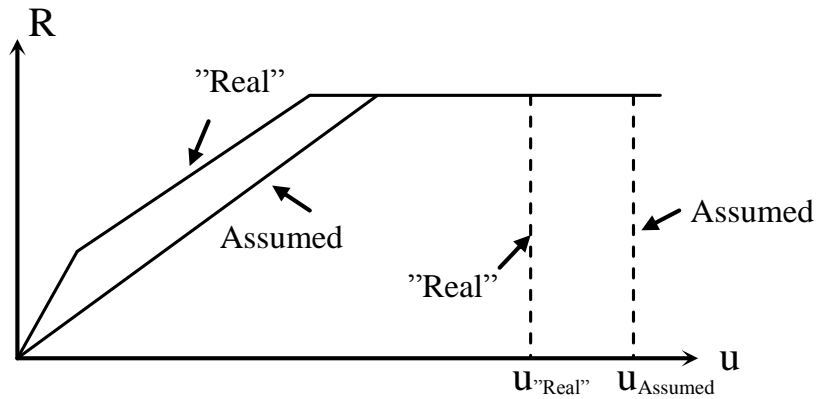


Figure 3.12 Assumed elastoplastic material response.

3.6.5 Required deformations

The total impulse load that acts on the beam is

$$I = w \cdot l \cdot i = 1.0 \cdot 2.7 \cdot 2800 = 7560 \text{ Ns} \quad (3.51)$$

The elastic deformation is then calculated as

$$u_{el} = \frac{I}{\sqrt{mk}} \quad (3.52)$$

which gives

for the uncracked state

$$u_I = \frac{7560}{\sqrt{1787 \cdot 4.2 \cdot 10^8}} = 8.7 \text{ mm} \quad (3.53)$$

and for the cracked state

$$u_{II} = \frac{7560}{\sqrt{1787 \cdot 5.6 \cdot 10^7}} = 23.9 \text{ mm} \quad (3.54)$$

The plastic deformation is given by

$$u_{pl} = \frac{I^2}{2Rm} \quad (3.55)$$

and with current indata

$$u_{III} = \frac{7560^2}{2 \cdot 444 \cdot 10^3 \cdot 1512} = 42.6 \text{ mm} \quad (3.56)$$

For the elastoplastic material the elastic part will add additional resistance and therefore less plastic deformation is needed. The maximum elastic deformation is calculated as

$$u_{ep,II} = \frac{R}{k} = \frac{444 \cdot 10^3}{5.6 \cdot 10^7} = 7.9 \text{ mm} \quad (3.57)$$

and the plastic reduction will therefore be

$$\Delta u_{III} = \frac{u_{ep,II}}{2} = 4.0 \text{ mm} \quad (3.58)$$

This will give the plastic deformation

$$u_{ep,III} = u_{III} - \Delta u_{III} = 42.6 - 4.0 = 38.6 \text{ mm} \quad (3.59)$$

and the total elastoplastic deformation can be calculated to

$$u_{ep} = u_{ep,II} + u_{ep,III} = 7.9 + 38.7 = 46.6 \text{ mm} \quad (3.60)$$

3.6.6 Equivalent static load

The equivalent static load is a static load that gives the same deformations as the impulse does. For structural engineers, it can be used to give a better understanding for the loads acting on the structure since they are more experienced with static loads and have developed a “feeling” for them.

The impulse is uniformly distributed so the equivalent static load will also be uniformly distributed. From equation (3.50) it can be calculated to

$$q_e = \frac{R}{l} \quad (3.61)$$

So for a beam with elastic response the equivalent static load is

$$q_{el} = \frac{R}{l} = \frac{ku_{el}}{l} \quad (3.62)$$

which for the uncracked state gives

$$q_{el} = \frac{4.2 \cdot 10^8 \cdot 8.7 \cdot 10^{-3}}{2.7} = 1353 \text{ kN/m} \quad (3.63)$$

and for the cracked state

$$q_{el} = \frac{5.6 \cdot 10^7 \cdot 23.9 \cdot 10^{-3}}{2.7} = 496 \text{ kN/m} \quad (3.64)$$

For a beam with a plastic response the equivalent static load can be calculated as

$$q_{pl} = \frac{R}{l} \quad (3.65)$$

and with current indata

$$q_{III} = \frac{444 \cdot 10^3}{2.7} = 164 \text{ kN/m} \quad (3.66)$$

With the equivalent static loads and equation (3.49) the maximum field moments can be calculated to

$$M_I = \frac{1353 \cdot 2.7^2}{8} = 1233 \text{ kNm} \quad (3.67)$$

$$M_{II} = \frac{496 \cdot 2.7^2}{8} = 452 \text{ kNm} \quad (3.68)$$

$$M_{III} = \frac{164 \cdot 2.7^2}{8} = 149 \text{ kNm} \quad (3.69)$$

It should be noticed that an assumed elastic response results in high demands on the moment capacity for the structure.

3.6.7 Maximum deformation capacity

For the elastic case there are no limits for the deformation capacity and therefore such a control is not necessary. Instead the maximum field moment, calculated from the equivalent load, is compared with the load capacity of the beam, i.e. the beam is controlled as a normal static case with the equivalent load as a uniformly distributed load. However, for the plastic case the rotation capacity will be the limiting factor for the beam and a deformation control according to Eurocode 2 CEN (2004) is therefore carried out.

According to Johansson and Laine (2009) the diagram in Eurocode 2 CEN (2004), see Figure 3.13, can be used for impulse loaded structures.

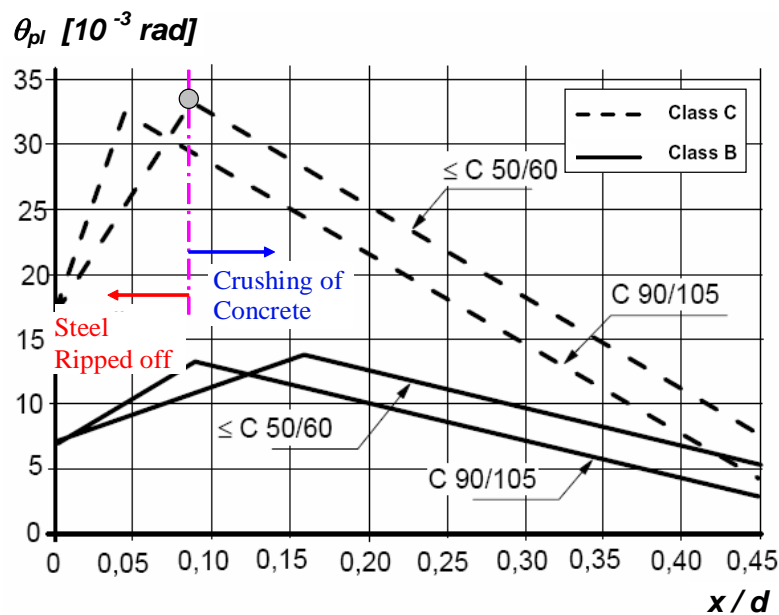


Figure 3.13 Diagram from Eurocode 2 CEN (2004) showing plastic rotation capacity. From Johansson and Laine (2009).

The diagram can only be used for concrete quality lower than C50/60 if

$$\frac{x}{d} \leq 0.45 \quad (3.70)$$

and with current indata

$$\frac{x}{d} = \frac{31}{310} = 0.1 \leq 0.45 \quad (3.71)$$

this is okay.

The diagram is only accurate if the shear slenderness $\lambda=3.0$, for other values the rotation capacity should be multiplied by a factor

$$k_\lambda = \sqrt{\frac{\lambda}{3}} \quad (3.72)$$

where λ is

$$\lambda = \frac{x_0}{d} \quad (3.73)$$

and x_0 is the distance between the maximum moment and the zero moment, see Figure 3.14.

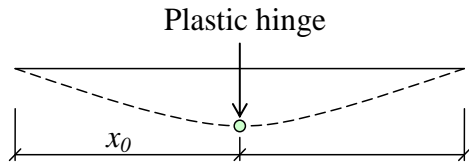


Figure 3.14 Simply supported beam showing distance x_0 .

For this example when the beam is simply supported the shear slenderness is

$$\lambda = \frac{x_0}{d} = \frac{l/2}{d} = \frac{2700/2}{310} = 4.35 \quad (3.74)$$

and the rotation capacity should be multiplied with a factor

$$k_\lambda = \sqrt{\frac{4.35}{3}} = 1.2 \quad (3.75)$$

So with a concrete quality of C20/25, the reinforcement in class B and the $x/d = 0.1$ the plastic rotation capacity is according to Figure 3.13

$$\theta = 11 \cdot 10^{-3} \text{ rad} \quad (3.76)$$

and with the k_λ factor the plastic rotation is

$$\theta_{pl} = \theta \cdot k_\lambda = 11 \cdot 10^{-3} \cdot 1.2 = 13.2 \cdot 10^{-3} \text{ rad} \quad (3.77)$$

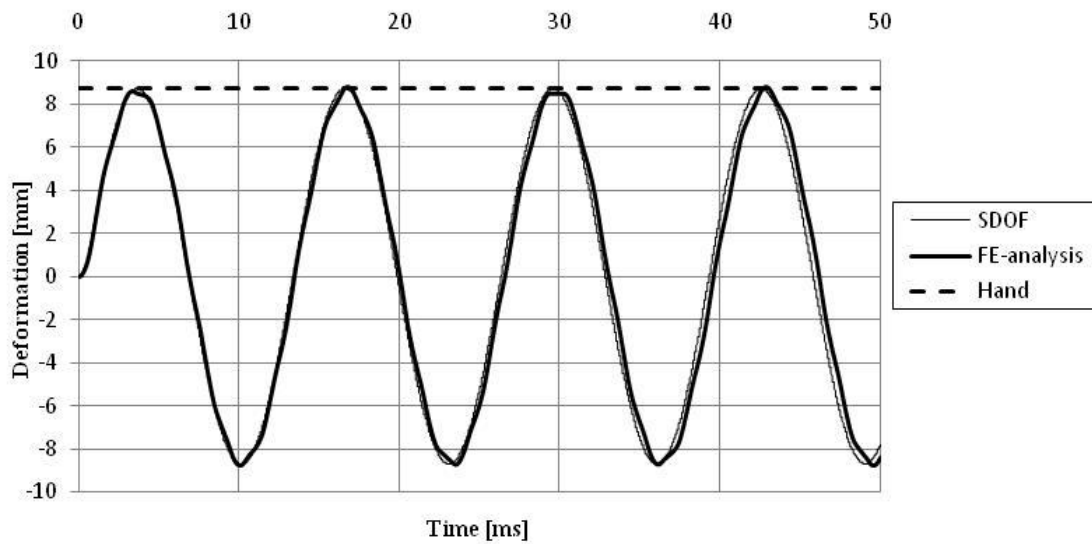
Now the maximum deformation capacity for the beam can be calculated to

$$u_{rd} = \frac{\theta \cdot l}{2} = \frac{13.2 \cdot 10^{-3} \cdot 2.7}{2} = 17.8 \text{ mm} \quad (3.78)$$

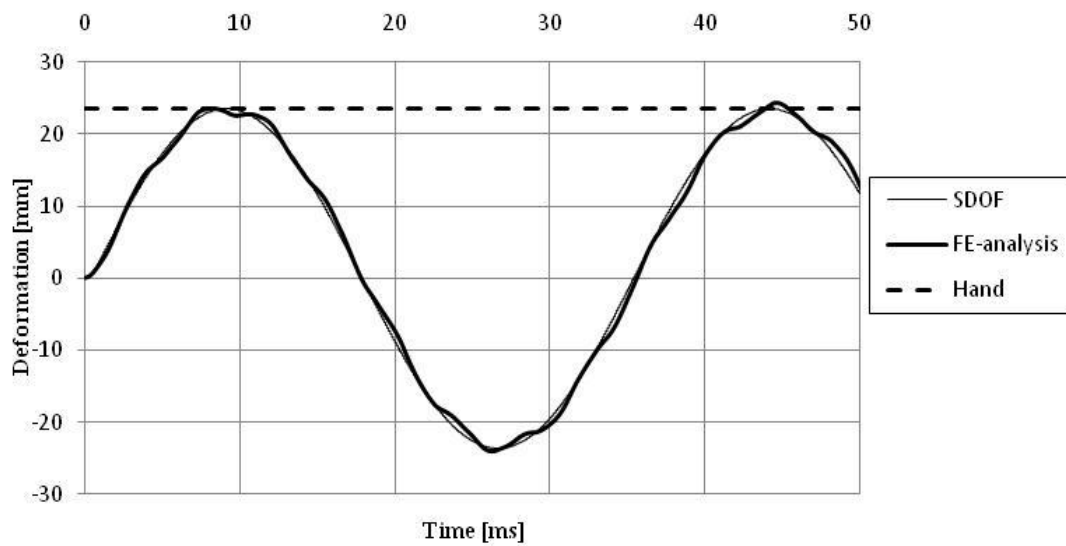
3.6.8 Results

The required deformation for the plastic and elastoplastic case is almost the double of what the beam can deform; i.e. the wall will not be able to resist the explosion. It will first crack, and then plasticise and when the rotation exceeds the capacity the wall will finally collapse. Since the plastic state is reached the elastic state has been passed and the elastic case does therefore not need to be controlled.

The deformation against time for the elastic material is plotted in Figure 3.15 for the different calculation methods. As can be seen the elastic analyses coincide very well in between the different methods. However, this is not the case for the plastic and elastoplastic analyses as shown in Figure 3.16 and further discussion on this subject is done in Section 3.7.

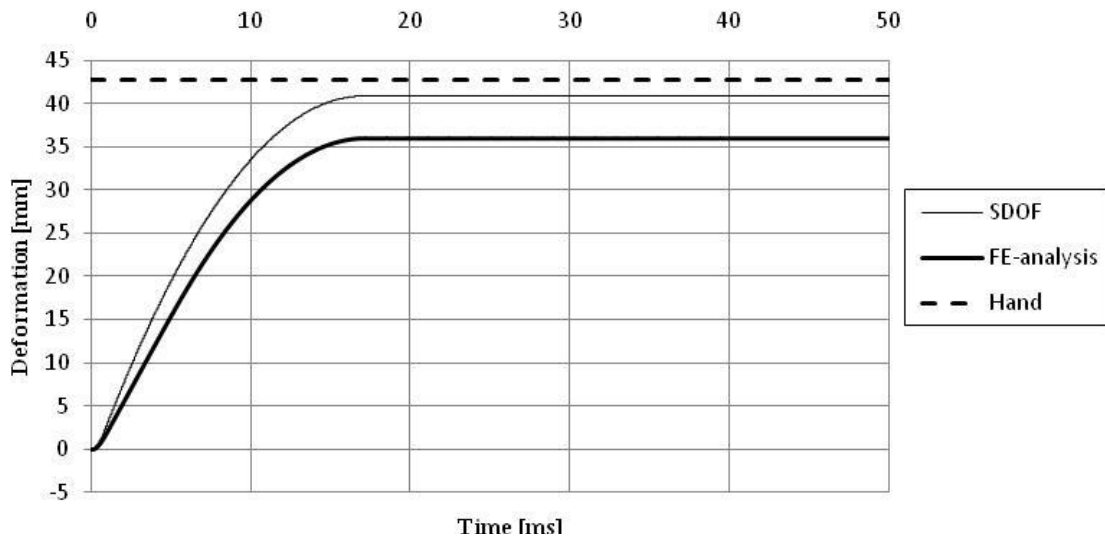


(a)

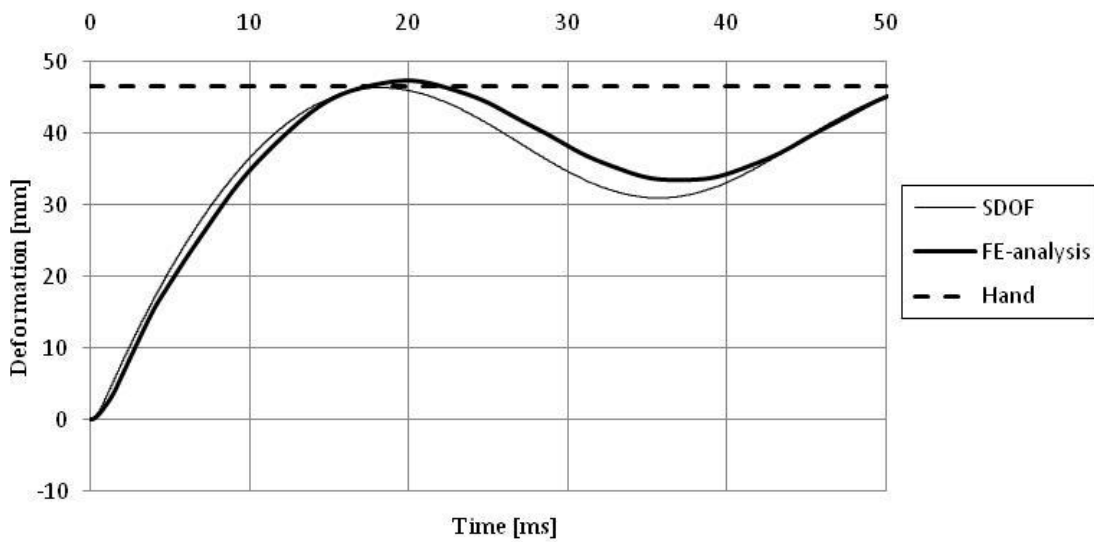


(b)

Figure 3.15 Deformations over time for (a) uncracked case (b) cracked case.



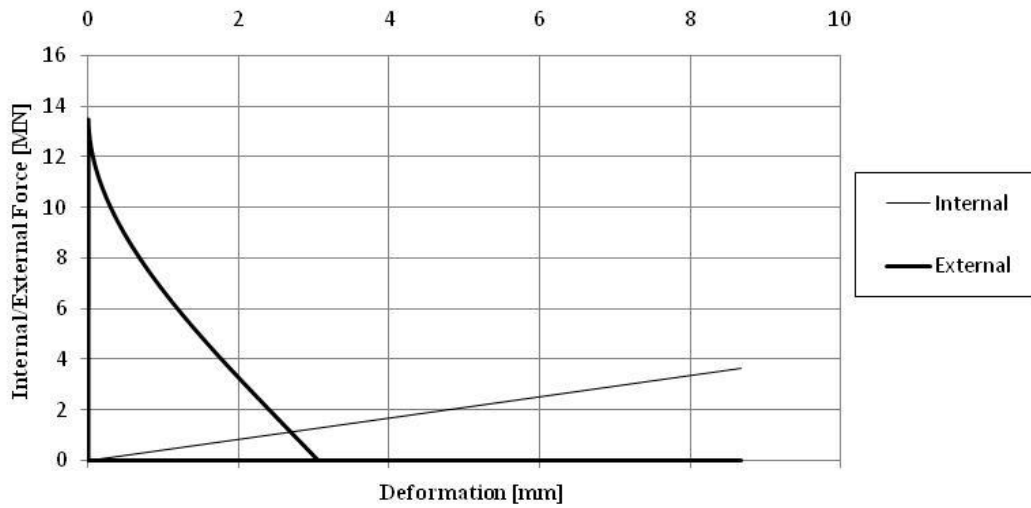
(a)



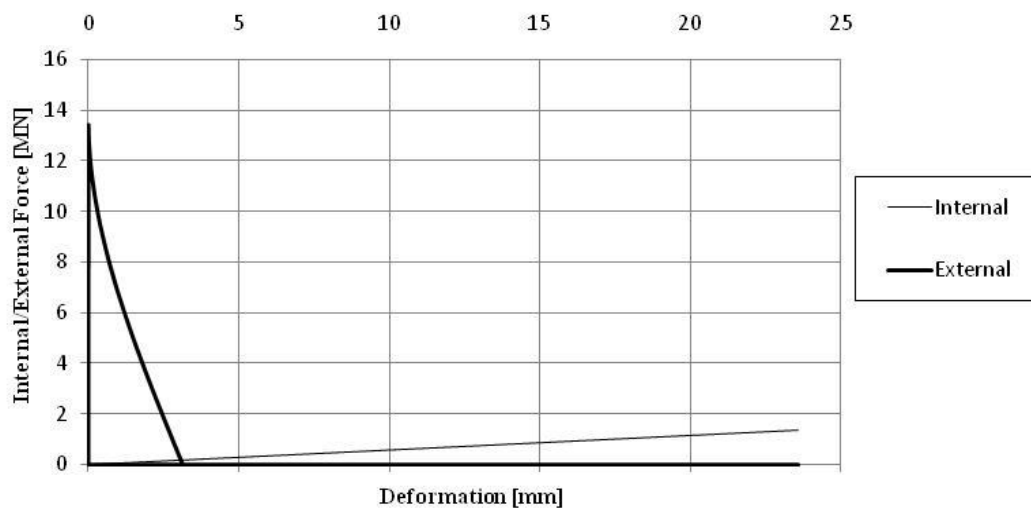
(b)

Figure 3.16 Deformations over time for (a) plastic case (b) elastoplastic case.

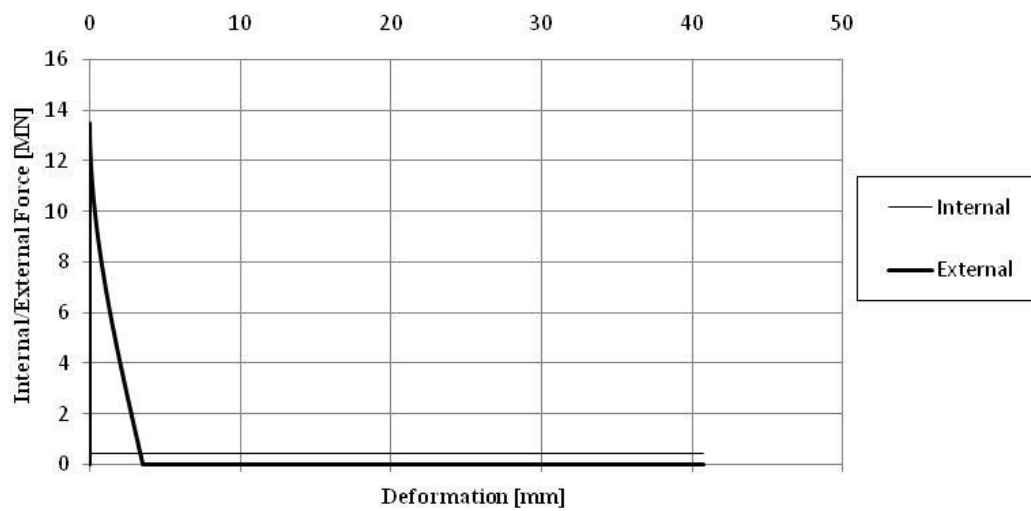
Figure 3.17 shows the relation between force and deformation for the two cases; elastic and plastic. The area under the curves is equal to the executed work and should be the same for both the internal and external work.



(a)



(b)



(c)

Figure 3.17 The relation between force and deformation for (a) uncracked case (b) cracked case (c) plastic case.

The internal work is calculated from the Figure 3.17 to

$$W_{I,i} = \frac{3629.5 \cdot 10^3 \cdot 8.7 \cdot 10^{-3}}{2} = 15.8 \text{ kJ} \quad (3.79)$$

$$W_{II,i} = \frac{1354.4 \cdot 10^3 \cdot 23.6 \cdot 10^{-3}}{2} = 16.0 \text{ kJ} \quad (3.80)$$

$$W_{III,i} = 442.5 \cdot 10^3 \cdot 42.7 \cdot 10^{-3} = 18.9 \text{ kJ} \quad (3.81)$$

The work for the plastic case has a higher value. This is because the effective mass is lower for the plastic case, compare equation (3.30) and (3.31), and will therefore be easier to set into motion, resulting in a larger external work. The external work is, for a characteristic impulse load, defined in Section 2.4.5 to

$$W_e = \frac{I_c^2}{2m} \quad (3.82)$$

and with current indata

$$W_{I,II,e} = \frac{7560^2}{2 \cdot 1787} = 16.0 \text{ kJ} \quad (3.83)$$

$$W_{III,e} = \frac{7560^2}{2 \cdot 1512} = 18.9 \text{ kJ} \quad (3.84)$$

which is the same as the internal energy for each case. The work against time is plotted in Figure 3.18 for elastic and plastic response. When the external work equals the internal work the maximum deformation is obtained.

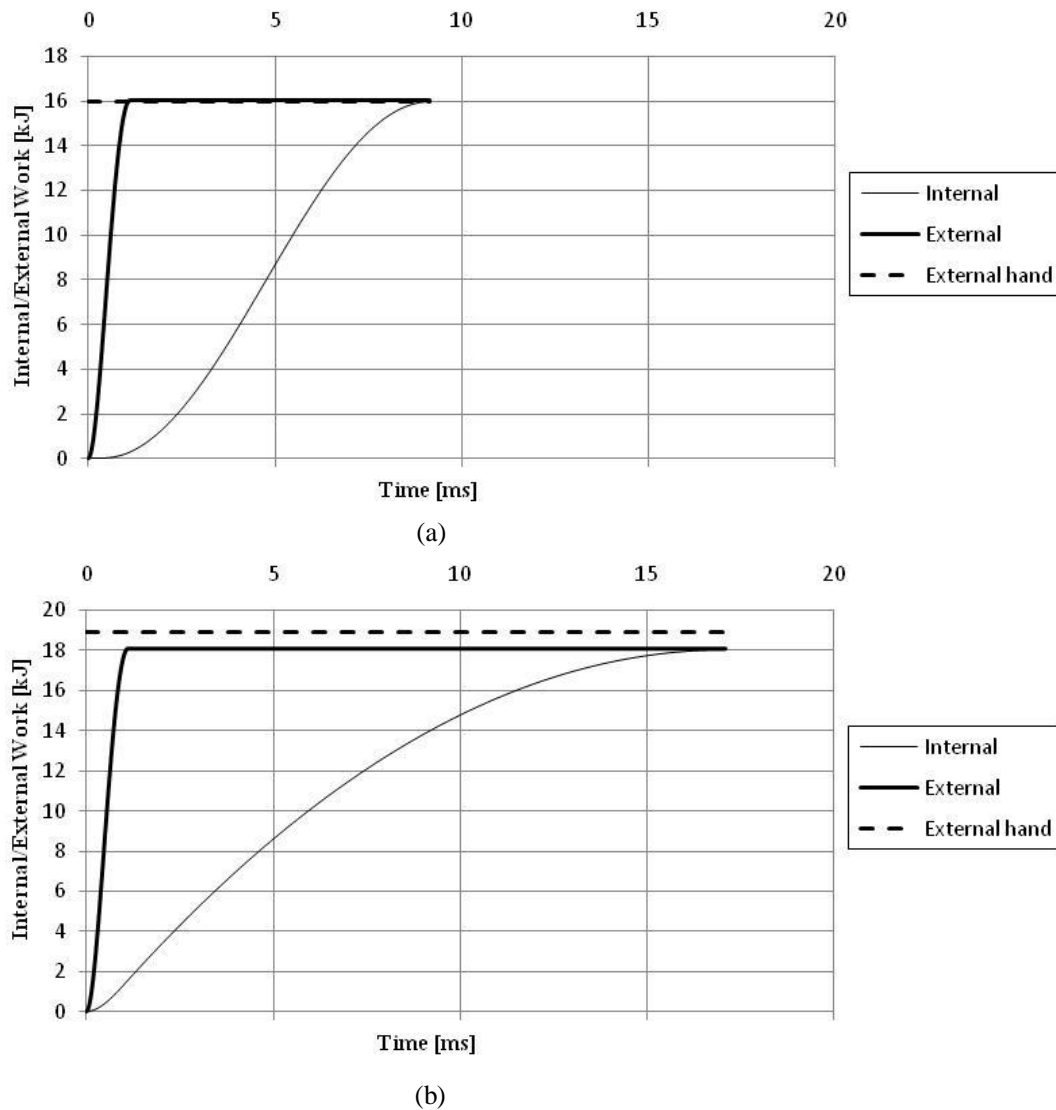


Figure 3.18 The relation between work and time for (a) elastic cracked case (b) plastic case.

As can be seen the hand calculations differs from the equation of motion calculations for the plastic case. This is because the hand calculations are based on the fact that the load has a characteristic form as shown in Figure 2.18, but in this example the load has been assumed to be triangular. The same problem arises for the elastic case, but here the difference is much smaller. One way to determine this error is by using so called damage curves, which is based on the knowledge that the divergence depends on the force $F(t)$ and the angular frequency ω for the elastic case and the force $F(t)$ and internal resistance R for the plastic case. Deeper studies on this subject will not be carried out here but instead the reader is referred to Johansson and Laine (2009).

3.7 Comments to divergence between analysis

3.7.1 Elastic response

When using linear elastic material in the different models there is not any significant difference between the results from SDOF and FE-model, as can be seen in

Figure 3.15. It can be stated that the assumed deformation shape, see Figure 3.19, when deriving the transformation factor κ for linear elastic material is a good assumption. One minor difference is the somewhat unsmooth response in the FE-analysis compared to the smooth response in the SDOF-analysis. This difference arises because ADINA considers higher order of eigenmodes while the SDOF-model only considers one mode.



Figure 3.19 Deformation shape when using linear elastic material.

It is also observed that there is a phase shift between the results from SDOF-analysis and FE-analysis. The reason for this phase shift is unknown, but a control of the eigenfrequencies for the two different models shows that they are the same.

3.7.2 Ideal plastic response

The difference between the FE-analysis compared to the hand calculations or the SDOF analysis is rather large for the ideal plastic material behaviour, about 5 and 14 percent, as can be seen in Figure 3.20. The difference between the SDOF- and hand calculation model depends on the assumption about a characteristic impulse load in the hand calculations and is described in Section 2.4.5.1.

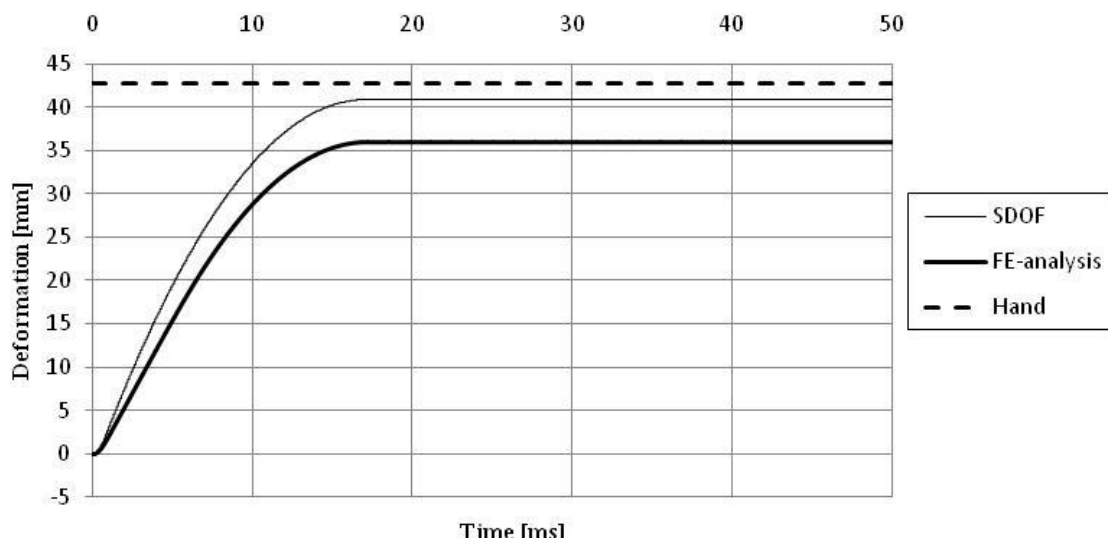


Figure 3.20 Deformations over time for plastic case.

The reason for the divergence between SDOF- and FE-analysis is believed to depend on the assumed deformation shape used when deriving the transformation factor κ , see Figure 3.21. In the derivation of the SDOF-model κ_{mF} is equal to 0.667, but in the FE-model the shape changes with time.

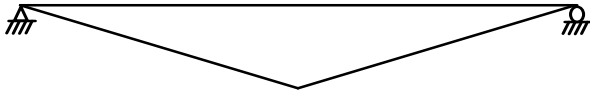


Figure 3.21 Deformation shape when using ideal plastic material.

A small comparison study between the models, SDOF and FEM, with three different loads and time duration has been made for better understanding and illustration of the problem. The three different cases are chosen to have a pressure of 5000, 2500 and 1000 kPa and time durations of 1.12, 2.24 and 5.60 ms. It should be pointed out that the total impulse for the three different cases is the same and that the first pressure and time duration, $P=5000$ kPa and $t_I=1.12$ ms, are the same as the example done in Section 3.6. Also, since the impulse intensity is the same, the results from hand calculations will be analogous.

As mentioned earlier, a large divergence can be seen for the pressure 5000 kPa and time duration 1.12 ms. The deformation shape for the FE-analysis in early stages is shown in Figure 3.22 where it is clear that the assumed deformation shape shown in Figure 3.21 have not yet been formed when the impulse load has ended. Thus, the assumption used when deriving κ_{mF} for the SDOF-model is not correct.

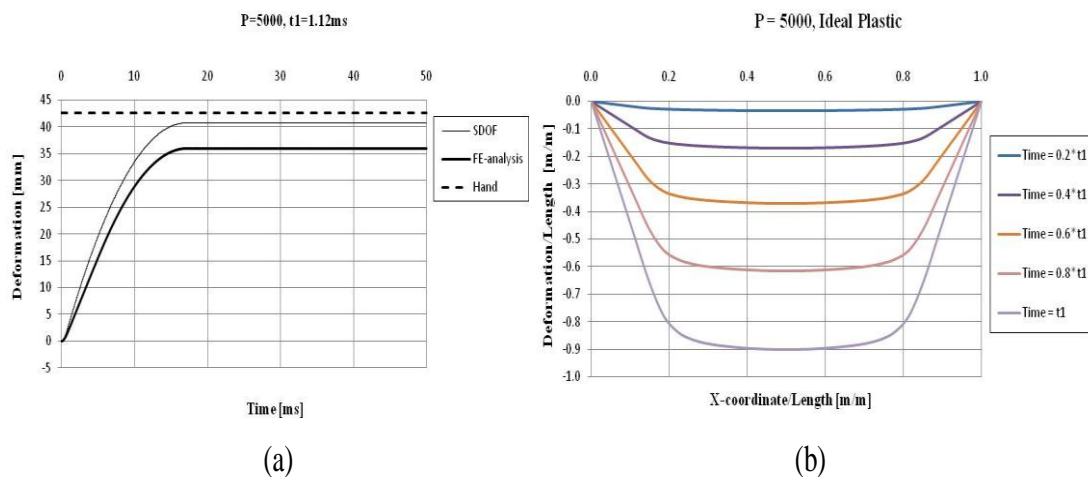
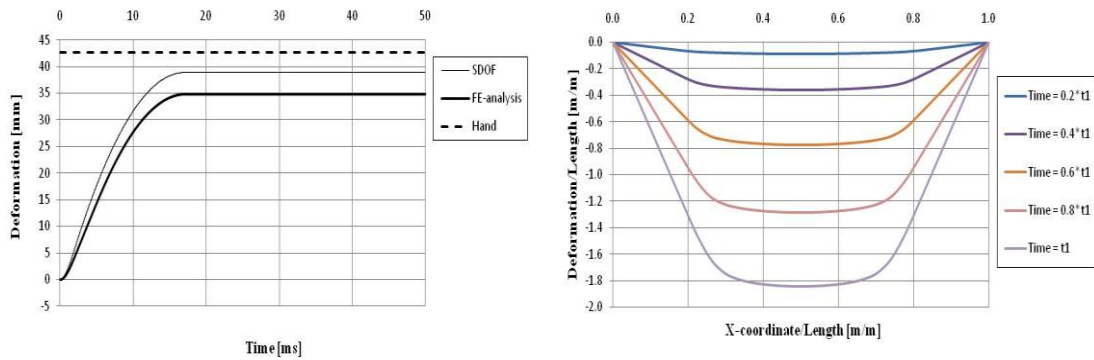
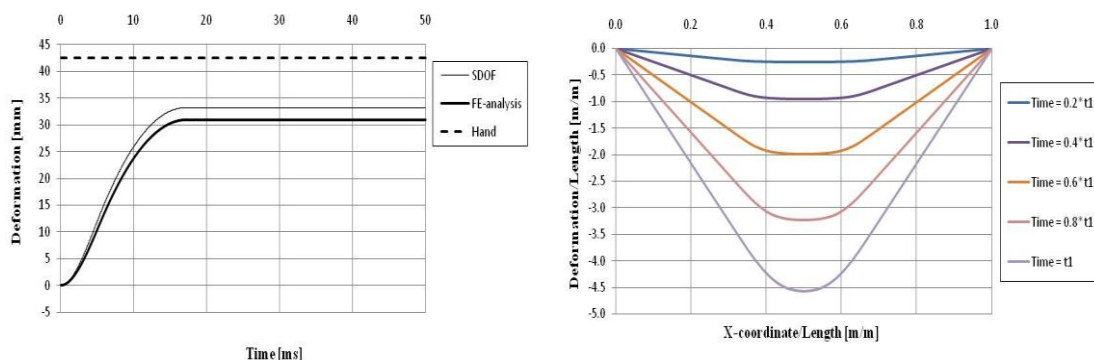


Figure 3.22 Response of beam with $P=5000$ kPa and $t_I=1.12$ ms. (a) Deformation vs. time. (b) Deformation shape along the beam at different time steps in FE-analysis.

However, when decreasing the pressure and increasing the time duration of the load a better convergence is reached, as can be seen in Figure 3.23a,c. This is because an increased load duration give more time for the structure to acquire a response more similar to that in Figure 3.21 and consequently, the results from the SDOF and FEM converge towards each other. Note here, that when studying the Figure 3.22b and Figure 3.23b,d the time t_I is not the same. The time $0.8t_I$ in Figure 3.22b is equal to $0.4t_I$ in Figure 3.23b and $0.2t_I$ in Figure 3.23d.



(a)



(b)

Figure 3.23 (a) Deformation vs. time and deformation shape along the beam at different time steps for $P=2500\text{kPa}$ and $t_1=2.24\text{ms}$ in FE-analysis. (b) Deformation vs. time and deformation shape along the beam at different time steps for $P=1000\text{kPa}$ and $t_1=5.6\text{ms}$ in FE-analysis.

Now when the “real” deformation shape is found for the example in 3.6, it is of interest to calculate a new transformation factors. This factor will be based on the deformation shape shown in Figure 3.24, which is a simplification of the shape in Figure 3.22b.

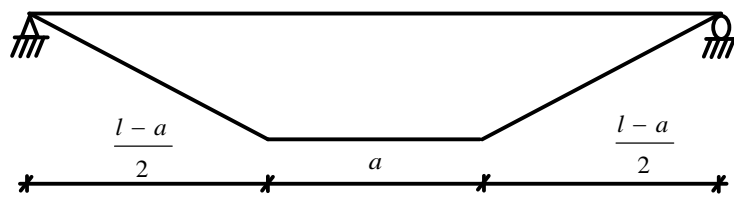


Figure 3.24 Modified deformation shape of the beam with ideal plastic material.

The derivation of the new transformation factors for this modified deformation shape is presented in APPENDIX A. By running SDOF-analysis with a pressure of 5000 kPa and time duration of 1.12 ms together with different length of a , a response close enough to the FE-analysis is found when a is equal to 0.5 m, see Figure 3.25. This value corresponds to a transformation factor κ_{mF} of 0.771. This indicates that when a load with short duration is acting on a structure the value of 0.667 for κ_{mF} cannot be used, but a new transformation factor needs to be calculated.

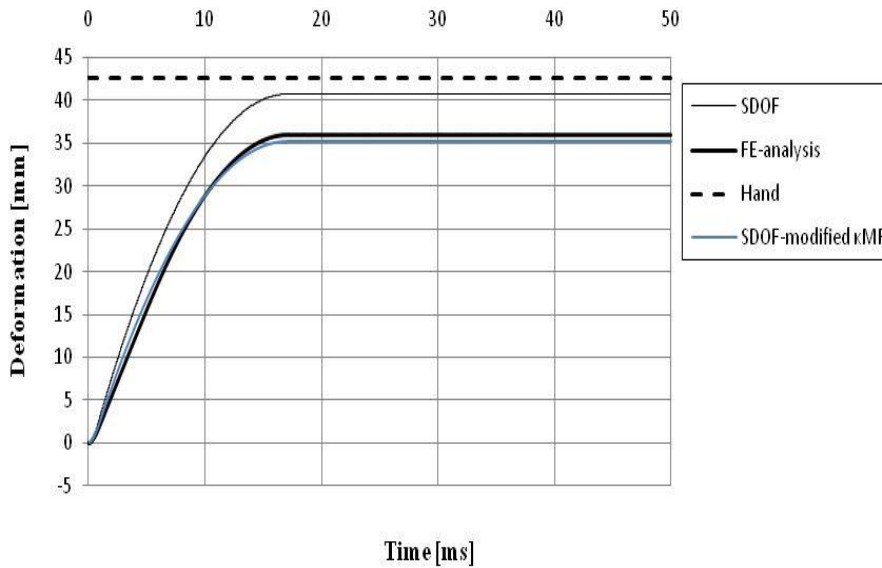


Figure 3.25 Deformation over time for old and new modified transformation factor for $P=5000\text{kPa}$ and $t_1=1.12\text{ms}$.

3.7.3 Elastoplastic response

The elastoplastic response of the different models is illustrated in Figure 3.26. The input data from Section 3.6 is used.

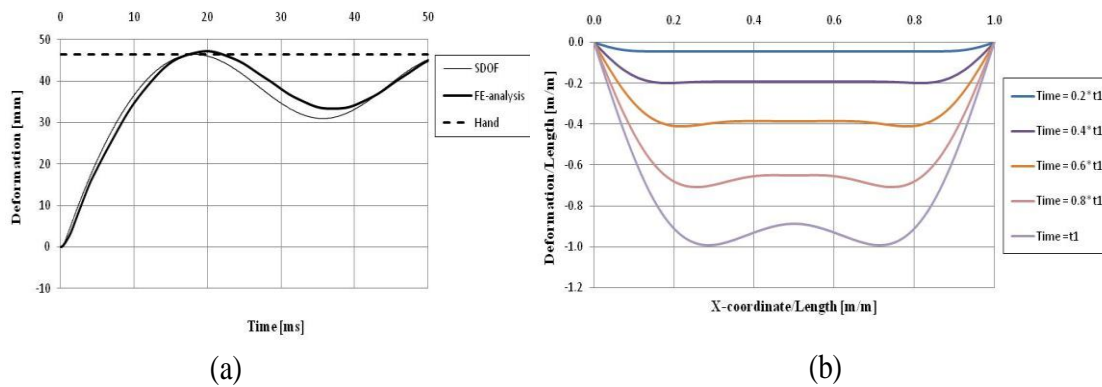


Figure 3.26 Response of beam with $P=5000\text{kPa}$ and $t_1=1.12\text{ms}$. (a) Deformation over time. (b) Deformation shape for the beam at different time steps in FE-analysis.

The same study as for the ideal plastic material, Section 3.7.2, with three different loads and time durations is also carried out here, see Figure 3.27. The reasoning about the assumed deformation shape is similar to the ideal plastic discussion, i.e. the longer load duration the closer the two analyses are to each other. However, the deformation shape here is more developed compared to the ideal plastic case and the difference between the SDOF-analysis and FE-analysis are smaller.

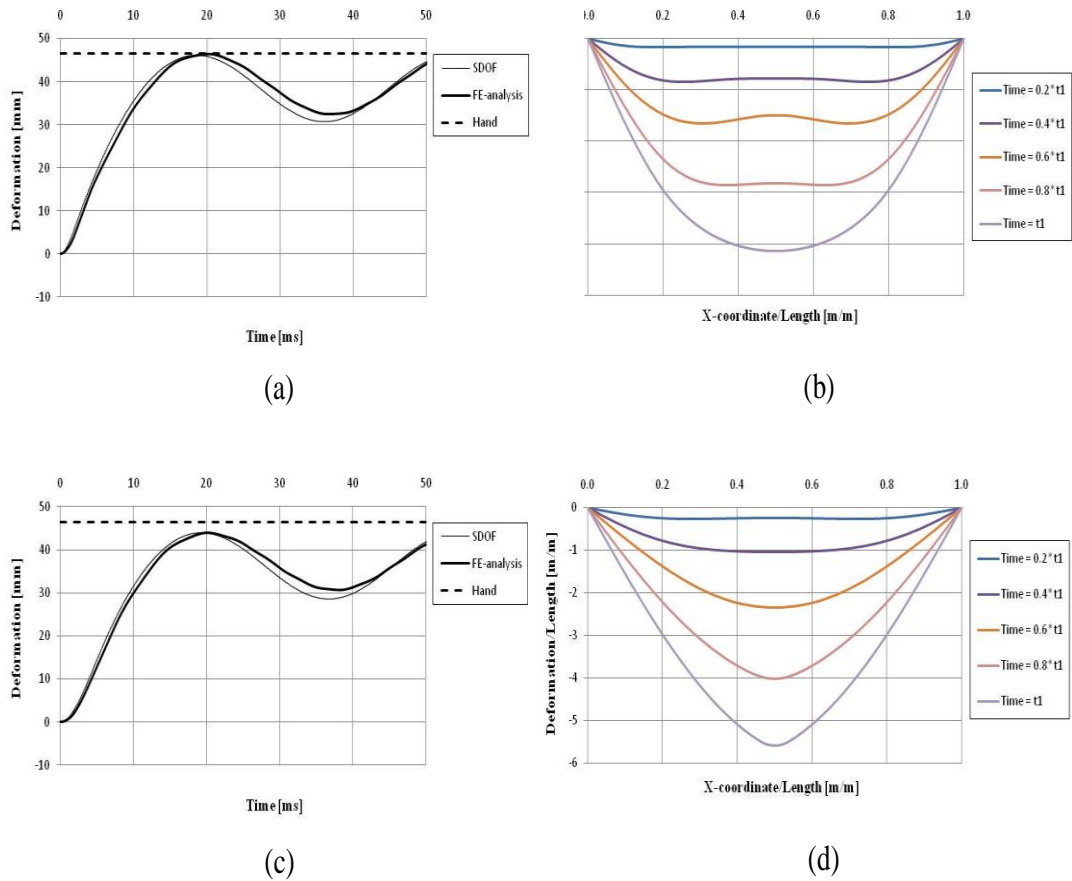


Figure 3.27 (a) Deformation vs. time for $P=2500\text{kPa}$ and $t_1=2.24\text{ms}$. (b) Deformation shape along the beam at different time steps for $P=2500\text{kPa}$ and $t_1=2.24\text{ms}$ in FE-analysis. (c) Deformation vs. time for $P=1000\text{kPa}$ and $t_1=5.6\text{ms}$. (d) Deformation shape along the beam at different time steps for $P=1000\text{kPa}$ and $t_1=5.6\text{ms}$ in FE-analysis.

The calculation of transformation factors κ_{mF} for different stages and with indata taken from the FE-analysis is done in APPENDIX C. The result is presented in Table 3.3. A misleading value of the transformation factor is found in the early stage. This is because the maximum deformation point is not in the chosen system point for the early stages as was assumed when the transformation factor where calculated.

Table 3.3 Variation of transformation factors from FE-analysis.

u_s [mm]	t [ms]	κ_m	κ_F	κ_{mF}
2.4	1.11	0.853	0.871	0.979
10	2.81	0.491	0.627	0.783
20	5.51	0.484	0.619	0.782
30	8.31	0.435	0.583	0.747
40	12.4	0.424	0.573	0.739

47.3	20	0.408	0.561	0.728
------	----	-------	-------	-------

Another notation is that the value of the transformation factor tends to approach a mean value between the elastic and plastic transformation factor. However, when using this mean value a larger divergence is found and the SDOF-analysis gives a result on the unsafe side.

It is also worth mentioning that the transformation factor κ_{mF} used in the SDOF-model for the elastoplastic material is the same as the ideal plastic transformation factor, i.e. $\kappa_{mF} = 0.667$. However, the elastoplastic material is elastic for an amount of time and should then have a transformation factor κ_{mF} equal to the elastic factor, which is higher. Since a higher value of the transformation factor results in a lower deformation this could be the reason for why the FE-analysis has a larger deformation than the SDOF-analysis.

3.7.4 Numerical solution methods

There are two different types of numerical solution methods in the software program ADINA, the implicit solution method Newmark and the explicit solution method central difference method. In the example the latter one has been used in the SDOF-model while the implicit Newmark solution method has been used for the FE-analysis. Since different solution methods for the SDOF- and FE-model are used it is of interest to perform a control in ADINA with the different solution methods to see if they differ.

When using 2D-beam elements there is not a significant difference in the response between the two solution methods, see Figure 3.28. As can be seen in the figure a better agreement is found for this example when both the FE-analysis and the SDOF system use the central difference method.

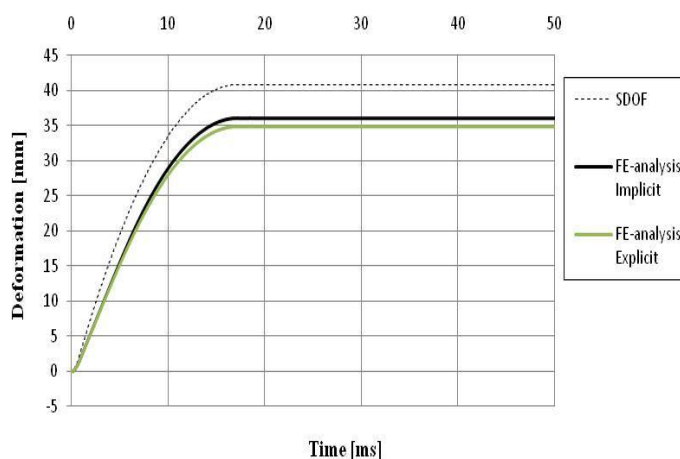


Figure 3.28 Response between explicit- and implicit solution method with 2D-beam elements.

In contrast to the 2D-beam elements the 3D-beam elements generates a significant difference for the two different solution methods, see Figure 3.29. The result when using the explicit solution method is on the unsafe side, i.e. it tends to overestimate the response. According to ADINA, the larger difference that arises for 3D-beam

elements depends on that more integration orders are used for the 3D-beam elements than for 2D-beam elements. Another reason for the difference in the 3D-beam element analysis is, according to ADINA, that too large time increment in the explicit solution method is used for a nonlinear analysis. However, this is not the case here since a control with smaller time increment has been carried out and the same result was obtained.

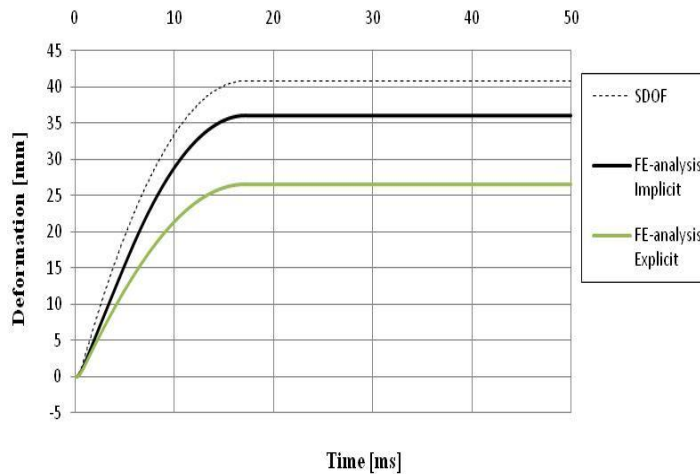


Figure 3.29 Response between explicit- and implicit solution method with 3D-beam elements.

The conclusions that can be drawn from these analyses is that both methods can be used in ADINA for 2D-beam element analysis while when nonlinear FE-analysis is carried out with 3D-beam elements it is of importance to choose the implicit solution method Newmark in order to gain satisfactory results.

4 Slabs

4.1 Introduction

A slab is supported on two supports or more. If the load is carried in one direction it is classified as a one-way slab and hence, only need reinforcement in this direction. If the load is carried in two directions it is classified as a two-way slab and will therefore need reinforcement in two directions. The amount of reinforcement can differ in the different directions of the slab resulting in a different stiffness and bearing capacity in these directions.

The behaviour of a one-way slab is similar to the behaviour of a beam described in Chapter 3. In this chapter, rectangular two-way slabs with constant thickness and support on all four sides is studied, see Figure 4.1. What should be pointed out here is that in contrast to the beam studies the parameters of a slab will always be per width unit, i.e. the parameters is calculated with a width of 1.0 m.

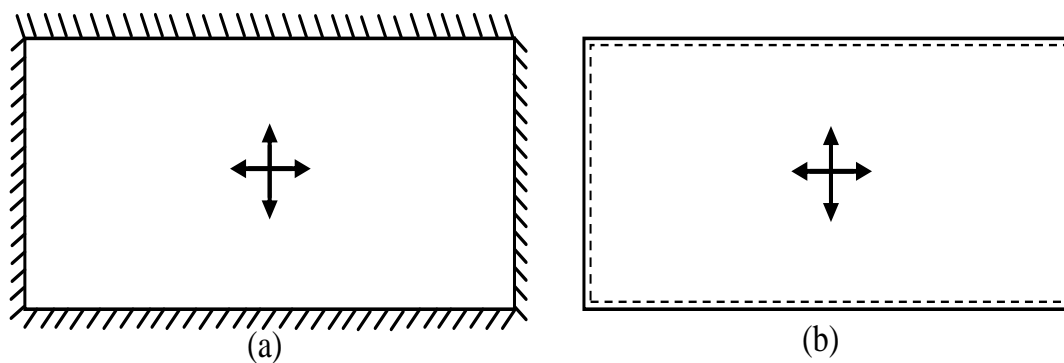


Figure 4.1 Rectangular two-way slabs: (a) fully fixed (b) simply supported.

4.2 Response of slabs subjected to impulse load

The response of the slab subjected to a uniformly distributed impulse load is rather similar to the response of a beam, but here the slab acts in two directions. The deformation shape at different stages for the slab is illustrated in Figure 4.2. A strip located in the middle of the slab in both the short and long direction is taken from the slab and is coupled together for the same stage.

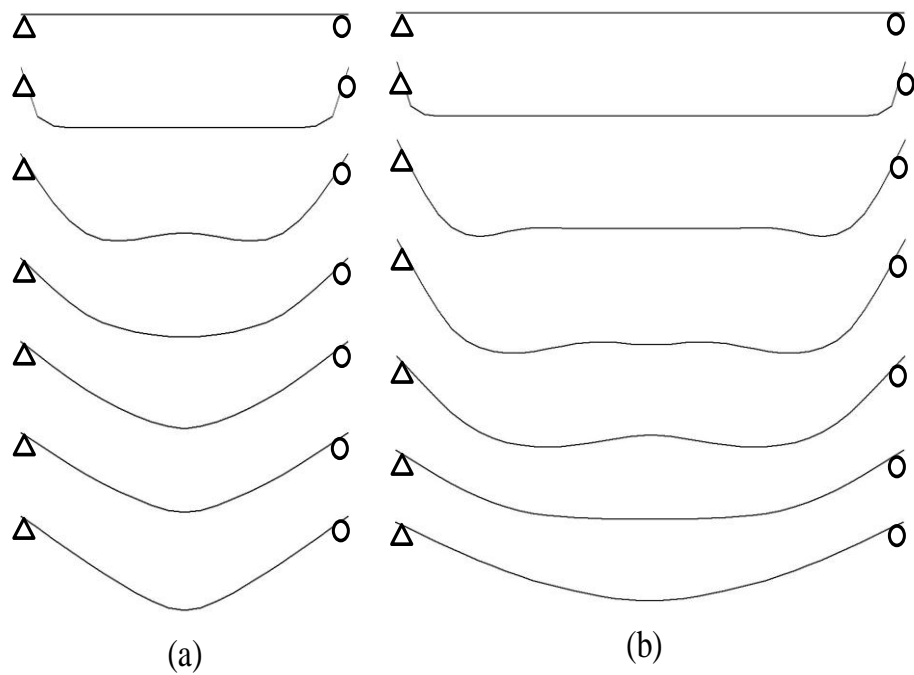


Figure 4.2 Response of slab subjected to an impulse load at different time.
 (a) Short side strip. (b) Long side strip.

The theory on why this deformation form appears is the same as for a beam and is described in Section 3.2. What can be noticed in Figure 4.2 is that more time is required for the long side to fully develop the final deformation shape.

The deformation distribution for a slab subjected to a static and impulse load can be seen in Figure 4.3. Notice that the maximum deformation at an early stage for the impulse loaded slab is not located in the centre of the slab, as it is for a static load. However, by studying the development of the deformation along time for the impulse loaded slab it can be seen that the response approaches the static response.

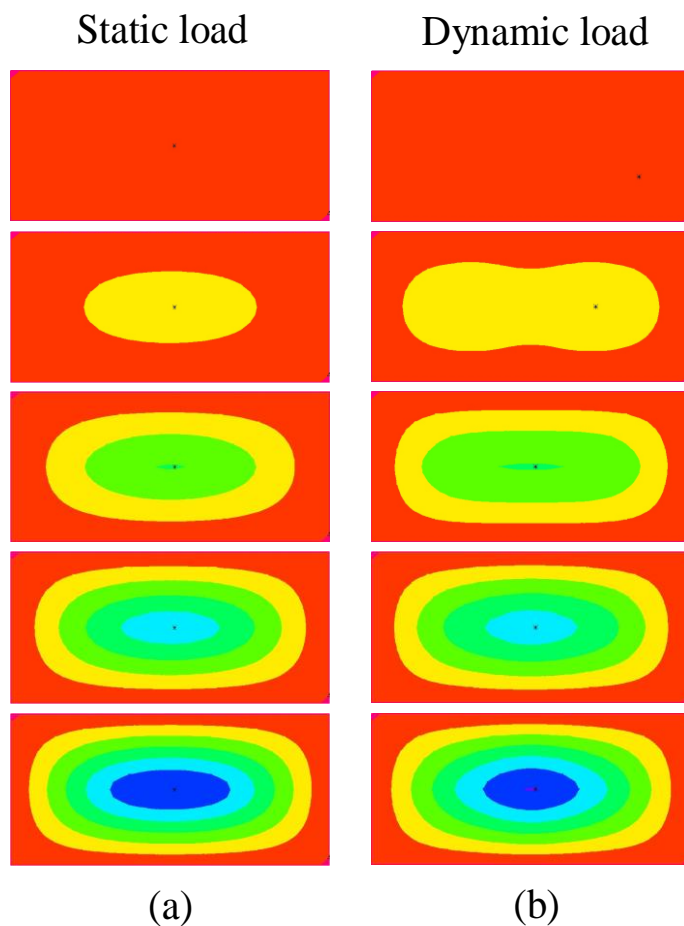


Figure 4.3 Deformation plots for (a) static load and (b) impulse (dynamic) load.

As can be seen in Figure 4.2 there appears to be large deformations near the supports in an early stage also for the slab. This will lead to large curvature and high shear stresses near the supports in the early loading stage with a significant risk of cracks at the underside of the slab, see Figure 4.4. As mentioned before in Section 3.2 this problem requires more investigation and it is outside the limits of this master thesis and will therefore not be further investigated.

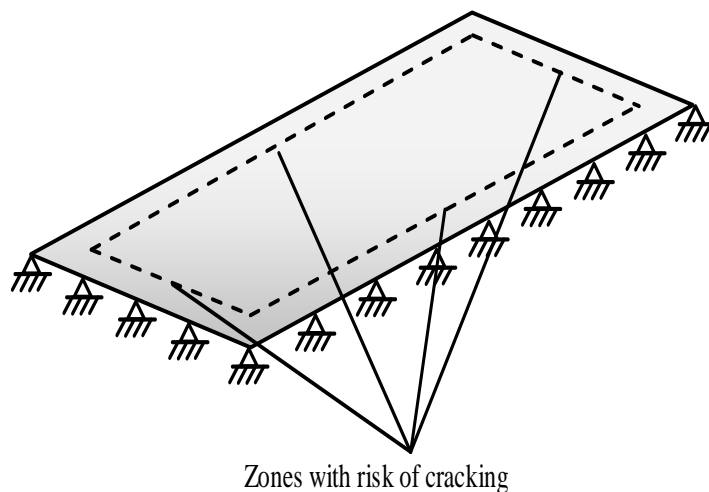


Figure 4.4 Zone where there is a high risk of cracking at the underside of the slab in the early stage.

4.3 Transformation from slab to SDOF-system

4.3.1 Introduction

The reduction of a slab to a SDOF system is similar to the reduction of beams. The equation of motion can be written, according to equation (2.55), as

$$\kappa_{mF} m \ddot{u} + R = F(t) \quad (4.1)$$

where

$$\kappa_{mF} = \frac{\kappa_m}{\kappa_F} \quad (4.2)$$

which is analogous with the beam calculations. However, while the beam could be assumed to only vary in one direction, i.e. length direction, the slab varies in two directions, i.e. length and width. This means that another dimension, read variable, needs to be added for slabs.

4.3.2 Transformation factor for the mass κ_m

The kinetic energy for a slab and a SDOF-system can then be stated as

$$E_k^{slab} = \frac{m \cdot v^2}{2} = \int_{y=0}^{y=l} \int_{x=0}^{x=w} \frac{v^2}{2} \cdot m'(x, y) dx dy \quad (4.3)$$

$$E_k^{SDOF} = \frac{m_e \cdot v_s^2}{2} \quad (4.4)$$

where the velocity is equal to

$$v(x) = \frac{du(x, y)}{dt} \quad (4.5)$$

$$v_s = \frac{du_s}{dt} \quad (4.6)$$

By combining equation (4.3) and (4.4) with the knowledge of equal kinetic energy and by using the relations from equation (4.5) and (4.6) the equivalent mass can be calculated to

$$m_e = \int_{y=0}^{y=l} \int_{x=0}^{x=w} \frac{v^2}{v_s^2} \cdot m'(x, y) dx dy = \int_{y=0}^{y=l} \int_{x=0}^{x=w} \frac{u^2}{u_s^2} \cdot m'(x, y) dx dy \quad (4.7)$$

The transformation factor for the mass κ_m is defined as

$$\kappa_m = \frac{m_e}{m} \quad (4.8)$$

and the final expression for the mass transformation factor is

$$\kappa_m = \frac{1}{m} \cdot \int_{y=0}^{y=l} \int_{x=0}^{x=w} \frac{v^2}{v_s^2} \cdot m'(x, y) dx dy = \int_{y=0}^{y=l} \int_{x=0}^{x=w} \frac{u^2}{u_s^2} \cdot m'(x, y) dx dy \quad (4.9)$$

By assuming that the mass is constant over the slab, the total mass can be calculated as

$$m = m' \cdot w \cdot l \quad (4.10)$$

and the equation (4.9) can then be reduced to

$$\kappa_m = \frac{1}{m' \cdot w \cdot l} \cdot \int_{y=0}^{y=l} \int_{x=0}^{x=w} \frac{v^2}{v_s^2} \cdot m' dx dy = \frac{1}{w \cdot l} \int_{y=0}^{y=l} \int_{x=0}^{x=w} \frac{u^2}{u_s^2} dx dy \quad (4.11)$$

4.3.3 Transformation factor for the load κ_F

The external work for an untransformed slab and a SDOF system is

$$W_e^{slab} = F \cdot u \quad (4.12)$$

$$W_e^{SDOF} = F_e \cdot u_s \quad (4.13)$$

The total force on the slab is

$$F = \int_{y=0}^{y=l} \int_{x=0}^{x=w} q(x, y) dx dy \quad (4.14)$$

and the external work for the untransformed slab can then be rewritten to

$$W_e^{slab} = \int_{y=0}^{y=l} \int_{x=0}^{x=w} q(x, y) \cdot u(x, y) dx dy \quad (4.15)$$

With the information of equal external work and equation (4.13) and (4.15) the equivalent force F_e can be expressed as

$$F_e = \int_{y=0}^{y=l} \int_{x=0}^{x=w} q(x, y) \cdot \frac{u(x, y)}{u_s} dx dy \quad (4.16)$$

The transformation factor for the load κ_F is defined as

$$\kappa_F = \frac{F_e}{F} \quad (4.17)$$

and together with equation (4.14) and (4.16) the final expression for the load transformation factor can be calculated to

$$\kappa_F = \frac{\int_{y=0}^{y=l} \int_{x=0}^{x=w} q(x, y) \cdot \frac{u(x, y)}{u_s} dx dy}{\int_{y=0}^{y=l} \int_{x=0}^{x=w} q(x, y) dx dy} \quad (4.18)$$

When considering a case with uniformly distributed load the total force on the slab can be rewritten to

$$F = \int_{y=0}^{y=l} \int_{x=0}^{x=w} q(x, y) dx dy = q \cdot l \cdot w \quad (4.19)$$

Inserting equation (4.19) into (4.18) the load transformation factor can be reduced to

$$\kappa_F = \frac{q \cdot \int_{y=0}^{y=l} \int_{x=0}^{x=w} \frac{u(x, y)}{u_s} dx dy}{q \cdot w \cdot l} = \frac{1}{l \cdot w} \cdot \int_{y=0}^{y=l} \int_{x=0}^{x=w} \frac{u(x, y)}{u_s} dx dy \quad (4.20)$$

4.3.4 Tabulated transformation factors

Due to the complex calculations that arise for slabs, only a few transformation factors for basic examples have been derived. The elastic factors are derived in APPENDIX D and the plastic factors are derived in APPENDIX E, the results are presented in Table 4.1. Note that the transformation factor for the internal force κ_k is, according to Biggs (1964), equal to the transformation factor for the load κ_F and is therefore not presented here.

Table 4.1 Tabulated transformation factors for a slab.

		Uniformly distributed load	
		Simply supported	Fully fixed
		Deformation curve elastic case	
κ_m		0.250	-
κ_F		$4/\pi^2$	-
κ_{mF}		0.617	-
		Deformation curve plastic case	
κ_m		$(1+a/w)/6$	$(1+a/w)/6$
κ_F		$(1+a/2w)/3$	$(1+a/2w)/3$

4.4 Equation of motion

The approach for solving the equation of motion for a slab is very similar to the beam approach described in Section 3.3. The energy absorbed by the slab can be described by studying the maximum deformation that occurs. This will happen in the middle of the slab for the elastic material and along the yield line in the middle for the plastic material, see Figure 2.25c. A point in the middle of the slab is chosen to represent the system point for the undamped SDOF-system. The equation of motion can then be stated as

$$\kappa_{mF} m_b \ddot{u} + R_b = F_b(t) \quad (4.21)$$

Similar to the beam model the equation of motion will be solved with the “central difference method” together with the software Matlab. This method is further described in Nyström (2006).

4.5 Hand calculations

Also here, the approach is very similar to the beam approach. The calculations are based on energy balance and the SDOF-system with a system point in the middle of the slab. As for the beam model, these calculations should only be used in preliminary design. The deformations for the different materials are calculated analogous with the calculations for the beam. The difference between the models is that different transformation factors are used and that the maximum internal force will be based on the yield line theory for the plastic material in the slab model.

4.6 FE-analysis

4.6.1 Restrictions

The FE-analysis is carried out using the software ADINA. The reinforcement and concrete will be modeled as one homogenous material. The cracked elasticity modulus and the choice of materials response in different sections of the structure is the same as for the beam, see Section 3.5 for more information. A slab has a more complex behaviour than a beam, for example will the Poisson’s ratio influence the slab stiffness. To have the same conditions as the hand- and SDOF-models some special arrangements have been made in the FE model.

4.6.2 How to model in ADINA

4.6.2.1 Choice of elements

Shell elements would probably be the most obvious and common choice of element when modeling a slab. However, when using shell elements in a two-way slab and in combination with plastic material a biaxial effect will appear that increase the moment

capacity of the slab. To avoid this increased capacity shell elements were not used to model the slab, instead a grid of beams were used to approximate the slab.

The effect can be described by studying a slab with supports on two opposite sides, i.e. a one-way slab. Figure 4.5 shows the response of the slab at different stages. The biaxial effect arises between point 2 and 3. If no biaxial effect appeared this part would have a constant resistance as the red bilinear response curve in Figure 4.5 has and hence, a constant reaction force. However, as can be seen there is an inclination of the curve which increase the bearing capacity of the slab in a way that is not intended.

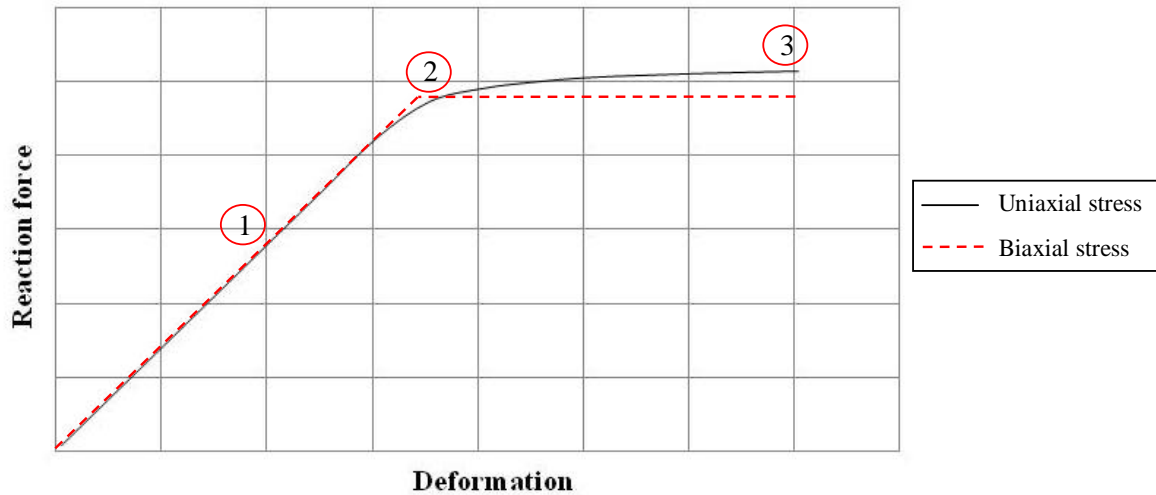


Figure 4.5 Comparison at different stages for a plastic beam response modeled by shell elements and subjected to a uniaxial or biaxial stress.

So for point 1 when the slab is elastic and the Poisson's ratio is set to zero there is only stresses in one direction, as can be seen in Figure 4.6. This means that there is zero moment around x-axis, M_x .

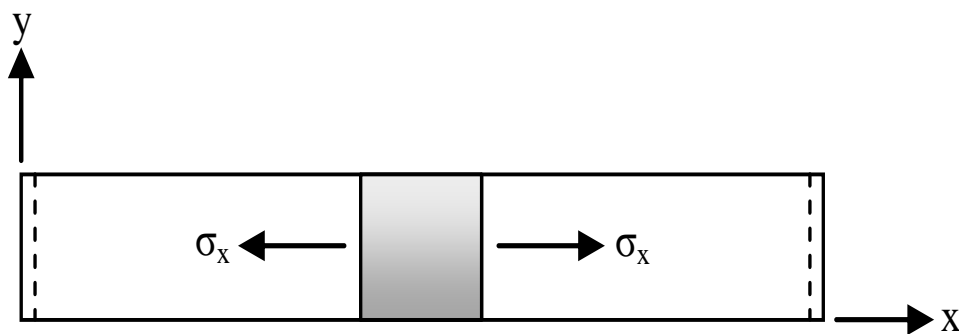


Figure 4.6 Stresses acting on one element in elastic state.

By continuing loading the slab it will enter the plastic stage, point 2 and forward, where the biaxial effect arises, see Figure 4.7. Here, the moment around the x-axis, M_x , is no longer zero and stresses arise in the y direction.

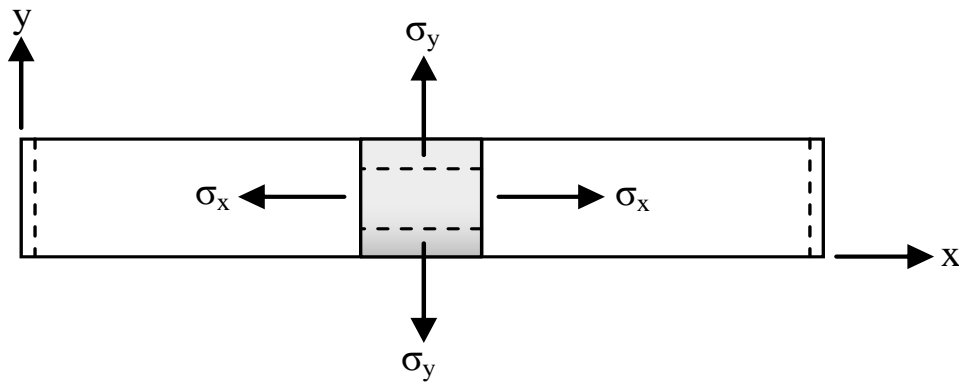


Figure 4.7 Stresses acting on one element in plastic state.

The reason for this effect is that the plastic material model used in ADINA is based on Von Mises plastic theory so no matter if the Poisson's ratio is set to zero or not, it automatically sets the Poisson's ratio to 0.5 in the plastic state. Because of this, a lateral contraction will take place and the stresses that arise can be calculated with Hooke's law.

So instead of using shell elements a model with beam elements in two directions is to be used, called beam grid. For this to work 3D beam elements in different directions must be connected with the same nodes at the intersection points, see Figure 4.8.

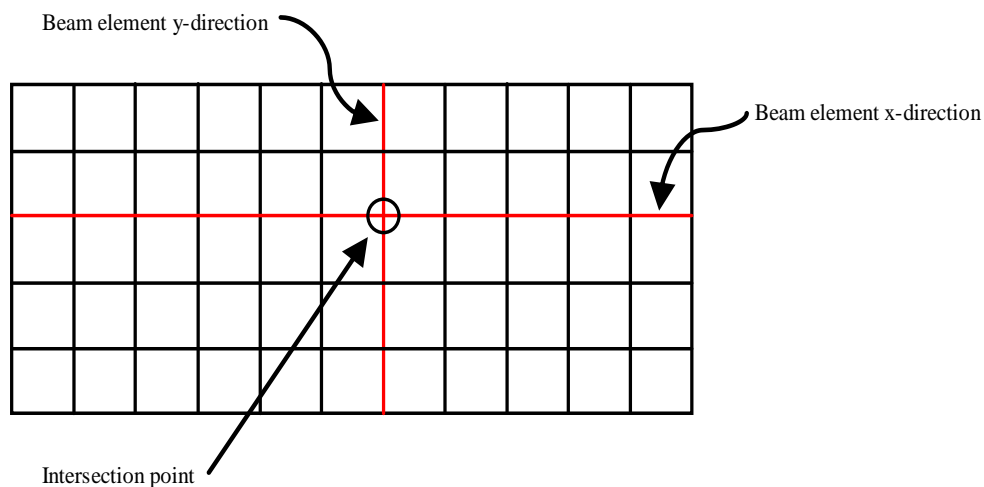


Figure 4.8 Arrangement of beam elements in slab model.

In this Master thesis, a slab with an area of 5x2.7 m and a thickness of 0.350 m is studied. The beam grid is then composed by beams with a cross section of 0.135x0.350 and with a distance of 0.135 m between each other, see Figure 4.9. Note that the width of the slab is 4.995 m. This is due to not exceed the limitation of 900 nodes in the evaluation copy of ADINA and also, to have a quadratic grid, i.e. the same distance between the nodes in both directions.

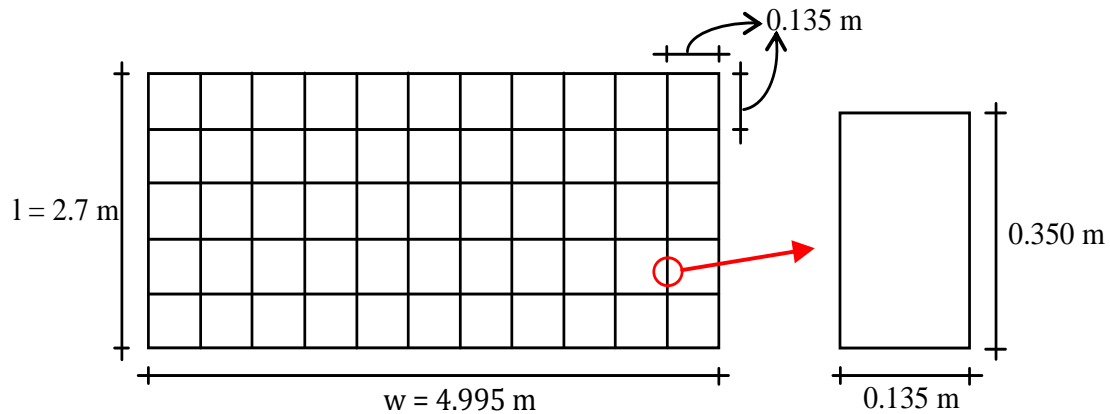


Figure 4.9 Arrangement of beam elements in slab model.

4.6.2.2 Element integration points

Previously when studying the beam in Chapter 3, 2D beam elements were used. However, 2D beam elements cannot be used when the purpose is to model a slab since a third direction needs to be considered, i.e. 3D beam elements have to be used. As mentioned in Section 3.5.4 there is a limitation of choice of number of integration points when using 3D beam elements in the software ADINA. ADINA automatically sets the number of integration points to seven in 3D beam elements. In earlier reports, Ek and Mattsson (2010), the stress distribution was expected to have the appearance as shown in Figure 4.10.

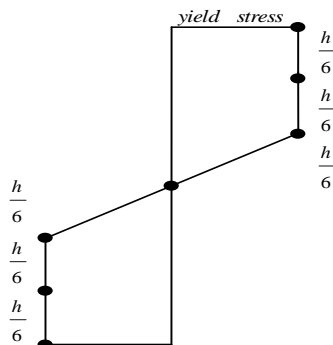


Figure 4.10 Expected stress distribution with seven integration points.

However, this is not the case in ADINA. Instead, ADINA calculates the stress distribution with a polynomial of order six as shown in figure Figure 4.11.

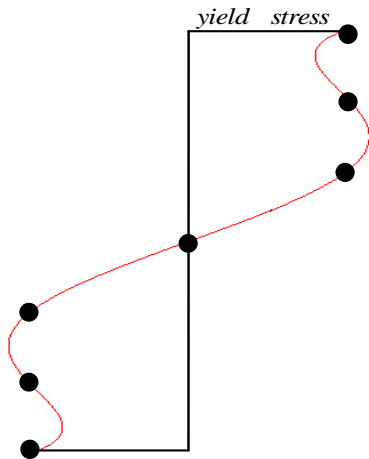


Figure 4.11 ADINA Stress distribution with a polynomial of order six.

When calculating the moment around the neutral axis for the stress distributions in Figure 4.10 and Figure 4.11 the latter is 4.2 % lower. Hence, to be able to use the expected stress distribution shown in Figure 4.10 a modified yield stress, f_y^{mod} , is to be used in ADINA. The equation for this modified yield stress is derived in APPENDIX F and is

$$f_y^{\text{mod}} = \frac{1}{\alpha} \frac{M_{rd}}{w \cdot h^2} \quad (4.22)$$

where α is a factor that consider the difference between the two different stress distributions. Note that equation (4.22) only works for rectangular homogenous cross sections.

4.6.2.3 Modified elasticity modulus

A problem that arises when using a beam grid is the reduction of the torsional stiffness. Depending on how fine mesh is used, i.e. how many beam elements each side has, the reduction will be different. That is, the finer mesh used the larger will de reduction be. The problem can be described by studying one beam element in each direction of the slab, see Figure 4.12. If for example the beam in x-direction is loaded by a uniformly distributed load it will deform as a normal beam. However, since the beam element in y-direction is connected to the loaded beam in the intersection point it will add an additional stiffness to the loaded beam, i.e. its torsional stiffness. Depending on how fine mesh is used, the beam elements will have different widths and since the torsional stiffness is greatly dependent on the width it will have a larger stiffness when fewer elements are used.

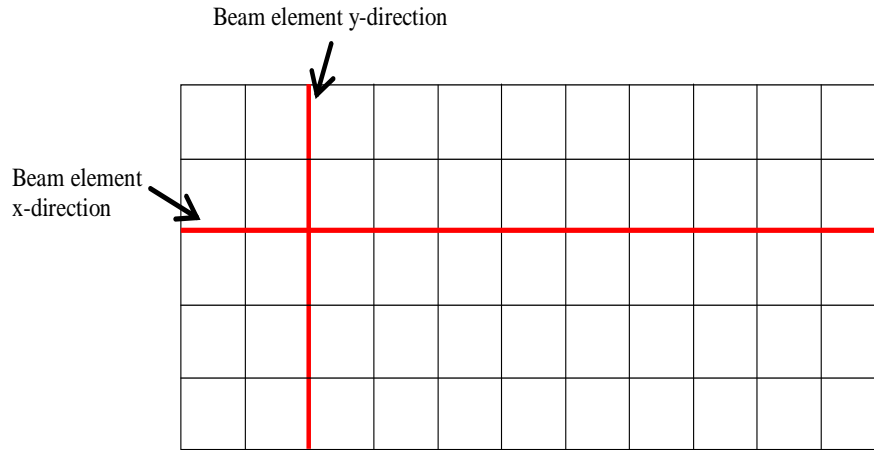


Figure 4.12 Studying one beam element in each direction.

Another way to describe the problem is by studying the equations for the torsional and bending stiffness stated as

$$K_v = c_1 \cdot a \cdot b^3 \quad \text{where} \quad a = \max(h, w) \quad , \quad b = \min(h, w) \quad (4.23)$$

$$EI = E \cdot \frac{wh^3}{12} \quad (4.24)$$

where c_1 is a factor depending on the ratio between the height and width of the cross-section. Since the bending stiffness is direct proportional to the width there is no effect on the bending stiffness when dividing the width into smaller parts. However, the torsional stiffness may be greatly reduced. If for example the width w would be divided into two elements, the new torsional moment would be

$$K_v = 2c_1 h \left(\frac{w}{2} \right)^3 = \frac{c_1}{4} h w^3 < c_1 h w^3 \quad (4.25)$$

To solve this problem the elasticity modulus has been modified as

$$E^{\text{mod}} = \alpha \cdot E \quad (4.26)$$

where α is a factor that is established by controlling that the eigenfrequency and the deformation are equal to the values from hand calculations. This will give the beam grid the same total stiffness as the studied slab.

4.6.3 Verification of the model

A static analysis of the beam grid in ADINA has been carried out to verify the model. Figure 4.13 shows where the model plasticises just before the structure collapses, i.e. it shows the maximum plastic strain in the two different directions which are parallel to the sides. As can be seen there are some difference compared to the yield line model, see Figure 2.25c, used in hand and SDOF calculations.

In difference with the yield line figure the plasticised area is much larger for the FE-model. The difference depends on that the yield line theory is based on the assumption that all the plastic deformations takes place in one small deformable element, while in reality the plastic strain will be spread out to a larger area. Another difference noted is that the yield line model assumes that all the yield lines at the sides reaches the corners, but this is not the case in the FE-analysis, compare Figure 2.25c and Figure 4.13b. This difference arises because the yield line method assumes that the ultimate moment capacity is reached along the yield lines all the way to the corners, while in reality the slab will collapse before this happens. The reason for this collapse is unknown, but a consequence of it is that the FE-model will collapse for a lower load than the hand and SDOF calculations.

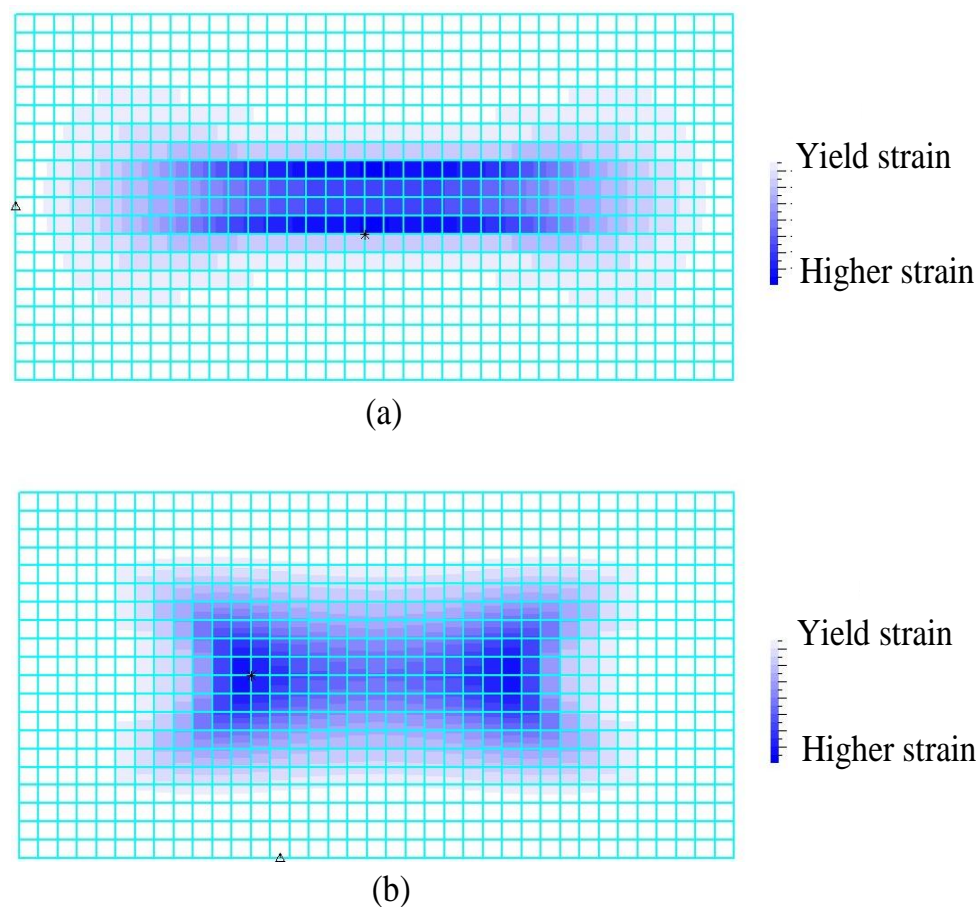


Figure 4.13 Plastic strain for an uniformly distributed static load. A very thin layer of shell elements are placed in the beam grid to get a visual effect. The strain is parallel to (a) long side (b) short side.

When verifying the ultimate moment capacity of a single beam in the beam grid for the FE-model it has a somewhat higher value than expected. The difference between the expected and obtained moment capacity corresponds to the torsional moment. As mentioned in Section 4.6.2.3 the torsional moment depends on the chosen mesh, so if an enough fine mesh is chosen the torsional moment will be small and the difference can be neglected.

4.7 Example – Simply supported slab

4.7.1 Scenario

A charge of 125 kg TNT detonates on a distance of 5 m from a building resulting in an impulse load of 2800 Ns/m^2 , with a maximum peak pressure of 5000 kPa, hitting one of the building sides. The building is a multi-story building with a height of 2.7 m for each floor. The wall facing the explosion is a reinforced concrete wall with a cross-section as shown in Figure 4.14. The amount of reinforcement is the same in both directions. Behind the wall there are columns placed at a distance of 5 meters from each other. The concrete wall is of quality C20/25 with reinforcement in class B500. Will the wall be able to resist the explosion?

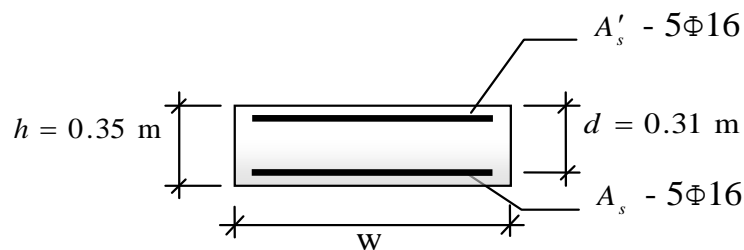


Figure 4.14 Rectangular cross-section of the studied wall.

The control will be made for four cases – uncracked (state I), cracked (state II), ideal plastic (state III) and the elastoplastic case.

4.7.2 Assumptions and simplifications

- The load is triangular and uniformly distributed over the entire wall.
- There are no windows or other irregularities in the wall.
- The connections between wall/slab and wall/column are free to rotate and the wall is not continuous over the floor slabs or columns.
- The supports are rigid.

With these assumptions the wall can be simplified to a $2.7 \times 5 \text{ m}$ long simply supported slab, see Figure 4.15.

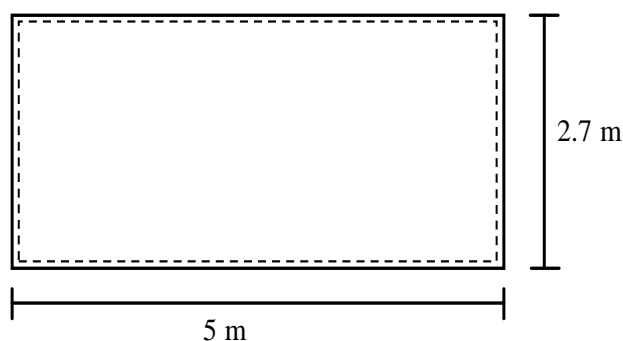


Figure 4.15 Dimensions of the slab.

This system can then further be simplified to a SDOF system with the equation of motion

$$\kappa_{mF} m \ddot{u} + R = F(t) \quad (4.27)$$

4.7.3 Transformed mass

The total mass for the slab is

$$m = \rho \cdot b \cdot h \cdot l = 2400 \cdot 5.0 \cdot 0.35 \cdot 2.7 = 11340 \text{ kg} \quad (4.28)$$

According to Table 4.1 the κ_{mF} is

$$\kappa_{mF,I} = \kappa_{mF,II} = 0.617 \quad (4.29)$$

for the elastic case and

$$\kappa_{mF,III} = 0.567 \quad (4.30)$$

for the plastic case. From equation (4.28), (4.29) and (4.30) the equivalent mass can be calculated to

$$m_I = m_{II} = \kappa_{mF,I} \cdot m = 0.617 \cdot 11340 = 6997 \text{ kg} \quad (4.31)$$

$$m_{III} = \kappa_{mF,III} \cdot m = 0.567 \cdot 11340 = 6430 \text{ kg} \quad (4.32)$$

4.7.4 Maximum static load

The maximum static load is here calculated with the virtual work principle and according to the yield line theory. The moment capacity for the slab per 1,0 m width in both directions is

$$M_{nd} = f_y A_s (d - \beta x) \quad (4.33)$$

The height of the compressed zone x is calculated as

$$x = \frac{f_y A_s}{\alpha f_{cc} w} = \frac{500 \cdot 1005}{0.81 \cdot 20 \cdot 1000} = 31 \text{ mm} \quad (4.34)$$

Equation (4.33) together with (4.34) gives the final moment capacity as

$$M_{nd} = 500 \cdot 1005 \cdot (310 - 0.416 \cdot 31) = 150 \text{ kNm} \quad (4.35)$$

The deformation has been normalized, i.e. set to 1, and Figure 4.16 can then be established.

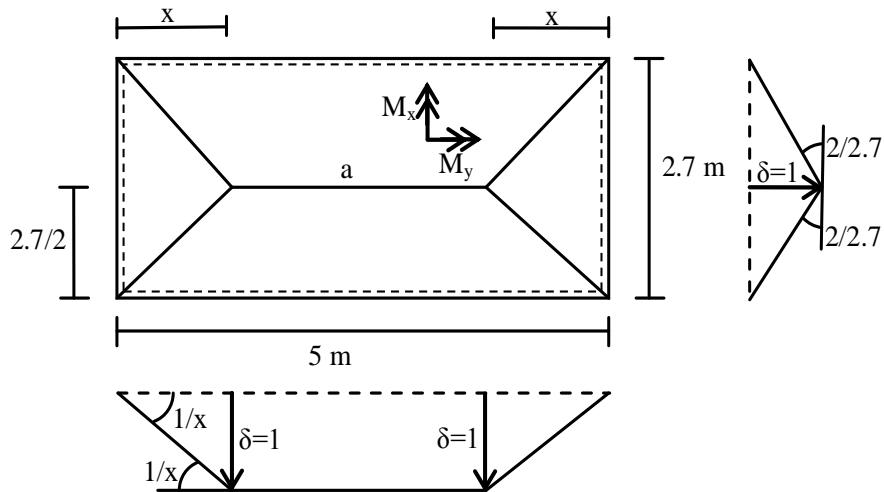


Figure 4.16 Collapse figure for a simply supported slab.

The external work is defined as

$$W_e = \sum q_i A_i \delta_{TP,i} \quad (4.36)$$

and by dividing the slab into different parts as shown in Figure 4.17, the external work can be calculated to

$$\begin{aligned} W_e &= q_1 \cdot A_1 \cdot \delta_{TP,1} \cdot 2 + q_2 \cdot A_2 \cdot \delta_{TP,2} \cdot 4 + q_3 \cdot A_3 \cdot \delta_{TP,3} \cdot 2 = \\ &= q_1 \cdot \frac{2.7}{2} \cdot (5 - 2x) \cdot \frac{1}{2} \cdot 2 + q_2 \cdot \frac{\frac{2.7}{2} \cdot x}{2} \cdot \frac{1}{3} \cdot 4 + q_3 \cdot \frac{2.7 \cdot x}{2} \cdot \frac{1}{3} \cdot 2 = \\ &= q \cdot \left((5 - 2 \cdot x) \cdot 2.7 \cdot \frac{1}{2} + 2 \cdot x \cdot l \cdot \frac{1}{3} \right) = q \cdot \left(\frac{5 \cdot 2.7}{2} - \frac{x \cdot 2.7}{3} \right) \end{aligned} \quad (4.37)$$

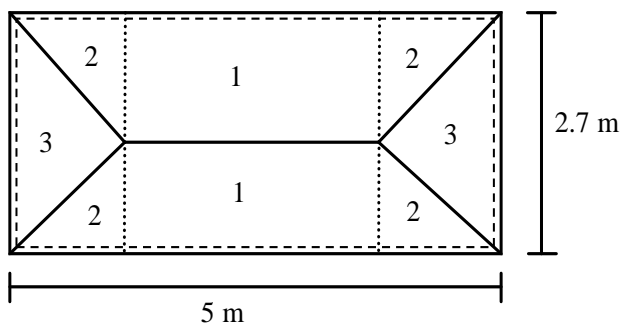


Figure 4.17 The slab divided into 3 different parts.

The internal work is defined as

$$W_i = \sum M_i l_i \theta_i \quad (4.38)$$

and with current indata

$$W_i = 150 \cdot 10^3 \cdot 2.7 \cdot \frac{1}{x} \cdot 2 + 150 \cdot 10^3 \cdot 5 \cdot \left(\frac{2}{2.7} + \frac{2}{2.7} \right) = \frac{810 \cdot 10^3}{x} + \frac{3000 \cdot 10^3}{2.7} \quad (4.39)$$

By setting the external work equal to the internal work the uniformly distributed load q can be described by a function of x as

$$q = \frac{810 \cdot 10^3}{6.75x - 0.9x^2} + \frac{\left(\frac{3 \cdot 10^6}{2.7} \right)}{6.75 - 0.9x} \quad (4.40)$$

The maximum distributed load is calculated by differentiating the equation (4.40) with regard to x and setting it equal to zero

$$\frac{dq}{dx} = \frac{1000 \cdot 10^3}{(6.75 - 0.9x)^2} - \frac{810 \cdot 10^3 \cdot (6.75 - 1.8x)}{(6.75x - 0.9x^2)^2} = 0 \quad x_1 = 1.720 \text{ m} \quad x_2 = -3.178 \text{ m} \quad (4.41)$$

The second value is obviously only a theoretical value since the length must be positive. The first value is shorter than the length of the slab so the right mechanism has been chosen. Inserting x_1 into equation (4.40) the maximum distributed load can be calculated to

$$q = \frac{810 \cdot 10^3}{6.75 \cdot 1.720 - 0.9 \cdot 1.720^2} + \frac{\left(\frac{3 \cdot 10^6}{2.7} \right)}{6.75 - 0.9 \cdot 1.720} = 304 \text{ kN/m}^2 \quad (4.42)$$

4.7.5 Stiffness and internal resistance

The stiffness of a slab can be expressed as

$$k = \frac{Q}{u} = \frac{qlw}{u_{\max}} \quad (4.43)$$

where the maximum deformation u_{\max} is according to equation (2.40)

$$u_{\max} = \frac{16q}{\pi^6 D} \sum_{m=1}^{\infty} \sum_{n=1}^{\infty} \frac{(-1)^{\frac{m+n}{2}-1}}{mn \left(\frac{m^2}{w^2} + \frac{n^2}{l^2} \right)^2} \quad (4.44)$$

and the flexural rigidity D is

$$D = \frac{EI}{1 - \nu^2} \quad (4.45)$$

Usually a Poisson's ratio of 0.2 is used for concrete. However, it has here been set to 0 in order to reduce the parameters that can differ between the models. Usually, a

Poisson's ratio of 0.2 is used for a concrete slab. The moment of inertia for the uncracked cross section is calculated in Section 3.6.4 and is according to equation (3.34)

$$I_I = 3.57 \cdot 10^9 \text{ mm}^4 \quad (4.46)$$

The cracked behaviour of a slab is rather complex. When the stresses increases the slab will crack and the stiffness in the different directions will no longer be equal. However, in this example the cracked behaviour has been simplified to have a constant stiffness, i.e. the same simplification as in the beam model. The moment of inertia can then be calculated in the same way as for the beam, i.e. the moment of inertia for the cracked cross section is according to equation (3.42)

$$I_{II} = 4.8 \cdot 10^8 \text{ mm}^4 \quad (4.47)$$

With current indata the flexural rigidity D can be calculated to

$$D_I = \frac{30 \cdot 10^3 \cdot 3.57 \cdot 10^9}{1 - 0^2} = 107.1 \cdot 10^{12} \text{ Nmm}^2 = 107.1 \cdot 10^6 \text{ Nm}^2 \quad (4.48)$$

$$D_{II} = \frac{30 \cdot 10^3 \cdot 4.8 \cdot 10^8}{1 - 0^2} = 14.8 \cdot 10^{12} \text{ Nmm}^2 = 14.8 \cdot 10^6 \text{ Nm}^2 \quad (4.49)$$

The double summation in equation (4.44) converges rapidly and a good approximation can be found by only taking the two first term of the series. The maximum deformation is then equal to

$$u_{\max, I} = \frac{16 \cdot q}{\pi^6 D_I} \sum_{m=1}^3 \sum_{n=1}^3 \frac{(-1)^{\frac{m+n}{2}-1}}{mn \left(\frac{m^2}{w^2} + \frac{n^2}{l^2} \right)^2} = \frac{16 \cdot q}{\pi^6 \cdot 107.1 \cdot 10^6} \cdot 30.32 = q \cdot 4.71 \cdot 10^{-9} \quad (4.50)$$

$$u_{\max, II} = \frac{16 \cdot q}{\pi^6 D_{II}} \sum_{m=1}^{\infty} \sum_{n=1}^{\infty} \frac{(-1)^{\frac{m+n}{2}-1}}{mn \left(\frac{m^2}{w^2} + \frac{n^2}{l^2} \right)^2} = \frac{16 \cdot q}{\pi^6 \cdot 14.8 \cdot 10^6} \cdot 30.32 = q \cdot 3.41 \cdot 10^{-8} \quad (4.51)$$

and the stiffness can finally be calculated to

$$k_I = \frac{Q}{u} = \frac{qlw}{u_{\max}} = \frac{q \cdot 2.7 \cdot 5}{q \cdot 4.71 \cdot 10^{-9}} = 2.86 \cdot 10^9 \quad (4.52)$$

$$k_{II} = \frac{Q}{u} = \frac{qlw}{u_{\max}} = \frac{q \cdot 2.7 \cdot 5}{q \cdot 3.41 \cdot 10^{-8}} = 3.96 \cdot 10^8 \quad (4.53)$$

The internal resistance is calculated as

$$R = q \cdot l \cdot w \quad (4.54)$$

And with current indata

$$R = 304 \cdot 10^3 \cdot 2.7 \cdot 5 = 4104 \text{ kN} \quad (4.55)$$

4.7.6 Required deformations

The total impulse load on the slab is

$$I = w \cdot l \cdot i = 5 \cdot 2.7 \cdot 2800 = 37800 \text{ Ns} \quad (4.56)$$

The elastic deformation is calculated as

$$u_{el} = \frac{I}{\sqrt{m_e k}} \quad (4.57)$$

which for the uncracked state gives

$$u_I = \frac{37800}{\sqrt{6997 \cdot 2.86 \cdot 10^9}} = 8.5 \text{ mm} \quad (4.58)$$

and for the cracked state

$$u_{II} = \frac{37800}{\sqrt{6997 \cdot 3.96 \cdot 10^8}} = 22.7 \text{ mm} \quad (4.59)$$

The plastic deformation is given by

$$u_{pl} = \frac{I^2}{2Rm_e} \quad (4.60)$$

and with current indata

$$u_{III} = \frac{37800^2}{2 \cdot 4104 \cdot 10^3 \cdot 6430} = 27.1 \text{ mm} \quad (4.61)$$

The elastoplastic material will have a larger total deformation than the ideal plastic material but less plastic deformations. Since it is only the plastic deformations that affect the capacity the elastoplastic material will be able to carry more load than the ideal plastic material. The maximum deformation for the elastic part is calculated as

$$u_{ep,II} = \frac{R}{k} = \frac{4104 \cdot 10^3}{3.96 \cdot 10^8} = 10.4 \text{ mm} \quad (4.62)$$

and the plastic reduction will therefore be

$$\Delta u_{III} = \frac{u_{ep,II}}{2} = 5.2 \text{ mm} \quad (4.63)$$

This will give the plastic deformation

$$u_{ep,III} = u_{III} - \Delta u_{III} = 27.1 - 5.2 = 21.9 \text{ mm} \quad (4.64)$$

and the total elastoplastic deformation can be calculated to

$$u_{ep} = u_{ep,II} + u_{ep,III} = 10.4 + 21.9 = 32.3 \text{ mm} \quad (4.65)$$

4.7.7 Equivalent static load

The equivalent static load for the elastic material can be calculated by rearranging equation (2.40) to

$$q_e = \frac{\pi^6 D}{16} \frac{u}{\sum_{m=1}^{\infty} \sum_{n=1}^{\infty} \frac{(-1)^{m+n-1}}{mn \left(\frac{m^2}{w^2} + \frac{n^2}{l^2} \right)^2}} \quad (4.66)$$

So, the equivalent static load for the uncracked state is

$$q_{e,I} = \frac{\pi^6 \cdot 107.1 \cdot 10^6}{16} \frac{8.5 \cdot 10^{-3}}{30.32} = 1084 \text{ kN/m}^2 \quad (4.67)$$

and for the cracked state

$$q_{e,II} = \frac{\pi^6 \cdot 14.8 \cdot 10^6}{16} \frac{22.7 \cdot 10^{-3}}{30.32} = 666 \text{ kN/m}^2 \quad (4.68)$$

The equivalent static load for the plastic material was calculated in Section 0 and is according to equation (4.42) equal to

$$q_{e,III} = 304 \text{ kN/m}^2 \quad (4.69)$$

The maximum field moments for the elastic material is according to Timoshenko (1959)

$$M_{x,\max} = \beta q a^2 \quad (4.70)$$

$$M_{y,\max} = \beta_1 q a^2 \quad (4.71)$$

where β and β_1 are tabulated values and a is the length of the shortest side. These values, β and β_1 , can be found in Timoshenko (1959, p. 120, table 8) and are for this example equal to

$$\beta = 0.09665 \quad (4.72)$$

$$\beta_1 = 0.0475 \quad (4.73)$$

The elastic maximum field moment can now be calculated for the uncracked state to

$$M_{x.\max} = 0.09665 \cdot 1084 \cdot 2.7^2 = 764 \text{ kNm} \quad (4.74)$$

$$M_{y.\max} = 0.0475 \cdot 1084 \cdot 2.7^2 = 375 \text{ kNm} \quad (4.75)$$

and for the cracked state to

$$M_{x.\max} = 0.09665 \cdot 666 \cdot 2.7^2 = 469 \text{ kNm} \quad (4.76)$$

$$M_{y.\max} = 0.0475 \cdot 666 \cdot 2.7^2 = 231 \text{ kNm} \quad (4.77)$$

The maximum moment for the plastic material is equal to the maximum moment capacity M_{rd} , which is according to (4.35)

$$M_{rd} = M_{x.\max} = 150 \text{ kNm} \quad (4.78)$$

Since the system point is in the middle of the slab and the yield line method only carry the load in one direction for this point, no moments will arise in the other direction. This means that the moment in y direction M_y is equal to zero.

4.7.8 Maximum deformation capacity

Similar to the beam model the deformation capacity for the elastic slab is controlled by a static calculation for the equivalent load. For the plastic and elastoplastic material a control of the rotation capacity will be done.

According to Johansson and Laine (2009) the diagram in Eurocode 2 CEN (2004), see Figure 4.18, can be used for impulse loaded structures.

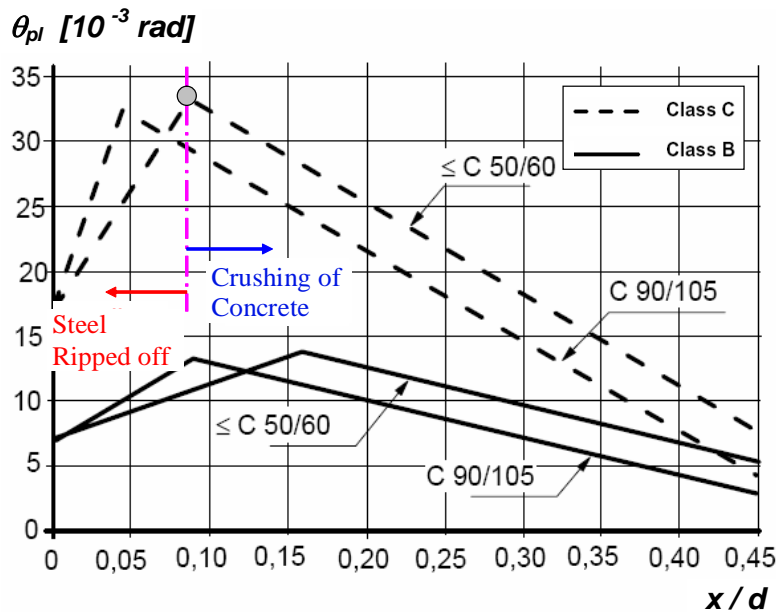


Figure 4.18 Diagram from Eurocode 2 CEN (2004) showing plastic rotation capacity. From Johansson and Laine (2009).

The diagram can only be used for concrete quality lower than C50/60 if

$$\frac{x}{d} \leq 0.45 \quad (4.79)$$

and with current indata

$$\frac{x}{d} = \frac{31}{310} = 0.1 \leq 0.45 \quad (4.80)$$

this is okay.

The shear slenderness is calculated as

$$\lambda = \frac{x_0}{d} \quad (4.81)$$

where x_0 is the distance between the maximum moment and the zero moment. To be on the safe side the minimum shear slenderness of the different directions is used, see Figure 4.19.

The shear slenderness can then be calculated for the different directions to

$$\lambda_x = \frac{x_{0,x}}{d} = \frac{2700 / 2}{310} = 4.35 \quad (4.82)$$

$$\lambda_y = \frac{x_{0,y}}{d} = \frac{1720}{310} = 5.55 \quad (4.83)$$

and since the shear slenderness is larger than three, the rotation capacity can be multiplied with a factor of

$$k_{\lambda} = \sqrt{\frac{4.35}{4}} = 1.2 \quad (4.84)$$

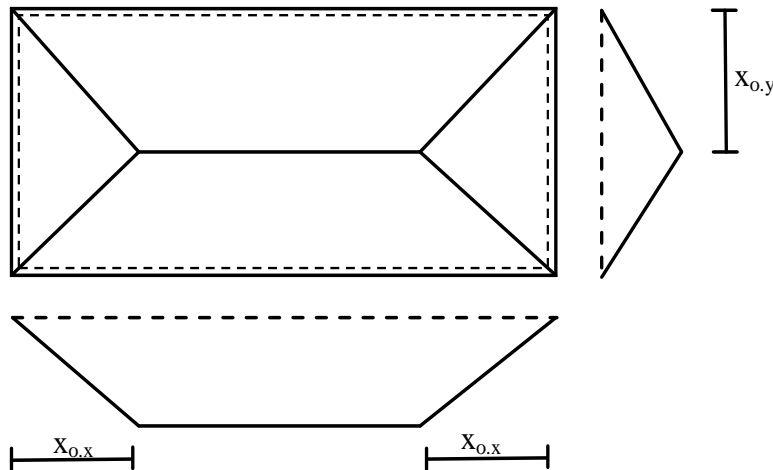


Figure 4.19 Simply supported slab showing distance x_0 .

So, with a concrete quality of C20/25, the reinforcement in class B and the x/d ratio of 0.1 the plastic rotation capacity is according to Figure 4.18

$$\theta = 11 \cdot 10^{-3} \text{ rad} \quad (4.85)$$

and with the k_{λ} factor the plastic rotation is

$$\theta_{pl} = \theta \cdot k_{\lambda} = 11 \cdot 10^{-3} \cdot 1.2 = 13.2 \cdot 10^{-3} \text{ rad} \quad (4.86)$$

The maximum deformation capacity for the slab can now be calculated to

$$u_{rd} = \frac{\theta \cdot l}{2} = \frac{13.2 \cdot 10^{-3} \cdot 2.7}{2} = 17.8 \text{ mm} \quad (4.87)$$

4.7.9 Results

The deformation required is larger than the deformation capacity for both plastic and elastoplastic case so the slab will not be able to resist the explosion. Since the plastic capacity, state III, is too low the cracked and uncracked, state I and state II, will also be too low and no calculations on elastic case is necessary.

The elastic deformations over the time are shown in Figure 4.20. As can be seen the different methods coincide rather well.

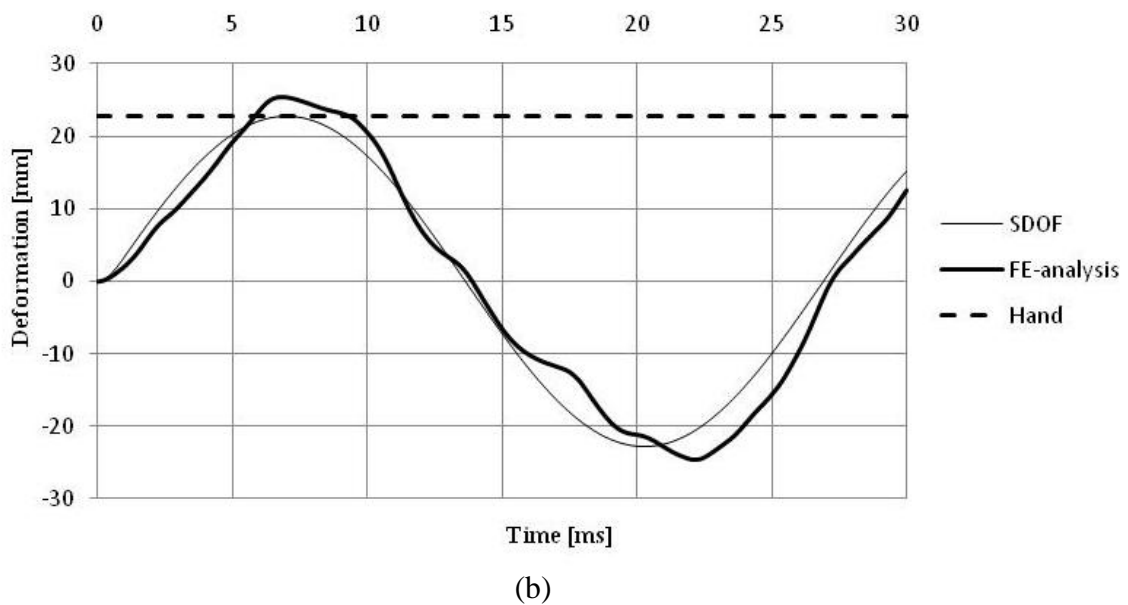
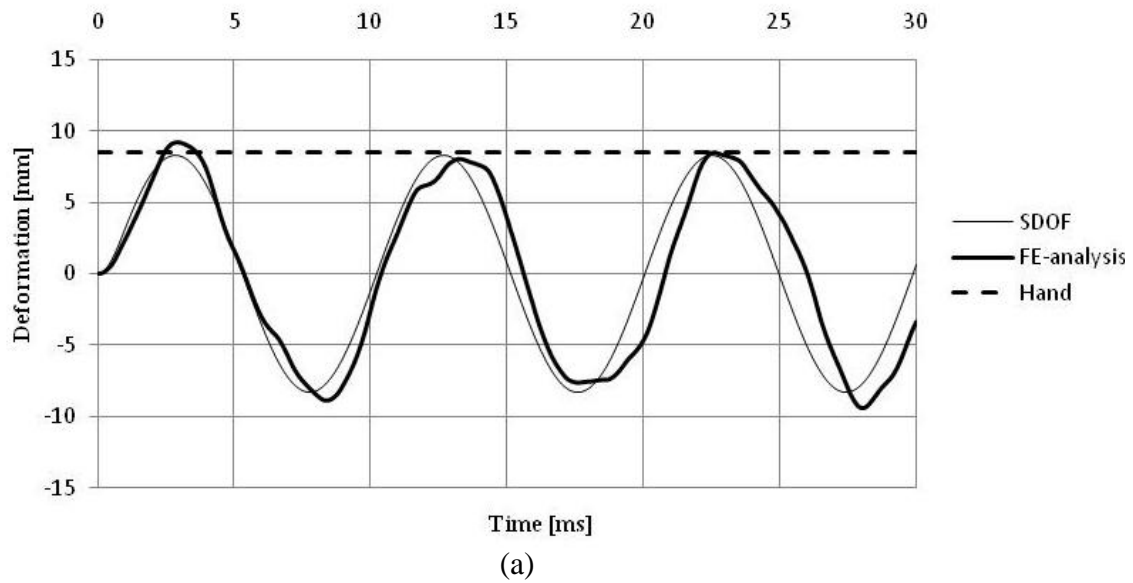
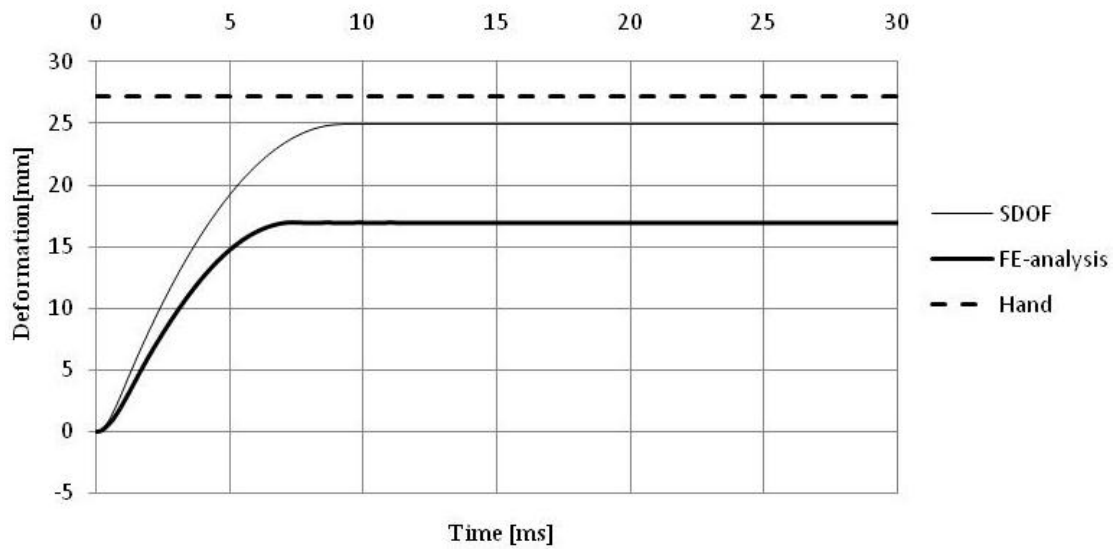
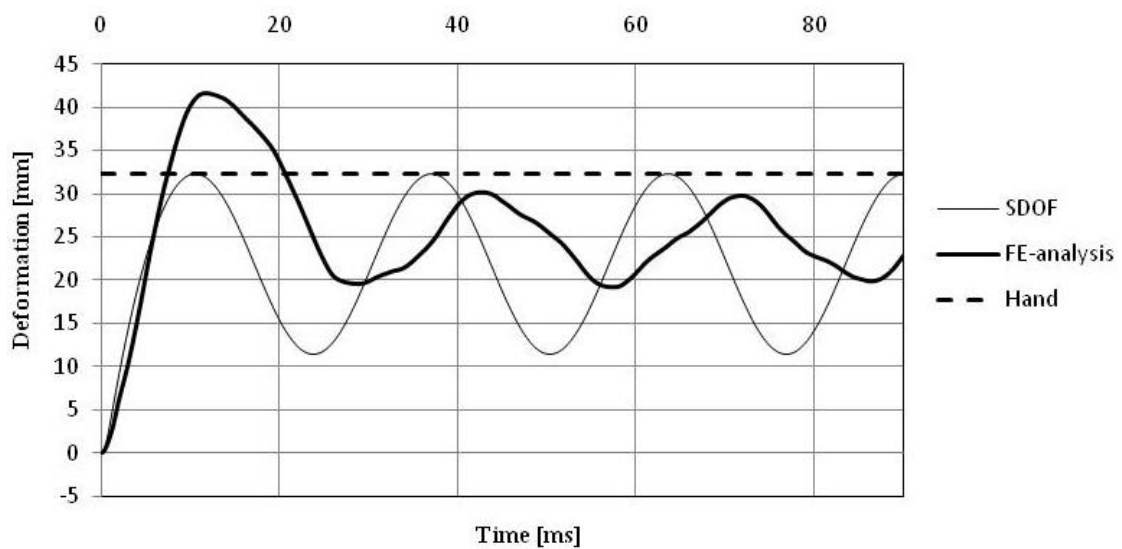


Figure 4.20 Deformations over time for (a) uncracked case (b) cracked case.

The plastic and elastoplastic deformations over time are shown in Figure 4.21. Here, a large divergence is found between the maximum values for SDOF and FE-analysis while the hand and SDOF calculations coincide well. Further discussion on the divergence that arises for the FE-analysis is carried out in Section 4.9.



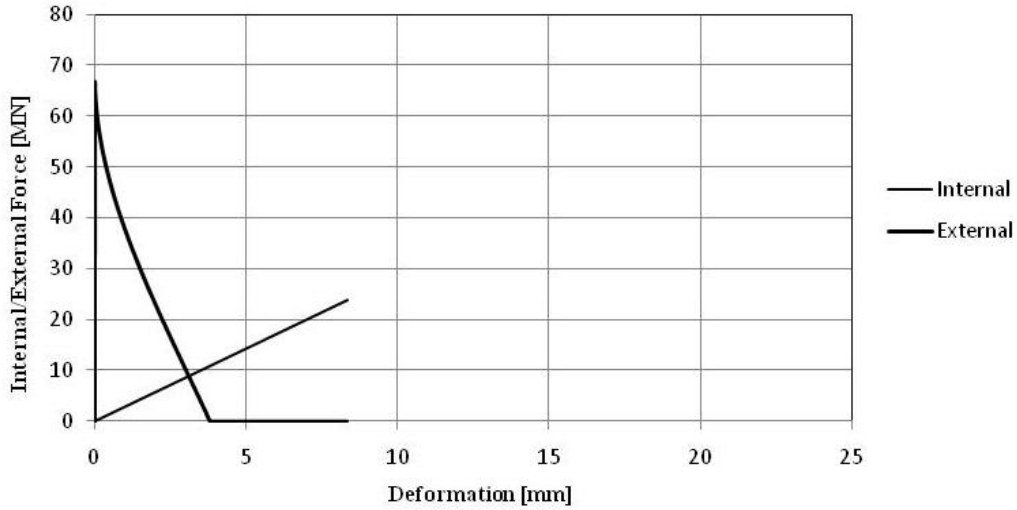
(a)



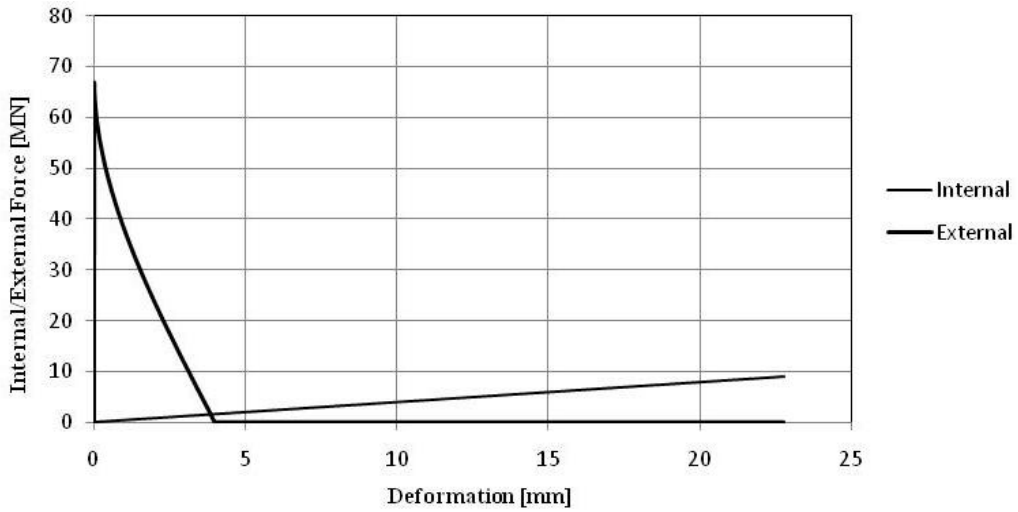
(b)

Figure 4.21 Deformations over time for (a) plastic case (b) elastoplastic case.

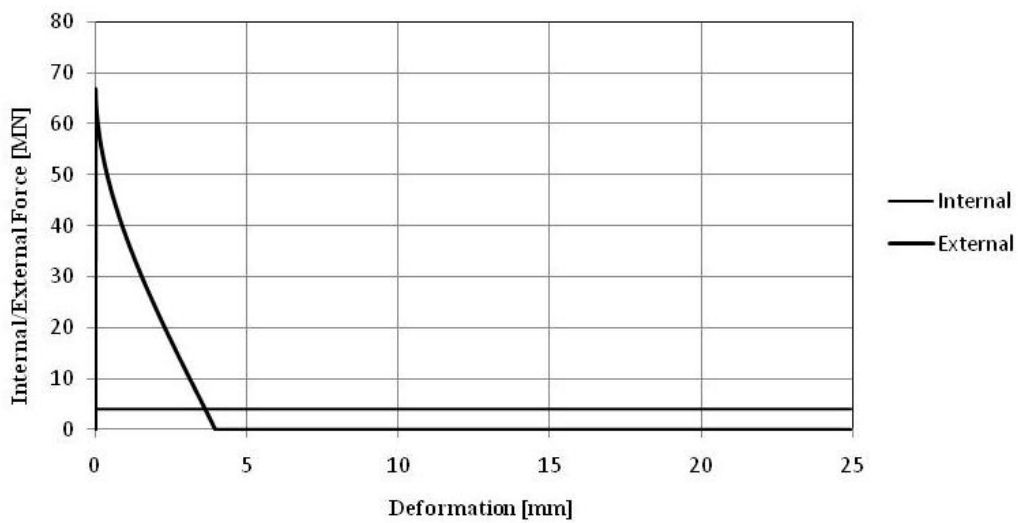
The relation between the force and deformation for elastic and plastic cases in the SDOF calculation is shown in Figure 4.22. The area under the curves is equal to the executed work and should be the same for both the internal and external work.



(a)



(b)



(c)

Figure 4.22 The relation between force and deformation for (a) uncracked case (b) cracked case (c) plastic case.

The internal work is calculated from Figure 4.22 to

$$W_{I,i} = \frac{2.38 \cdot 10^7 \cdot 8.34 \cdot 10^{-3}}{2} = 99.2 \text{ kJ} \quad (4.88)$$

$$W_{II,i} = \frac{8.92 \cdot 10^6 \cdot 22.78 \cdot 10^{-3}}{2} = 101.6 \text{ kJ} \quad (4.89)$$

$$W_{III,i} = 4.09 \cdot 10^6 \cdot 24.94 \cdot 10^{-3} = 101.89 \text{ kJ} \quad (4.90)$$

The external work is calculated with the equation

$$W_e = \frac{I_c^2}{2m} \quad (4.91)$$

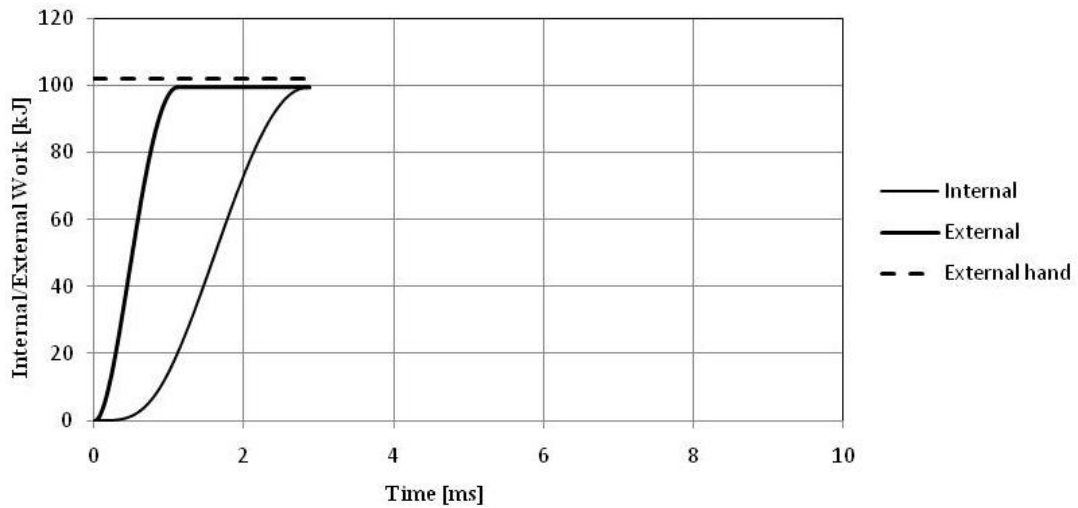
and with current indata

$$W_{I,II,e} = \frac{37800^2}{2 \cdot 6997} = 102.10 \text{ kJ} \quad (4.92)$$

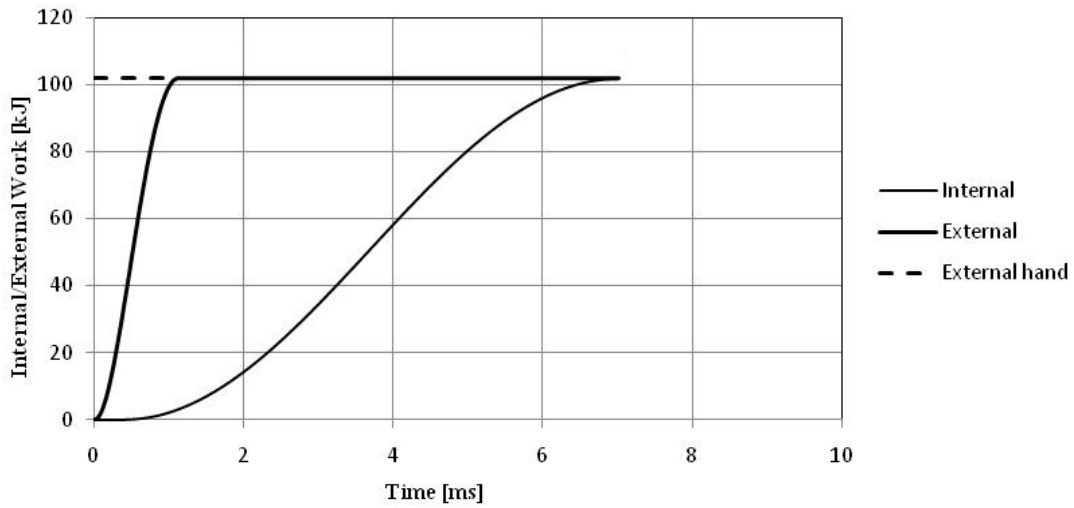
$$W_{III,e} = \frac{37800^2}{2 \cdot 6430} = 111.11 \text{ kJ} \quad (4.93)$$

The difference between the internal and external work depends on the assumption about a characteristic load in the hand calculations. The internal work that is based on the SDOF system will always be lower or equal to the external work that is based on the hand calculations. The divergence will be smaller the shorter the load is applied. This difference can be calculated with so called damage curves, the reader is referred to Johansson and Laine (2009). What can be seen for this example is that the difference is larger for the plastic case than for the elastic case.

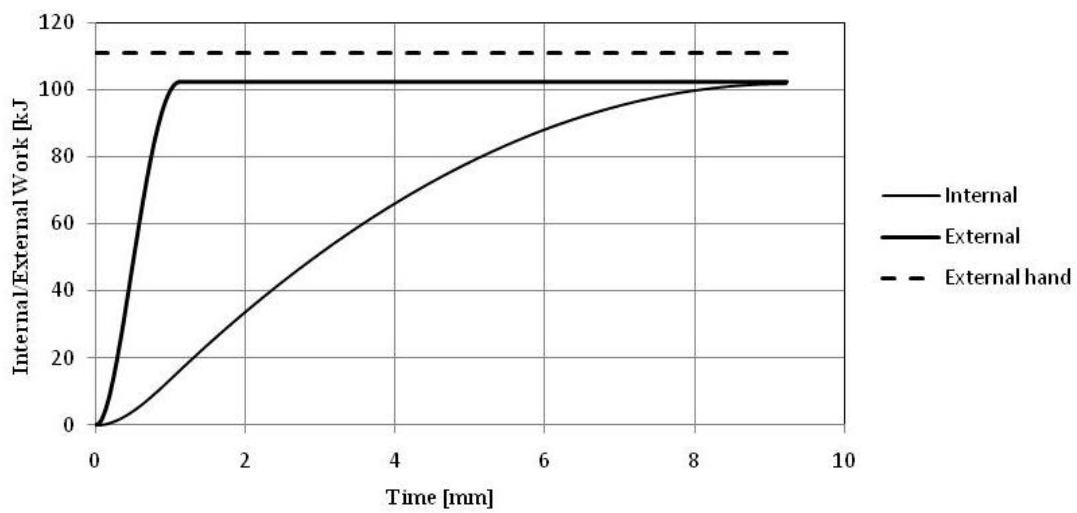
The work over time is shown in Figure 4.23. What can be seen here, except for the divergence between hand and SDOF calculations, is that the plastic case needs the longest time to fully develop its internal resistance while the cracked case has the shortest time. This is logical since the plastic case also has the largest deformation while the uncracked case has the smallest.



(a)



(b)



(c)

Figure 4.23 The relation between work and time for (a) uncracked case (b) cracked case (c) plastic case.

4.8 Example – Fully fixed slab

4.8.1 Scenario, assumptions and simplifications

The same scenario as in the previous example, Section 4.7, is here studied. The only difference is the connections wall to slab which are assumed to be fully fixed in contrast to previous example, where they were assumed to be free to rotate. The control will be made for two cases – Ideal plastic (state III) and elastoplastic case.

With these assumptions the wall can be simplified to a 2.7x5 m long fully fixed slab, see Figure 4.24, and further on to a SDOF system with the equation of motion equal to

$$\kappa_{mF} m \ddot{u} + R = F(t) \quad (4.94)$$

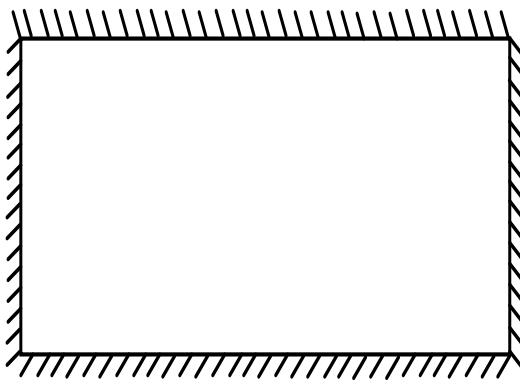


Figure 4.24 A fully fixed slab

4.8.2 Transformed mass

The total mass for the slab is

$$m = \rho \cdot b \cdot h \cdot l = 2400 \cdot 5.0 \cdot 0.35 \cdot 2.7 = 11340 \text{ kg} \quad (4.95)$$

According to Table 4.1 the κ_{mF} is

$$\kappa_{mF,III} = 0.567 \quad (4.96)$$

for the plastic case. From equation (4.95) and (4.96) the equivalent mass can be calculated to

$$m_{III} = \kappa_{mF,III} \cdot m = 0.567 \cdot 11340 = 6430 \text{ kg} \quad (4.97)$$

which is the same as for the simply supported slab studied in previous example.

4.8.3 Maximum static load

The field and support moment capacity for the fully fixed slab is also the same as the field moment capacity for the simply supported slab, i.e.

$$M_{nd} = 500 \cdot 1005 \cdot (310 - 0.416 \cdot 31) = 150 \text{ kNm} \quad (4.98)$$

The deformation figure is assumed to have the shape as shown in Figure 4.30.

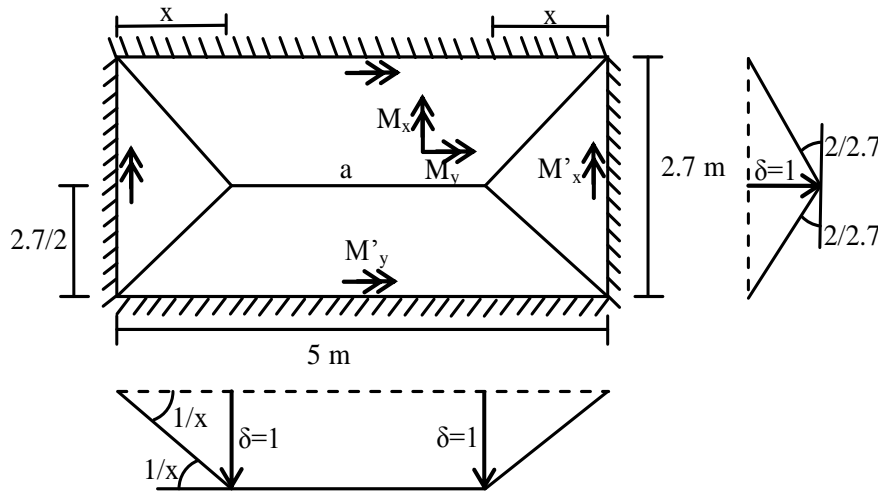


Figure 4.25 Collapse figure for a fully fixed slab.

The external work is defined as

$$W_e = \sum q_i A_i \delta_{TP,i} \quad (4.99)$$

and by dividing the slab into different parts as shown in Figure 4.29, the external work can be calculated to

$$\begin{aligned} W_e &= q_1 \cdot A_i \cdot \delta_{TP,i} \cdot 2 + q_2 \cdot A_i \cdot \delta_{TP,i} \cdot 4 + q_3 \cdot A_i \cdot \delta_{TP,i} \cdot 2 = \\ &= q_1 \cdot \frac{2.7}{2} \cdot (5 - 2x) \cdot \frac{1}{2} \cdot 2 + q_2 \cdot \frac{2.7}{2} \cdot x \cdot \frac{1}{2} \cdot 4 + q_3 \cdot \frac{2.7}{2} \cdot x \cdot \frac{1}{2} \cdot 2 = \\ &= q \cdot \left((5 - 2 \cdot x) \cdot 2.7 \cdot \frac{1}{2} + 2 \cdot x \cdot l \cdot \frac{1}{3} \right) = q \cdot \left(\frac{5 \cdot 2.7}{2} - \frac{x \cdot 2.7}{3} \right) \end{aligned} \quad (4.100)$$

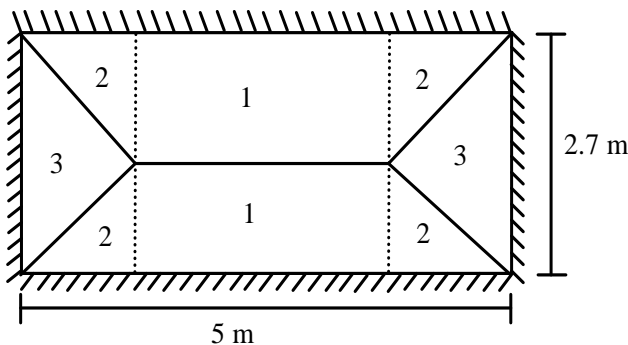


Figure 4.26 The slab divided into 3 different parts.

The internal work is defined as

$$W_i = \sum M_i l_i \theta_i \quad (4.101)$$

and with current indata

$$W_i = 150 \cdot 10^3 \cdot 2.7 \cdot \frac{1}{x} \cdot 2 + 150 \cdot 10^3 \cdot 5 \cdot \left(\frac{2}{2.7} + \frac{2}{2.7} \right) + 150 \cdot 10^3 \cdot 2.7 \cdot \frac{1}{x} + 150 \cdot 10^3 \cdot 5 \cdot \frac{1}{\left(\frac{2.7}{2} \right)} \cdot 2 = \frac{1620 \cdot 10^3}{x} + \frac{6000 \cdot 10^3}{2.7} \quad (4.102)$$

By setting the external work equal to the internal work the uniformly distributed load q can be described by a function of x as

$$q = \frac{1620 \cdot 10^3}{6.75x - 0.9x^2} + \frac{\left(\frac{6 \cdot 10^6}{2.7} \right)}{6.75 - 0.9x} \quad (4.103)$$

The maximum distributed load is calculated by differentiating the equation (4.103) with regard to x and setting it equal to zero

$$\frac{dq}{dx} = \frac{2000 \cdot 10^3}{(6.75 - 0.9x)^2} - \frac{1620 \cdot 10^3 \cdot (6.75 - 1.8x)}{(6.75x - 0.9x^2)^2} = 0 \quad (4.104)$$

$$x_1 = 1.720 \text{ m} \quad x_2 = -3.178 \text{ m}$$

The second value is obviously only a theoretical value since the length must be positive. The first value is shorter than the length of the slab so the right mechanism has been chosen. Inserting x_1 into equation (4.103) the maximum distributed load can be calculated to

$$q = \frac{1620 \cdot 10^3}{6.75 \cdot 1.720 - 0.9 \cdot 1.720^2} + \frac{\left(\frac{6 \cdot 10^6}{2.7} \right)}{6.75 - 0.9 \cdot 1.720} = 608 \text{ kN/m}^2 \quad (4.105)$$

4.8.4 Stiffness and internal resistance

The stiffness of a fully fixed slab can be expressed as

$$k = \frac{Q}{u} = \frac{qlw}{u_{\max}} \quad (4.106)$$

where maximum deformation u_{\max} for a slab with the length and width ratio of 1.75 can, according to Timoshenko (1959), be calculated as

$$u_{\max} = \frac{0.00247 \cdot q \cdot l^4}{D} \quad (4.107)$$

The flexural rigidity D is calculated in the same way as for the simply supported slab and is for the cracked case equal to

$$D_{II} = 14.8 \cdot 10^6 \text{ Nm}^2 \quad (4.108)$$

The maximum deformation can then be calculated to

$$u_{\max} = \frac{0.00247 \cdot q \cdot 2.7^4}{14.8 \cdot 10^6} = q \cdot 8.869 \cdot 10^{-9} \quad (4.109)$$

and the stiffness is then equal to

$$k_{II} = \frac{Q}{u} = \frac{qlw}{u_{\max}} = \frac{q \cdot 2.7 \cdot 5}{q \cdot 8.869 \cdot 10^{-9}} = 1.52 \cdot 10^9 \quad (4.110)$$

The internal resistance is calculated as

$$R = q \cdot l \cdot w \quad (4.111)$$

And with current indata

$$R = 608 \cdot 10^3 \cdot 2.7 \cdot 5 = 8208 \text{ kN} \quad (4.112)$$

4.8.5 Required deformations

The total impulse load on the slab is

$$I = w \cdot l \cdot i = 5 \cdot 2.7 \cdot 2800 = 37800 \text{ Ns} \quad (4.113)$$

The plastic deformation is given by the equation

$$u_{pl} = \frac{I^2}{2Rm_e} \quad (4.114)$$

and with current indata

$$u_{III} = \frac{37800^2}{2 \cdot 8208 \cdot 10^3 \cdot 6430} = 13.5 \text{ mm} \quad (4.115)$$

The maximum deformation for the elastic part is calculated to

$$u_{ep,II} = \frac{R}{k} = \frac{8208 \cdot 10^3}{1.52 \cdot 10^9} = 5.4 \text{ mm} \quad (4.116)$$

and the plastic reduction will therefore be

$$\Delta u_{III} = \frac{u_{ep,II}}{2} = 2.7 \text{ mm} \quad (4.117)$$

This will give the plastic deformation

$$u_{ep.III} = u_{III} - \Delta u_{III} = 13.5 - 2.7 = 10.8 \text{ mm} \quad (4.118)$$

and the total elastoplastic deformation can be calculated to

$$u_{ep} = u_{ep.II} + u_{ep.III} = 5.4 + 10.8 = 16.2 \text{ mm} \quad (4.119)$$

4.8.6 Maximum deformation capacity

The diagram in Figure 4.18 can only be used for concrete quality lower than C50/60 if

$$\frac{x}{d} \leq 0.45 \quad (4.120)$$

and with current indata

$$\frac{x}{d} = \frac{31}{310} = 0.1 \leq 0.45 \quad (4.121)$$

which is okay.

The shear slenderness is calculated as

$$\lambda = \frac{x_0}{d} \quad (4.122)$$

where x_0 is the distance between the maximum moment and the zero moment. Since the maximum moment will occur both in the middle of the slab and at the supports, x_0 will be approximately half of the length of x , see Figure 4.25, in the x-direction and approximately a fourth of the length l in y-direction. To be on the safe side the minimum shear slenderness of the different directions is used, see Figure 4.27.

The shear slenderness can then be calculated for the different directions to

$$\lambda_x = \frac{x_{0,x}}{d} = \frac{2700 / 4}{310} = 2.18 \quad (4.123)$$

$$\lambda_y = \frac{x_{0,y}}{d} = \frac{1720 / 2}{310} = 2.77 \quad (4.124)$$

and since the shear slenderness is less than three, no modification of the rotation capacity is needed.

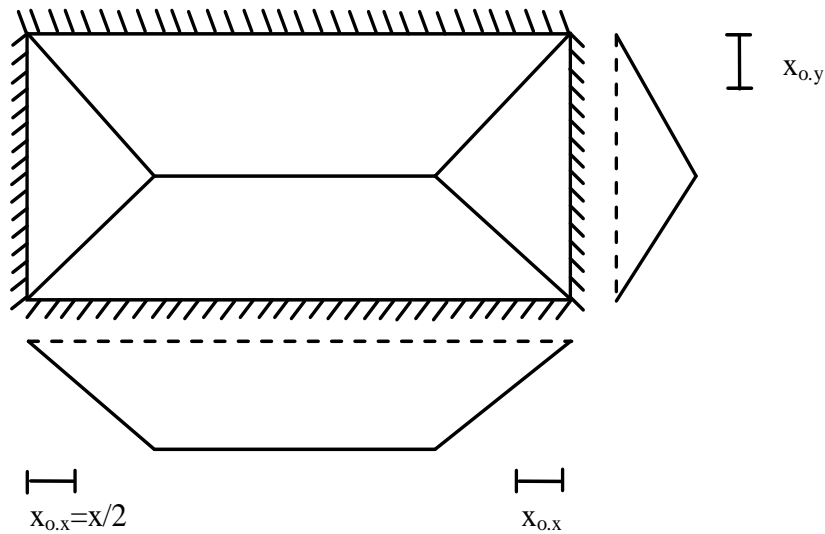


Figure 4.27 Fully fixed slab showing distance x_0 .

So, with a concrete quality of C20/25, the reinforcement in class B and the x/d ratio of 0.1 the plastic rotation capacity is according to Figure 4.18

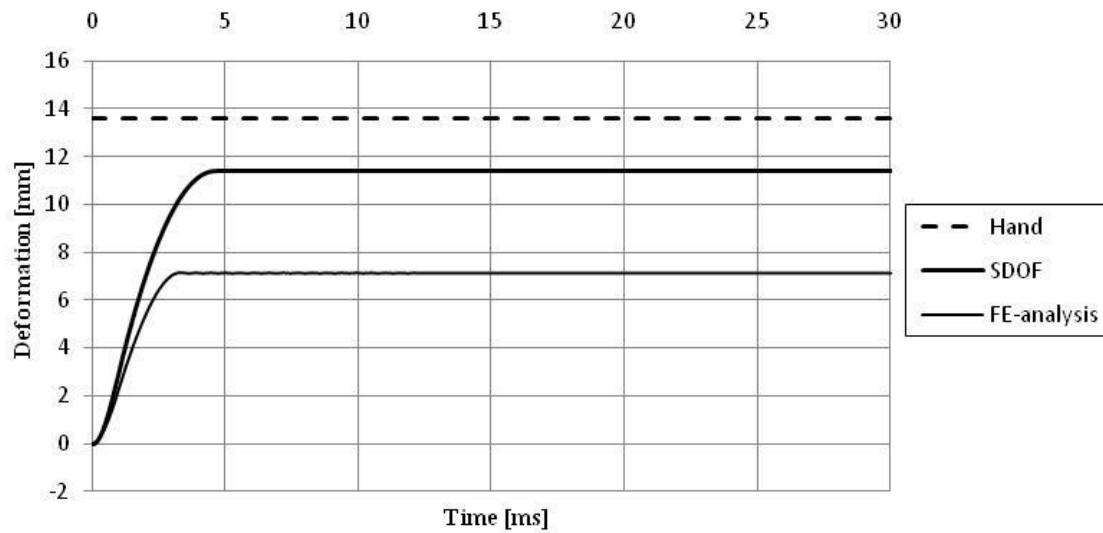
$$\theta = 11 \cdot 10^{-3} \text{ rad} \quad (4.125)$$

The maximum deformation capacity for the slab can now be calculated to

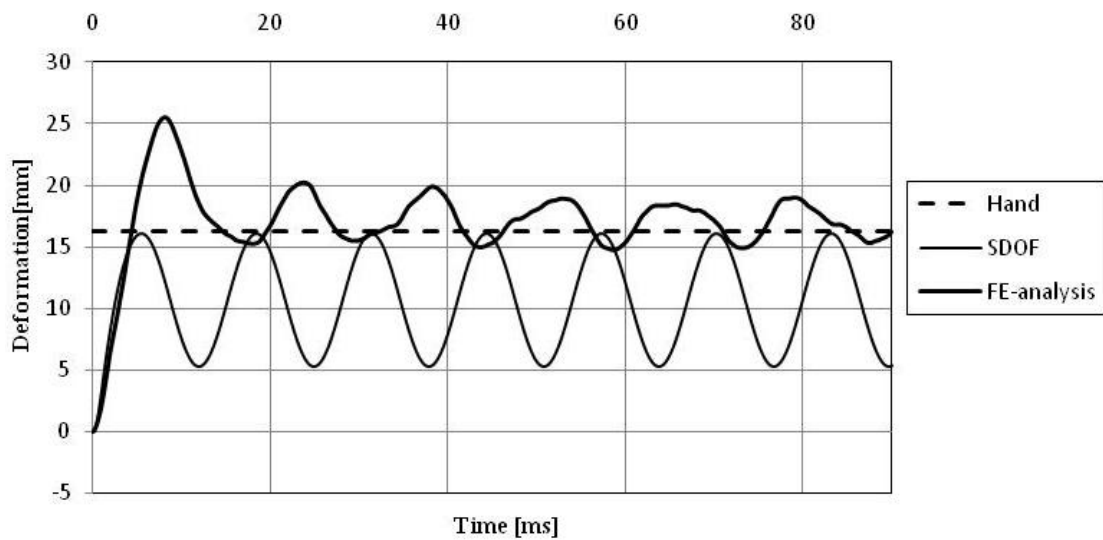
$$u_{rd} = \frac{\theta \cdot l}{2} = \frac{11 \cdot 10^{-3} \cdot 2.7}{2} = 14.8 \text{ mm} \quad (4.126)$$

4.8.7 Results

The slab will be able to resist the load for both the plastic and elastoplastic response. The deformation over time for the different cases is shown in Figure 4.28. As in the simply supported analyses a divergence is found between the SDOF and FE-analysis, but here it is larger. Further discussion on this subject is presented in Section 4.9.



(a)



(b)

Figure 4.28 Deformations over time for (a) plastic case (b) elastoplastic case.

4.9 Comments to divergence between analysis

4.9.1 Introduction

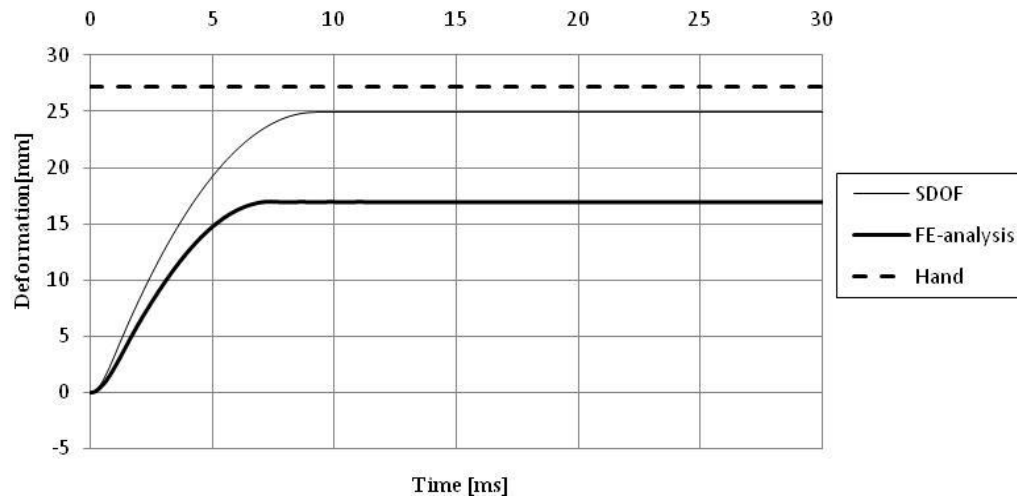
The response for the simply supported and fully fixed slabs, Section 4.7 and Section 4.8, is rather similar. The fully fixed slab has a decreased deformation compared to the simply supported slab and the divergences between SDOF and FE-analyses have different magnitudes, but the principle is the same. Therefore, only the results from the simply supported slab are presented in this Section, the comments made though also hold true for the fixed slab.

4.9.2 Elastic

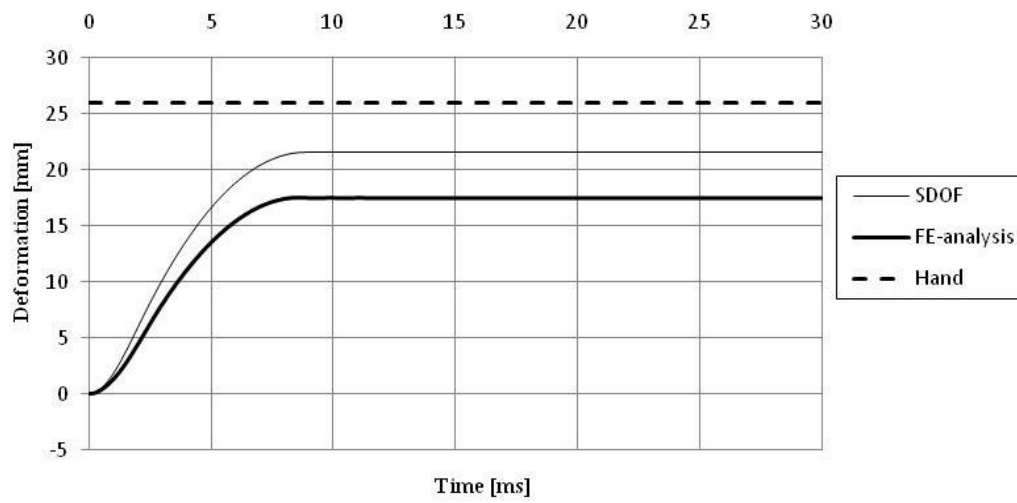
The response of the slab for linear elastic material is similar for the SDOF, hand calculations and FE-model, see Figure 4.20. As for beams, the agreement can be explained by a good assumption of the deformation shape used when deriving the transformation factors. Also as for the beam, the unsmooth response in the FE analysis arises due to the influence of higher order eigenmodes in the latter. However, the influence of these higher order eigenmodes is larger than for a beam, perhaps due to more possible eigenmodes. A phase shift between the SDOF-analysis and FE-analysis is also found here. The reason for this phase shift is not known but a control of the eigenfrequency shows that they do not explain the difference.

4.9.3 Ideal plastic

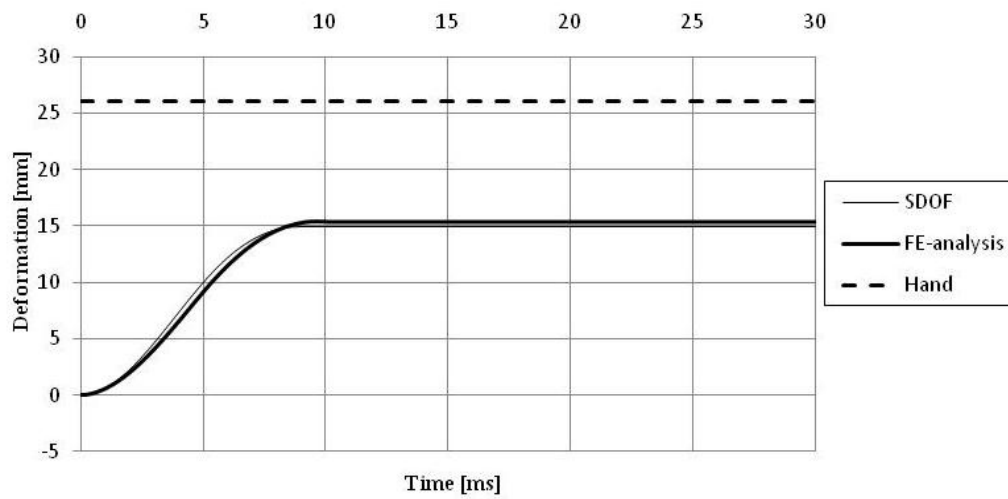
The difference between the SDOF-analyses and hand calculations depends on the assumption of a characteristic impulse load in the hand calculations as described in Section 2.4.5.1. When the same study as for the beam is carried out here, i.e. a different pressure and load duration but the same impulse, the same response as in the beam is observed, see Figure 4.29. This means that the more static the load is the better agreement between the different methods is reached. The reason for this is believed to depend on the assumption of a constant deformation shape when deriving the κ transformation factor, see Figure 4.30. The longer the load is applied, the less effect on the total response will the time when the deformation shape is assumed wrong have and the smaller will the divergence between the different analyses be.



(a)



(b)



(c)

Figure 4.29 Response of the slab subjected to (a) $P=5000$ kPa and $t_1=1.12$ ms (b) $P=2500$ kPa and $t_1=2.24$ ms (c) $P=1000$ kPa and $t_1=5.6$ ms.

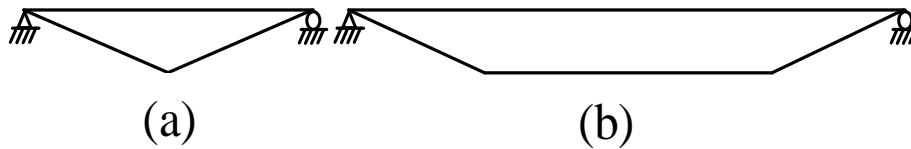


Figure 4.30 Deformation shape for the slab when using ideal plastic material. (a) short side and (b) long side.

However, as can be seen in Figure 4.29c the deformation in the SDOF system bypasses the deformation in the FE-analysis and when studies with longer load durations are done it can be seen that this divergence increases. One reason for this is that the static FE-analysis results in a lower capacity for the slab, and since the same amount of energy must be absorbed more deformation is required for the FE-analyses. However, this difference cannot be the only reason for the divergence between the SDOF and FE-analysis and the main reason for it remains unknown.

4.9.4 Elastoplastic

A large divergence in the maximum deformation for the elastoplastic slab is found between the SDOF, hand and FE-analysis, see Figure 4.21 and Figure 4.28. One reason can be found by studying the slabs response in a static analysis, see Figure 4.31. The assumed bilinear structural response used in the SDOF model overestimate the stiffness of the slab, resulting in lower deformations. This divergence has also been observed for the beam, but is there much less significant and has therefore been neglected. The energy absorbed by the structure is the same for the different structural responses, i.e. $\Delta W_{i,1} = \Delta W_{i,2}$.

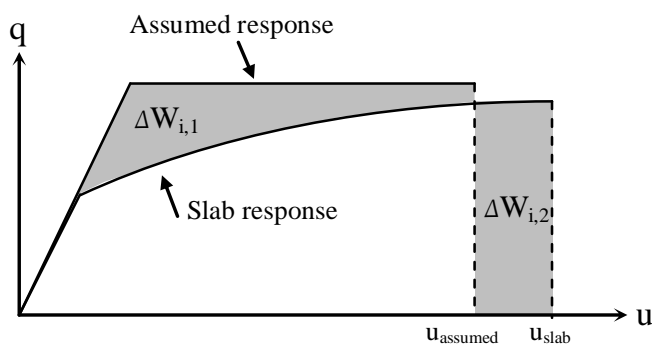


Figure 4.31 Elastoplastic material response with different approaches.

When modifying the response for the SDOF system with a multi linear response that corresponds to the slabs response shown in Figure 4.31, a better agreement is found between SDOF and FEM, see Figure 4.28. However, there is still a difference between SDOF and FE analysis and the reason for this remains unknown.

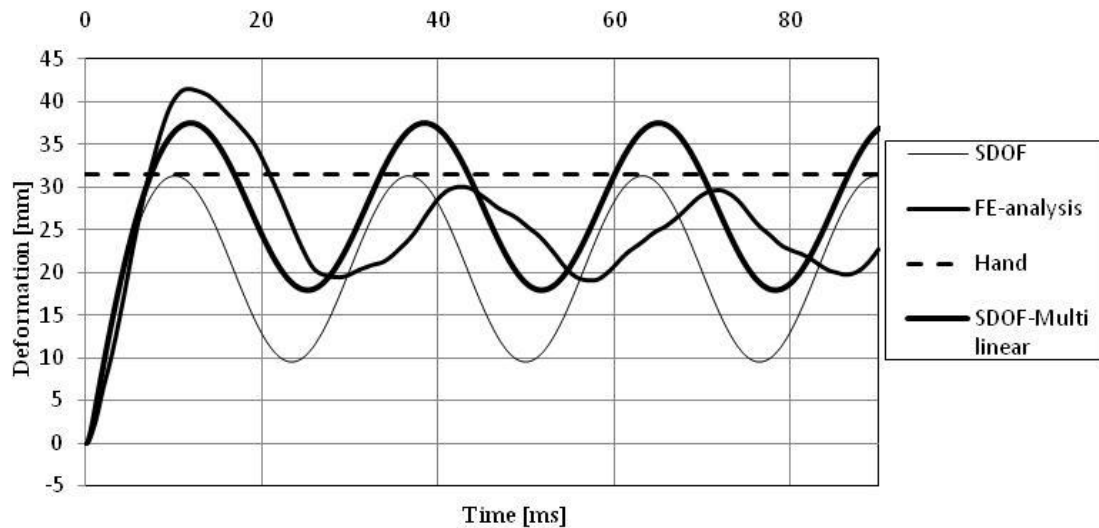


Figure 4.32 Response of the slab subjected to a load of $P=5000$ kPa and $t_1=1.12$ ms.

A study of the variation for the transformation factors has also been carried out here for different pressure and load durations but with the same impulses. The transformation factors are calculated from the FE model and are presented in APPENDIX G. Figure 4.33 illustrate the development of the κ_{mF} factor for two different loads. As can be seen the difference for the two loads is very small. The final value is reached for both loads after approximately 8 ms, which corresponds to the theoretical plastic value of the transformation factor. This shows, as mentioned in Section 4.9.3, that the longer load duration the longer time is needed, and the less effect on the total response will the time when the deformation shape is assumed wrong have.

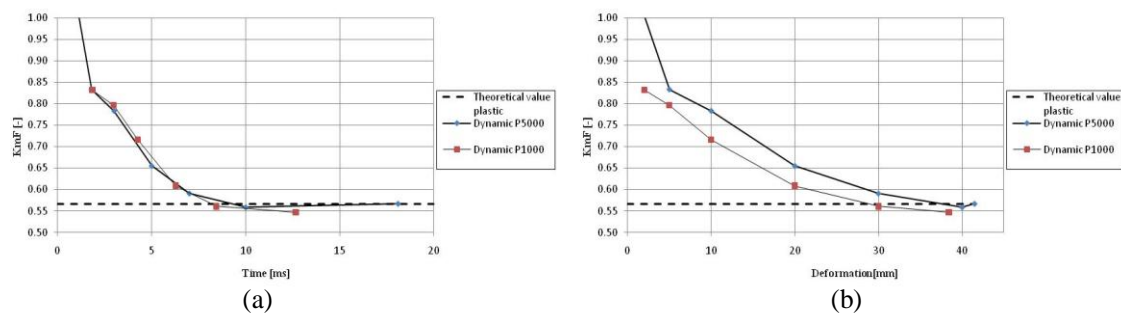


Figure 4.33 Variation of transformation factor κ_{mF} (a) over time and (b) over deformation.

An interesting notation is done for the transformation factor κ_{mF} in a static analysis, see Figure 4.34. The value starts close to the theoretical elastic value and ends close to the theoretical plastic value. The factor should, according to theory, gradually approach the theoretical plastic value the more load is applied, i.e. the longer the time goes. The higher value of the transformation factor found in the beginning is considered to depend on that the maximum deformation is not found in the system point, as was assumed in the theory. Note that the scale for both axis in Figure 4.34 is different compared to Figure 4.33.

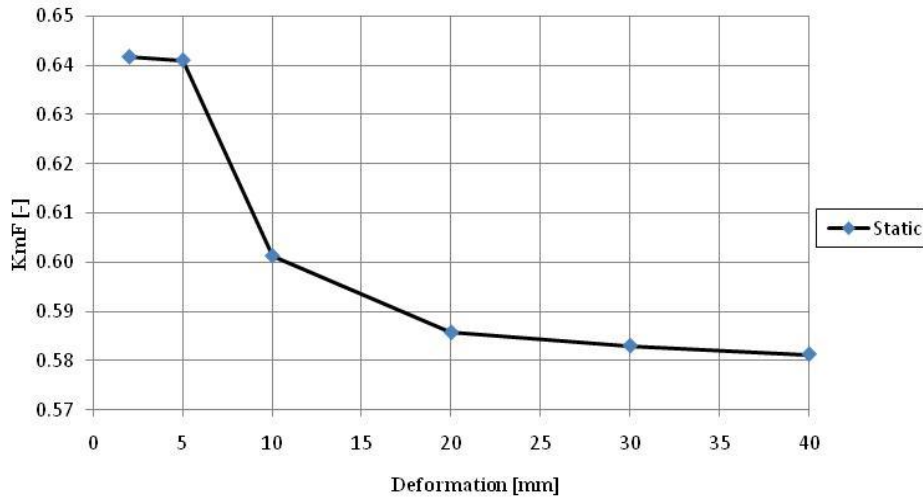


Figure 4.34 Variation of transformation factor κ_{mF} over time for a static load

Another notation done is that a large divergence in the deformation appears between the first and the rest cycles for the FE analysis. A control is done by checking the moments in the system point for three different time stages in order to acquire a better understanding for why the difference appears. Figure 4.35 shows that the maximum moment capacity is reached in both directions for point 1 and 2, but not for point 3. However, the moments are gradually decreasing indicating a small damping, but this cannot be the reason for the divergence found between the first and second cycle and the reason for the divergence remains unknown.

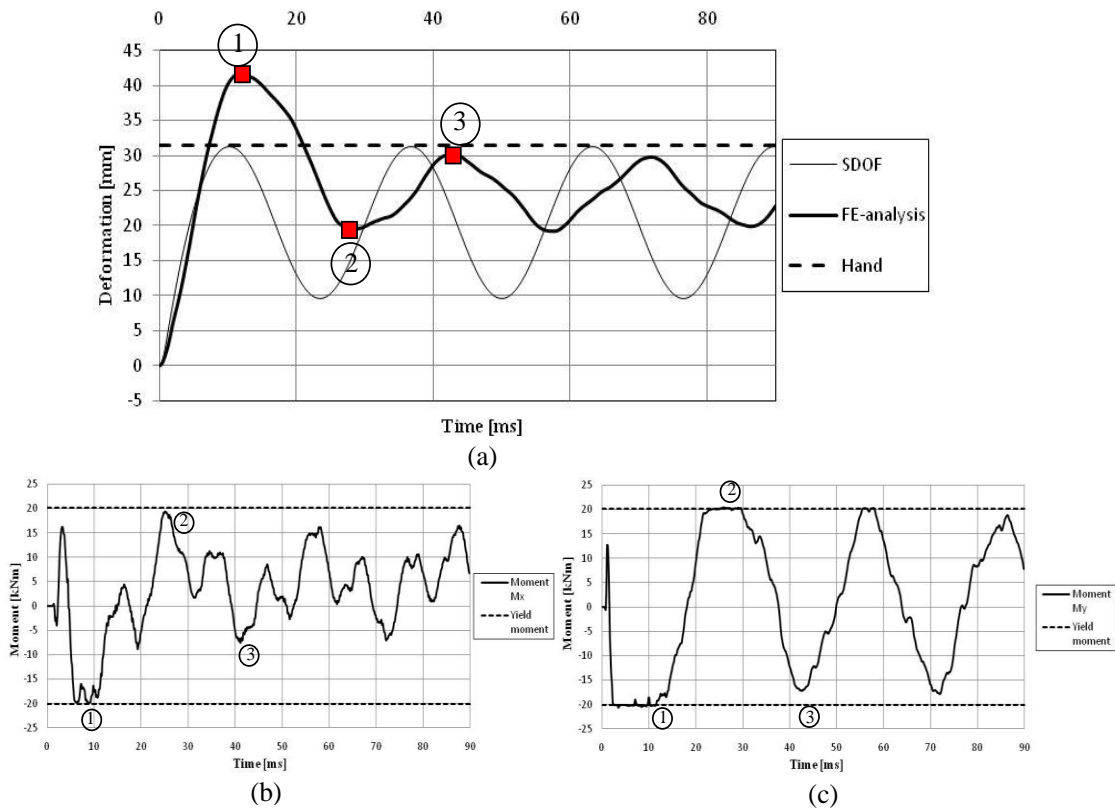


Figure 4.35 Investigation of moments at critical points. (a) Response of slab (b) moment in x-direction, M_x (c) moment in y-direction, M_y . Yield moment is 20.16 kNm.

5 Final remarks

5.1 Conclusions

In this master thesis different design approaches for structures exposed to explosions has been gathered. The reliability of these methods has then been controlled by comparing the results to FE analyses. The two different methods presented are hand calculations based on work equations and a numerical solution method based on the equation of motion. The analysis has been carried out on beams and slabs which has been reduced to a SDOF system.

The reliability of the design approaches for elastic response is good for both beams and slabs. The divergence found for the hand calculations depends on the assumption about a characterized impulse load, and can be predetermined.

The plastic response shows a large divergence for both beams and slabs and cannot be assumed to be reliable. The divergence is believed to depend on that a constant deformation shape is assumed when calculating the transformation factor κ_{mF} while in reality, the deformation shape changes with time. This theory is strengthened by analyses showing that the transformation factor greatly changes in the early stage for impulse loaded structures. However, the results for the design approaches are on the safe side so the methods can be used for preliminary design.

The elastoplastic response has a good reliability for beams, but because of the divergence found for the plastic response more studies are needed before it can be said to be reliable. A divergence is found for the elastoplastic slab analyses which are not acceptable. One reason for this is that the structure has a multi linear response that differs a lot from the bilinear response that was first assumed. To receive relatively reliable results for the elastoplastic slab, this multi linear structural response needs to be considered.

5.2 Further studies

Some simplifications of the behaviour for both slabs and beams have been done in this Master's thesis. A sequel to this thesis could be to investigate a slab with the reinforcement correctly modeled. Another important investigation is to control the residual strength of the beam or slab after it has been exposed to an impulse load. Is the residual strength greatly reduced in comparison with an equivalent static load?

In the examples carried out in this thesis, a reference bomb provided by the authorities is used, but only three of four structures are able to resist the load. A reason for this could be effects that increase the capacity of the structure but is not considered in this Master thesis. Another reason could be that the graph used from Eurocode 2 CEN (2004) when calculation the maximum rotation capacity may be on the safe side. Further investigation is here needed to check if the capacity of the slab can be utilized more.

6 References

WRITTEN SOURCES:

- ADINA (2009): *Theory and Modelling Guide*, Vol 1: ADINA Solids & Structures Report ARD 09-5, ADINA R & D, Inc., Watertown, USA.
- Al-Emrani, M. Engstöm, B. Johansson, M. Johansson. P. (2006): *Bärande konstruktioner*. Chalmers University of Technology, Division of Structural Engineering, Göteborg, Sweden.
- Balazs P. (1997): *Beräkningsmetoder vid stötvågsbelastade konstruktioner*. Försvarets forskningsanstalt, Avdelningen för vapen och skydd, FOA-R – 97-00473-311 – SE, Stockholm.
- Biggs J.M. (1964): *Introduction to Structural Dynamics*. McGraw-Hill, New-York, USA.
- CEN (2004): Eurocode 2: Design of concrete Structures – Part 1-1: General rules and rules for buildings. European Committee for Standardization, Bryssel, Belgien.
- Craig, R. Kurdila, A. (2006): *Fundamentals of Structural Dynamics*. John Wiley & Sons, Inc, New Jersey, USA.
- Ek K.J. och Mattsson P. (Planned to be published in 2010): *Design with Regard to Blast- and Fragment Loading*. Division of Structural Engineering, Concrete Structures, Chalmers University of Technology, Master Thesis 2009:81, Göteborg, Sweden.
- Engström B. (2008): *Design and analysis of continuous beams and columns*. Division of Structural Engineering, Concrete Structures, Chalmers University of Technology, Göteborg, Sweden.
- Engström B. (2009): *Design and analysis of slabs and flat slabs*. Division of Structural Engineering, Concrete Structures, Chalmers University of Technology, Göteborg, Sweden.
- Granström S. (1958): *Beräkningsmetod för stötvågsbelastade konstruktioner*. Forskning och försökssektionen, Befästningsbyrån, Kungliga Fortifikationsförvaltningen, Rapport nr 103:18, Stockholm.
- Hultin E. (1983): *Betongplattor Föreläsningskoncept*. Avdelningen för Betongbyggnad, Chalmers Tekniska Högskola, Kompendium 90:4, Göteborg.
- Johansson M. (2002): *Stötvågsutbredning i luft*. Räddningsverket, Rapport B54-223/02, Karlstad.
- Johansson M. och Laine L. (2007): *Begyggelsens motståndsförmåga mot extrem dynamisk belastning*, Delrapport 1: *Last av luftstötvåg*. Räddningsverket, Rapport B54-232/07, Karlstad.
- Johansson M. och Laine L. (2009): *Begyggelsens motståndsförmåga mot extrem dynamisk belastning*, Delrapport 3: *Kapacitet hos byggnader*. MSB, Rapport MSB 0142-10, Sverige.
- Johannesson P. och Vretblad B. (2005): *Byggformler och tabeller*. Liber, Stockholm.
- MATLAB R2010a

Nyström, U. (2006): *Design with regard to explosions*. Division of Structural Engineering, Concrete Structures, Chalmers University of Technology, Master Thesis 2006:14, Göteborg, Sweden.

Ottosen, N. and Petersson, H. (1992): *Introduction to the Finite Element Method*. Prentice Hall, England.

Råde, L. och Westergren, B. (1988): *Mathematics Handbook for Science and Engineering*. Studentlitteratur Lund.

Samuelsson, A. och Wiberg, N.E. (1988): *Byggnadsmekanik Hållfasthetslära*. Studentlitteratur Lund.

Samuelsson, A. och Wiberg, N.E. (1995): *Byggnadsmekanik Strukturmekanik*. Studentlitteratur Lund.

Timoshenko S. (1959): *Theory of plates and shells*. McGraw-Hill, New-York, USA.

WEB SOURCE:

http://www.msb.se/Upload/Insats_och_beredskap/Olycka_kris/Skyddsrum/Artiklar_forskning/Dynamisk%20lastp%C3%A5verkan%20referensbok.pdf

APPENDIX A Central difference method

The basic equation of motion can be written as equation (A.1) where u is solved for $t+\Delta t$ by equilibrium in time t .

$$m {}^t \ddot{u} + c {}^t \dot{u} + {}^t R = {}^t F(t) \quad (\text{A.1})$$

The acceleration for time t in the central difference method is

$${}^t \ddot{u} = \frac{1}{\Delta t^2} ({}^{t+\Delta t} u - 2 {}^t u + {}^{t-\Delta t} u) \quad (\text{A.2})$$

and the velocity for time t is

$${}^t \dot{u} = \frac{1}{2\Delta t} ({}^{t+\Delta t} u - {}^{t-\Delta t} u) \quad (\text{A.3})$$

When inserting equation (A.2) and (A.3) into equation (A.1) the deformation u for time $t+\Delta t$ can be stated as

$${}^{t+\Delta t} u = \left(\frac{{}^t m}{\Delta t^2} + \frac{{}^t c}{2\Delta t} \right)^{-1} \left({}^t F - {}^t R + \frac{2 {}^t m {}^t u}{\Delta t^2} - \left(\frac{{}^t m}{\Delta t^2} - \frac{{}^t c}{2\Delta t} \right) {}^{t-\Delta t} u \right) \quad (\text{A.4})$$

The central difference method requires information about the previous deformation ${}^{t-\Delta t} u$ to be able to calculate the new deformation at time $t+\Delta t$. This deformation is calculated as

$${}^{t-\Delta t} u = {}^0 u - \Delta t \cdot {}^0 \dot{u} + \frac{\Delta t^2}{2} {}^0 \ddot{u} \quad (\text{A.5})$$

APPENDIX B Modified transformation factor for the ideal plastic material for a beam

In Section 3.7.2 there was a discussion about the reliability of the assumed deformation shape in the SDOF-model when using ideal plastic material. Here, a derivation of a modified transformation factor for the ideal plastic material is done. The deformation shape derived is illustrated in Figure B.1.

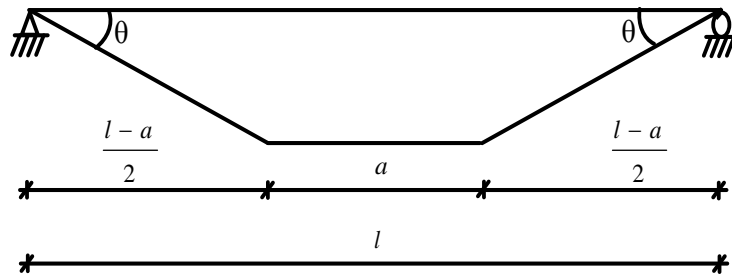


Figure B.1 Modified deformation shape for the ideal plastic material.

The deformation shape along the simply supported beam subjected to a uniformly distributed load is in this case

$$u(x) = \frac{u_s}{\frac{l-a}{2}} x, \quad 0 \leq x \leq \frac{l-a}{2} \quad (\text{B.1})$$

$$u(x) = u_s, \quad \frac{l-a}{2} \leq x \leq \frac{l}{2} \quad (\text{B.2})$$

The definition of the transformation factor for the mass is derived in Section 3.3.2 to

$$K_m = \frac{1}{l} \frac{\int_{x=0}^{x=l} u(x)^2 dx}{u_s^2} \quad (\text{B.3})$$

By inserting equation (B.1) and (B.2) into (B.3) the expression for the mass transformation factor can be calculated to

$$\begin{aligned} K_m &= \frac{1}{l} \frac{\int_{x=0}^{\frac{l-a}{2}} \left(\frac{u_s}{\frac{l-a}{2}} x \right)^2 dx}{u_s^2} + \frac{1}{l} \frac{\int_{x=\frac{l-a}{2}}^{\frac{l}{2}} u_s^2 dx}{u_s^2} = \frac{1}{l} \frac{\left(\frac{l-a}{2} \right)^2 \left[\frac{x^3}{3} \right]_0^{\frac{l-a}{2}}}{u_s^2} + \frac{1}{l} \frac{u_s^2}{u_s^2} \left[x \right]_{\frac{l-a}{2}}^{\frac{l}{2}} = \\ &= \frac{1}{2} - \frac{l-a}{3 \cdot l} \end{aligned} \quad (\text{B.4})$$

The definition of the transformation factor for the load is derived in Section 3.3.3 to

$$\kappa_F = \frac{1}{l} \frac{\int_{x=0}^{x=l} u(x) dx}{u_s} \quad (\text{B.5})$$

By inserting equation (B.1) and (B.2) into (B.5) the expression for the load transformation factor can be calculated to

$$\begin{aligned} \kappa_F &= \frac{1}{l} \frac{\int_{x=0}^{\frac{l-a}{2}} \frac{u_s}{l-a} x dx}{u_s} + \frac{1}{l} \frac{\int_{x=\frac{l-a}{2}}^{\frac{l}{2}} u_s dx}{u_s} = \frac{1}{l} \frac{2}{u_s} \left[\frac{u_s}{l-a} \left[\frac{x^2}{2} \right]_0^{\frac{l-a}{2}} \right] + \frac{1}{l} \frac{u_s}{u_s} \left[x \right]_{\frac{l-a}{2}}^{\frac{l}{2}} = \\ &= \frac{1}{2} - \frac{l-a}{4 \cdot l} \end{aligned} \quad (\text{B.6})$$

The transformation factor κ_{mF} can now be calculated

$$\kappa_{mF} = \frac{\kappa_m}{\kappa_F} = \frac{\frac{1}{2} - \frac{l-a}{3 \cdot l}}{\frac{1}{2} - \frac{l-a}{4 \cdot l}} \quad (\text{B.7})$$

Table B.1 Tabulated transformation factor κ_{mF} for different a .

κ_{mF}	a
0.667	0
0.690	0.1
0.713	0.2
0.733	0.3
0.753	0.4
0.771	0.5
0.788	0.6
0.804	0.7
0.819	0.8
0.833	0.9
0.847	1.0

APPENDIX C Modified transformation factor for the elastoplastic material for a beam

In Section 3.7.3 there was a discussion about the reliability of the assumed deformation shape for the elastoplastic response in the SDOF-model. Here, a calculation of a modified transformation factor for the elastoplastic material is done for a beam with a length of 2.7m and with an applied load of $P=5000\text{kPa}$, $t_1=1.12\text{ms}$. The deformation shape used is taken from FE-analysis at time $t_1=1.12\text{ms}$ and is illustrated in Figure C.1.

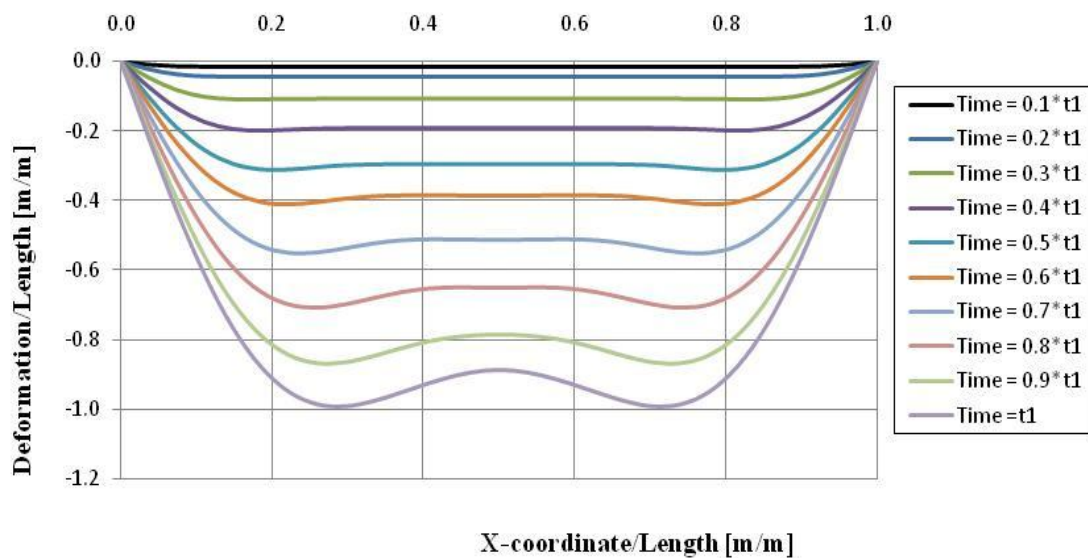


Figure C.1 Deformation shape for the elastoplastic material at time $t_1=1.12\text{ms}$.

The definition of the transformation factor for the mass is derived in Section 3.3.2 to

$$\kappa_m = \frac{1}{l} \frac{\int_{x=0}^{x=l} u(x)^2 dx}{u_s^2} \quad (\text{C.1})$$

and can be rewritten to be

$$\kappa_m = \frac{1}{l} \sum_{i=1}^n \frac{u_i^2 \cdot l}{u_s^2 \cdot n} \quad (\text{C.2})$$

where n is the number of free nodes in the FE-model, i.e. the nodes which is not fixed at the supports.

The definition of the transformation factor for the load is derived in Section 3.3.3 to

$$\kappa_F = \frac{1}{l} \frac{\int_{x=0}^{x=l} u(x) dx}{u_s} \quad (\text{C.3})$$

and can be rewritten to

$$\kappa_F = \frac{1}{l} \sum_{i=1}^n \frac{u_i \cdot l}{u_s \cdot n} \quad (\text{C.4})$$

where n is the number of free nodes in the FE-model.

The transformation factors for different time stages can be seen in Table C.1.

Table C.1 Transformation factors taken from FE-analysis for the elastoplastic beam.

u_s [mm]	t [ms]	κ_m	κ_F	κ_{mF}
2.4	1.11	0.853	0.871	0.979
10	2.81	0.491	0.627	0.783
20	5.51	0.484	0.619	0.782
30	8.31	0.435	0.583	0.747
40	12.4	0.424	0.573	0.739
47.3	20	0.408	0.561	0.728

APPENDIX D Elastic transformation factors for a simply supported slab with uniformly distributed load

D.1 Indata

The slab can, according to Granström (1958), be assumed to have a sinusoidal shape. The deformation along the slab can then be calculated as

$$u(x, y) = \sin(\pi x / w) \cdot \sin(\pi y / l) \cdot u_{\max} \quad (\text{D.1})$$

The maximum deformation u_{\max} is found in the middle of the slab and the system point is therefore chosen to the middle of the slab, see Figure D.1.

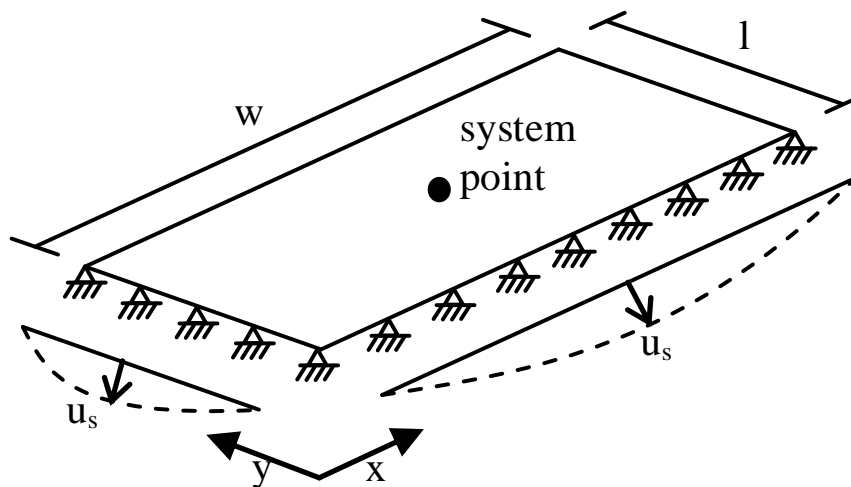


Figure D.1 Deformation shape for an elastic slab.

D.2 Transformation factor for the mass κ_m

The transformation factor for the mass is according to equation (4.11)

$$\kappa_m = \frac{1}{w \cdot l} \int_{y=0}^{y=l} \int_{x=0}^{x=w} \frac{u^2}{u_s^2} dx dy \quad (\text{D.2})$$

Inserting equation (D.1) into (D.2) gives

$$\begin{aligned}
\kappa_m &= \frac{1}{w \cdot l} \int_{y=0}^{y=l} \int_{x=0}^{x=w} (\sin(\pi x / w) \cdot \sin(\pi y / l))^2 dx dy = \\
&= \frac{1}{w \cdot l} \int_{y=0}^{y=l} (\sin(\pi y / l))^2 \cdot \left[\frac{x}{2} - \frac{\sin(2 \cdot \frac{\pi}{w} \cdot x)}{4 \cdot \frac{\pi}{w}} \right]_0^w dy = \frac{1}{w \cdot l} \int_{y=0}^{y=l} (\sin(\pi y / l))^2 \cdot \frac{w}{2} = \\
&= \frac{1}{w \cdot l} \cdot \frac{w}{2} \left[\frac{y}{2} - \frac{\sin(2 \cdot \frac{\pi}{l} \cdot y)}{4 \cdot \frac{\pi}{l}} \right]_0^l = \frac{1}{w \cdot l} \cdot \frac{w}{2} \cdot \frac{l}{2} = 0.25
\end{aligned} \tag{D.3}$$

D.3 Transformation factor for the load κ_F

The transformation factor for the load is according to equation (4.20)

$$\kappa_F = \frac{1}{l \cdot w} \cdot \int_{y=0}^{y=l} \int_{x=0}^{x=w} \frac{u(x, y)}{u_s} dx dy \tag{D.4}$$

Inserting equation (D.1) into (D.4) gives

$$\begin{aligned}
\kappa_F &= \frac{1}{l \cdot w} \cdot \int_{y=0}^{y=l} \int_{x=0}^{x=w} (\sin(\pi x / w) \cdot \sin(\pi y / l)) dx dy = \\
&= \frac{1}{l \cdot w} \cdot \int_{y=0}^{y=l} \sin(\pi y / l) \cdot \left[-\cos(\pi \cdot \frac{x}{w}) \cdot \frac{w}{\pi} \right]_0^w = \\
&= \frac{1}{l \cdot w} \cdot \int_{y=0}^{y=l} \sin(\pi y / l) \cdot \left[-(-1) \cdot \frac{w}{\pi} - (-1 \cdot \frac{w}{\pi}) \right] dy = \\
&= \frac{1}{l \cdot w} \cdot \int_{y=0}^{y=l} \sin(\pi y / l) \cdot 2 \cdot \frac{w}{\pi} dy = \frac{1}{l \cdot w} \cdot 2 \cdot \frac{w}{\pi} \cdot \left[-\cos(\pi \cdot \frac{y}{l}) \cdot \frac{l}{\pi} \right]_0^l = \\
&= \frac{1}{l \cdot w} \cdot 2 \cdot \frac{w}{\pi} \cdot \left[-(-1) \cdot \frac{l}{\pi} - (-1 \cdot \frac{l}{\pi}) \right] = \frac{1}{l \cdot w} \cdot 2 \cdot \frac{w}{\pi} \cdot 2 \cdot \frac{l}{\pi} = \frac{4}{\pi^2}
\end{aligned} \tag{D.5}$$

APPENDIX E Plastic transformation factors for a simply supported and fully fixed slab with uniformly distributed load

E.1 Indata

The calculations done here are based on the yield line theory. The assumed deformation shape is shown in Figure E.1.

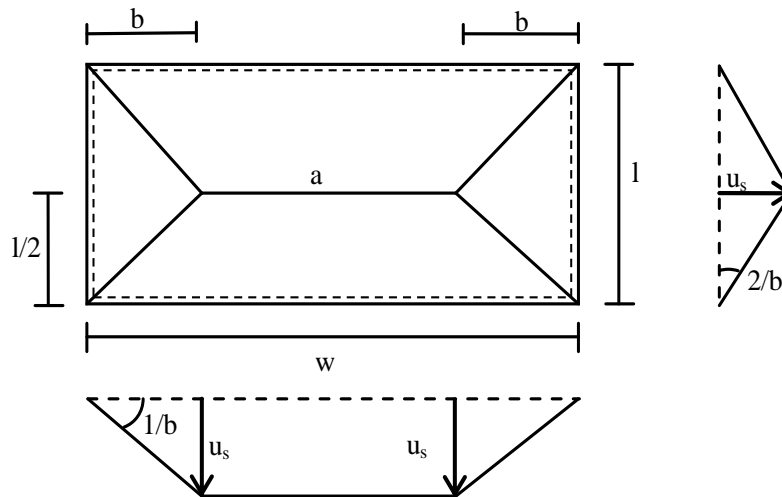


Figure E.1 Deformation shape for an elastic slab.

From the figure and by normalising the system point, i.e. setting u_s to 1, the following relations can be stated:

$$b = \frac{w - a}{2} \quad (\text{E.1})$$

$$u(x, y) = \frac{x}{b} \quad \text{for } 0 \leq x \leq b \text{ and } \frac{l}{2 \cdot b} \cdot x \leq y \leq \frac{l}{2} \quad \left(0 \leq x \leq \frac{2 \cdot b}{l} \cdot y \right) \quad (\text{E.2})$$

$$u(x, y) = \frac{2 \cdot y}{l} \quad \text{for } b \leq x \leq \frac{w}{2} \text{ and } 0 \leq y \leq \frac{l}{2} \quad (\text{E.3})$$

$$u(x, y) = \frac{2 \cdot y}{l} \quad \text{for } 0 \leq x \leq b \text{ and } 0 \leq y \leq \frac{l}{2} \cdot \frac{x}{b} \quad \left(\frac{2 \cdot b}{l} \cdot y \leq x \leq b \right) \quad (\text{E.4})$$

E.2 Transformation factor for the mass κ_m

The transformation factor for the mass is according to equation (4.11)

$$\kappa_m = \frac{1}{w \cdot l} \int_{y=0}^{y=l} \int_{x=0}^{x=w} \frac{u^2}{u_s^2} dx dy \quad (\text{E.5})$$

Inserting the deformation conditions stated by equation (E.2), (E.3) and (E.4) into (E.5) gives

$$\kappa_m = \frac{4}{w \cdot l} \left\{ \int_{x=0}^b \int_{y=\frac{l}{2 \cdot b} \cdot x}^{\frac{l}{2}} \left(\frac{x}{b} \right)^2 dx dy + \int_{x=0}^b \int_{y=0}^{\frac{l}{2 \cdot b} \cdot x} \left(\frac{2 \cdot y}{l} \right)^2 dx dy + \right. \\ \left. + \int_{x=b}^{\frac{w}{2}} \int_{y=0}^{\frac{l}{2}} \left(\frac{2 \cdot y}{l} \right)^2 dx dy \right\} = \frac{4}{w \cdot l} [(1) + (2) + (3)] \quad (\text{E.6})$$

$$(1) \int_{x=0}^b \int_{y=\frac{l}{2 \cdot b} \cdot x}^{\frac{l}{2}} \frac{x^2}{b^2} dx dy = \int_{x=0}^b \left[\frac{y \cdot x^2}{b^2} \right]_{\frac{l}{2 \cdot b} \cdot x}^{\frac{l}{2}} dx = \frac{l}{2 \cdot b^2} \int_{x=0}^b x^2 \left(1 - \frac{x}{b} \right) dx = \\ = \frac{l}{2 \cdot b^2} \left[\frac{x^3}{3} - \frac{x^4}{4 \cdot b} \right]_0^b = \frac{l \cdot b}{2} \left(\frac{1}{3} - \frac{1}{4} \right) = \frac{1}{24} \cdot l \cdot b \quad (\text{E.7})$$

$$(2) \int_{x=0}^b \int_{y=0}^{\frac{l}{2 \cdot b} \cdot x} \frac{4 \cdot y^2}{l^2} dx dy = \int_{x=0}^b \left[\frac{4}{l^2} \cdot \frac{y^3}{3} \right]_0^{\frac{l}{2 \cdot b} \cdot x} dx = \frac{4}{l^2} \cdot \frac{l^3}{8 \cdot b^3} \int_{x=0}^b \frac{x^3}{3} dx = \\ = \frac{l}{2 \cdot b^3} \left[\frac{x^4}{3 \cdot 4} \right]_0^b = \frac{l \cdot b}{2 \cdot 12} = \frac{1}{24} \cdot l \cdot b = (1) \text{ OK!} \quad (\text{E.8})$$

$$(3) \int_{x=b}^{\frac{w}{2}} \int_{y=0}^{\frac{l}{2}} \frac{4 \cdot y^2}{l^2} dx dy = \int_{x=b}^{\frac{w}{2}} \frac{4}{l^2} \left[\frac{y^3}{3} \right]_0^{\frac{l}{2}} dx = \frac{4}{l^2} \cdot \frac{l^3}{8} \int_{x=b}^{\frac{w}{2}} \frac{1}{3} dx = \\ = \frac{l}{6} [x]_b^{w/2} = \frac{l}{6} \left(\frac{w}{2} - b \right) = \frac{1}{12} \cdot l \cdot b \cdot \left(\frac{w}{b} - 2 \right) = \frac{2}{24} \cdot \left(\frac{w}{b} - 2 \right) \cdot l \cdot b \quad (\text{E.9})$$

$$\begin{aligned}
\kappa_m &= \frac{4}{w \cdot l} [(1) + (2) + (3)] = \frac{4}{w \cdot l} \cdot \frac{l \cdot b}{24} \left(1 + 1 + 2 \left(\frac{w}{b} - 2 \right) \right) = \\
&= \frac{8}{24} \cdot \left(\frac{w}{b} - 1 \right) \cdot \frac{l \cdot b}{l \cdot w} = \frac{1}{3} \cdot \left(\frac{w}{b} - 1 \right) \cdot \frac{b}{w} = \frac{1}{3} \left(1 - \frac{b}{w} \right) = \frac{1}{3} \left(1 - \frac{\left(\frac{w-a}{2} \right)}{w} \right) = \quad (E.10) \\
&\frac{1}{3} \left(1 - \frac{1}{2} + \frac{a}{2 \cdot w} \right) = \frac{1}{6} \left(1 + \frac{a}{w} \right)
\end{aligned}$$

E.3 Transformation factor for the load κ_F

The transformation factor for the load is according to equation (4.20)

$$\kappa_F = \frac{1}{l \cdot w} \cdot \int_{y=0}^{y=l} \int_{x=0}^{x=w} \frac{u(x, y)}{u_s} dx dy \quad (E.11)$$

Inserting the deformation conditions stated by equation (E.2), (E.3) and (E.4) into (E.11) gives

$$\begin{aligned}
\kappa_m &= \frac{4}{w \cdot l} \left(\int_{x=0}^b \int_{y=\frac{l}{2-b} \cdot x}^{\frac{l}{2}} \frac{x}{b} dx dy + \int_{x=0}^b \int_{y=0}^{\frac{l}{2-b} \cdot x} \frac{2 \cdot y}{l} dx dy + \right. \\
&\left. + \int_{x=b}^{\frac{w}{2}} \int_{y=0}^{\frac{l}{2}} \frac{2 \cdot y}{l} dx dy \right) = \frac{4}{w \cdot l} [(1)' + (2)' + (3)'] \quad (E.12)
\end{aligned}$$

$$\begin{aligned}
(1)' \int_{x=0}^b \int_{y=\frac{l}{2-b} \cdot x}^{\frac{l}{2}} \frac{x}{b} dx dy &= \int_{x=0}^b \left[\frac{y \cdot x}{b} \right]_{\frac{l}{2-b} \cdot x}^{\frac{l}{2}} dx = \frac{l}{2 \cdot b} \int_{x=0}^b \left(x - \frac{x^2}{b} \right) dx = \\
&= \frac{l}{2 \cdot b} \left[\frac{x^2}{2} - \frac{x^3}{3 \cdot b} \right]_0^b = \frac{l \cdot b}{2} \left(\frac{1}{2} - \frac{1}{3} \right) = \frac{l \cdot b}{12} \quad (E.13)
\end{aligned}$$

$$\begin{aligned}
(2)' \int_{x=0}^b \int_{y=0}^{\frac{l}{2-b} \cdot x} \frac{2 \cdot y}{l} dx dy &= \frac{2}{l} \int_{x=0}^b \left[\frac{y^2}{2} \right]_0^{\frac{l}{2-b} \cdot x} dx = \frac{2}{l} \cdot \frac{l^2}{4 \cdot b^2} \cdot \frac{1}{2} \int_{x=0}^b x^2 dx = \\
&= \frac{l}{4 \cdot b^2} \left[\frac{x^3}{3} \right]_0^b = \frac{l \cdot b}{12} = (1) \text{ OK!} \quad (E.14)
\end{aligned}$$

$$\begin{aligned}
(3)' \int_{x=b}^{\frac{w}{2}} \int_{y=0}^{\frac{l}{2}} \frac{2 \cdot y}{l} dx dy &= \frac{2}{l} \int_{x=b}^{\frac{w}{2}} \left[\frac{y^2}{2} \right]_0^{\frac{l}{2}} dx = \frac{2}{l} \cdot \frac{l^2}{4} \cdot \frac{1}{2} \int_{x=b}^{\frac{w}{2}} dx = \\
&= \frac{l}{4} [x]_b^{\frac{w}{2}} = \frac{l}{4} \left(\frac{w}{2} - b \right) = \frac{1}{8} \cdot \left(\frac{w}{b} - 2 \right) \cdot l \cdot b
\end{aligned} \tag{E.15}$$

$$\begin{aligned}
\kappa_m &= \frac{4}{w \cdot l} [(1)' + (2)' + (3)'] = \frac{4}{w \cdot l} \cdot \frac{l \cdot b}{24} \left(2 + 2 + 3 \left(\frac{w}{b} - 2 \right) \right) = \\
&= \frac{1}{6} \left(3 - \frac{2 \cdot b}{w} \right) = \frac{1}{6} \left(3 - \frac{2 \cdot \left(\frac{w-a}{2} \right)}{w} \right) = \frac{1}{6} \left(3 - 1 + \frac{a}{w} \right) = \frac{1}{6} \left(\frac{a}{w} + 2 \right)
\end{aligned} \tag{E.16}$$

APPENDIX F Modified alpha factor for the fictitious yield stress when using seven integration points

When Newton-Cotes integration method with seven integration points is used in ADINA, the software replaces the actual stress distribution with a polynomial of order six. Here, a derivation is done to acquire a factor that can transform ADINA's stress distribution to the expected stress distribution.

The equation of the ultimate moment capacity for the expected stress distribution, see Figure F.1 can be stated as

$$\begin{aligned}
 M_{rd} &= \left(\left(f_y' \cdot \frac{h \cdot 2}{6} \right) \cdot 2 \cdot \frac{h}{6} + \left(f_y' \cdot \frac{h}{6} \cdot \frac{1}{2} \right) \cdot \frac{h}{6} \cdot \frac{2}{3} \right) \cdot w \cdot 2 = f_y' \cdot w \cdot h^2 \cdot \left(\frac{2}{9} + \frac{1}{6} \cdot \frac{1}{6} \cdot \frac{1}{3} \right) \\
 &= f_y' \cdot w \cdot h^2 \cdot \left(\frac{12}{54} + \frac{1}{54} \right) = \frac{13}{54} \cdot f_y' \cdot w \cdot h^2
 \end{aligned}
 \tag{F.1}$$

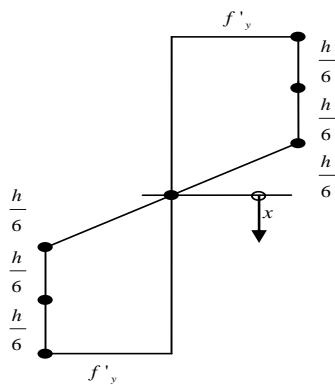


Figure F.1 Expected stress distribution.

By normalizing the height to 2 and yield stress to 1 the polynomial of order six can be stated as

$$\sigma = 3.7x - 6.75x^3 + 4.05x^5 \quad -1 < x < 1
 \tag{F.2}$$

and have the appearance as shown in Figure F.2.

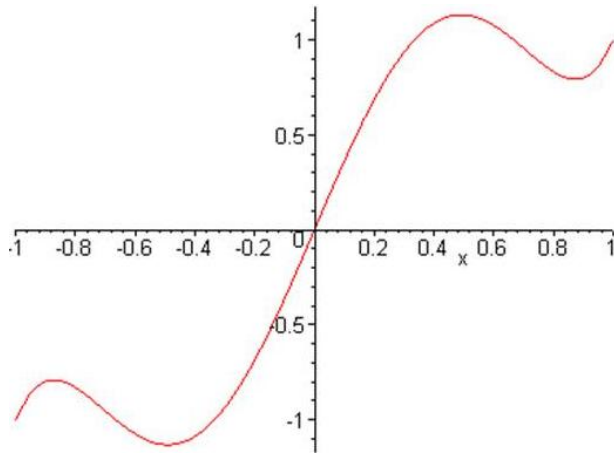


Figure F.2 Deformation shape for an elastic slab.

The moment for the normalized stress distribution in ADINA can now be stated as

$$M_{Adina} = \int_0^1 (3.7x - 6.75x^3 + 4.05x^5)x \cdot dx = 0.4619 \quad (F.3)$$

And the moment for the normalized expected stress distribution can be stated as

$$M_{expected} = \int_0^{1/3} (3x)x \cdot dx + \int_{1/3}^1 x \cdot dx = 0.4815 \quad (F.4)$$

The difference between ADINA's stress distribution and the expected stress distribution is

$$\frac{0.4619}{0.4815} = 0.9593 \quad (F.5)$$

So, ADINA's stress distribution generates 4.07% smaller value compared to the expected stress distribution, i.e.

$$f_y' = 0.9593 \cdot f_y'_{expected} \quad (F.6)$$

This lead to

$$M_{rd} = \frac{13}{54} \cdot f_y' \cdot w \cdot h^2 = \left\{ f_y' = 0.9593 \cdot f_y'_{expected} \right\} = \alpha \cdot f_y'_{actual} \cdot w \cdot h^2 \quad (F.7)$$

where α is

$$\alpha = \frac{13}{54} \cdot 0.9593 = 0.231 \quad (F.8)$$

APPENDIX G Transformation factors for elastoplastic slab

Transformation factors are here tabulated for a simply supported respectively fully fixed slab with different loads. The transformation factors are calculated for the same principle as in APPENDIX C, i.e. with information from the FE analysis.

$$\kappa_m = \frac{1}{l \cdot w} \sum_{i=1}^n \frac{u_i^2 \cdot l \cdot w}{u_s^2 \cdot n} \quad (\text{G.1})$$

$$\kappa_F = \frac{1}{l \cdot w} \sum_{i=1}^n \frac{u_i \cdot l \cdot w}{u_s \cdot n} \quad (\text{G.2})$$

$$\kappa_{mF} = \frac{\kappa_m}{\kappa_F} \quad (\text{G.3})$$

Table G.1 Transformation factors for a simply supported slab subjected to the uniformly distributed impulse load $P=5000\text{kPa}$ and $t_1=1.12\text{ms}$.

u_s [mm]	t [ms]	κ_m	κ_F	κ_{mF}
2	1.11	0.844	0.838	1.008
5	1.81	0.543	0.651	0.834
10	3.01	0.440	0.561	0.784
20	5.01	0.295	0.450	0.655
30	7.01	0.226	0.383	0.591
40	10.01	0.196	0.350	0.558
41.5	11.81	0.203	0.358	0.567

Table G.2 Transformation factors for a simply supported slab subjected to the uniformly distributed impulse load $P=1000\text{kPa}$ and $t_1=5.6\text{ms}$.

u_s [mm]	t [ms]	κ_m	κ_F	κ_{mF}
2	1.85	0.548	0.656	0.833
5	2.97	0.460	0.577	0.796
10	4.28	0.360	0.503	0.717
20	6.27	0.243	0.399	0.609

30	8.43	0.192	0.342	0.561
38.4	12.66	0.181	0.331	0.547

Table G.3 Transformation factors for a simply supported slab subjected to a uniformly distributed static load (loaded until failure).

u_s [mm]	t [ms]	κ_m	κ_F	κ_{mF}
2	185	0.279	0.435	0.642
5	455	0.278	0.434	0.641
10	650	0.238	0.396	0.601
20	810	0.220	0.375	0.586
30	885	0.216	0.370	0.583
40	910	0.214	0.368	0.581

Table G.4 Transformation factors for a fully fixed slab subjected to the uniformly distributed impulse load $P=5000\text{kPa}$ and $t_1=1.12\text{ms}$.

u_s [mm]	t [ms]	κ_m	κ_F	κ_{mF}
2	1.01	0.673	0.713	0.944
5	1.71	0.414	0.531	0.780
10	3.01	0.324	0.439	0.737
20	5.41	0.185	0.325	0.568
25.5	8.21	0.143	0.274	0.522

Table G.5 Transformation factors for a fully fixed slab subjected to the uniformly distributed impulse load. $P=1000\text{kPa}$ and $t_1=5.6\text{ms}$.

u_s [mm]	t [ms]	κ_m	κ_F	κ_{mF}
0.7	1.11	0.534	0.618	0.864
2	1.81	0.359	0.482	0.745
5	3.11	0.325	0.442	0.735
10	4.71	0.240	0.380	0.631
19.2	8.51	0.132	0.257	0.515

Table G.6 Transformation factors for a fully fixed slab subjected to a uniformly distributed static load (loaded until failure).

u_s [mm]	t [ms]	κ_m	κ_F	κ_{mF}
2	345	0.210	0.338	0.622
5	560	0.204	0.335	0.610
10	670	0.198	0.333	0.594
20	750	0.181	0.321	0.563
25	775	0.174	0.315	0.552
30	795	0.170	0.312	0.545
33.5	810	0.173	0.315	0.550